ABSTRACT

Title of Document: ISOTOPE AND ORGANIC GEOCHEMISTRY OF A UNIQUE PROTEROZOIC, POSTGLACIAL SUCCESSION: THE LAPA FORMATION, VAZANTE GROUP, BRAZIL

Kristina Bartlett Brody, Master of Science, 2007

Directed By: Dr. Alan J. Kaufman, Department of Geology

This study is the second to investigate biological characteristics associated with Proterozoic glaciation via molecular fossils from organic matter preserved in shale. In the Vazante Group, Minas Gerais, Brazil, the Serra da Lapa Formation unconformably overlies a formation recently dated to *ca.* 1.13 Ga. Lithologic and isotopic data suggest the Lapa represents deposition immediately after either an early Neoproterozoic "snowball Earth" ice age or a possible regional, but still low-latitude, late Mesoproterozoic ice age. The relative abundances of biomarkers and other organic molecules show variations that match lithologic and isotopic changes observed in 40 meters of exploration drill core studied. Inconsistencies among biomarker abundances as well as differences between the organic matter of the Lapa Formation and that of the underlying formation hint at heterogeneity among and within formations. A more complete picture of the Vazante Group is warranted before characteristics of preserved organic matter can be interpreted in the context of depositional environments or postdepositional processes.

ISOTOPE AND ORGANIC GEOCHEMISTRY OF A UNIQUE PROTEROZOIC, POSTGLACIAL SUCCESSION: THE LAPA FORMATION, VAZANTE GROUP, BRAZIL

By

Kristina Bartlett Brody.

Thesis submitted to the Faculty of the Graduate School of the
University of Maryland, College Park, in partial fulfillment
of the requirements for the degree of
Master of Science
2007

Advisory Committee:
Associate Professor Alan J. Kaufman, Chair
Associate Professor James Farquhar
Professor Richard J. Walker

Acknowledgements

I could not have completed this project without the many people who generously shared their time, knowledge and resources with me. Thank you first to Alan J. Kaufman, who agreed to take on an English major and science writer-editor as a master's student, and additionally entrusted me with a difficult and fascinating project. I thank him for his patience combined with high expectations that challenged me to make this happen. Thank you to James Farquhar and Richard Walker both for helpful and enjoyable conversations and for taking the time to serve on my committee and share their knowledge.

To our colleagues in Brazil I say, "obrigada." Marly Babinksi, Julio Murio Pinho and Aroldo Misi showed us great kindness and drove us many miles to share with us the beauty and geology of Brazil. Thank you also to Tolentino Flavio de Oliveira for setting aside three days of time at the Paracatú mine so that we could collect many, many core samples. I thank him also for answering my many emails, and I thank all the employees of the mining company for helping us to collect and cut core samples.

George Cody of the Geophysical Lab at the Carnegie Institution of Washington warmly invited me to use is lab and GCMS, making it possible for me to collect my data. Jennifer Eigenbrode spent many hours helping me to understand biomarkers and how to do biomarker work. I thank her enthusiastically for serving as a mentor. Elizabeth Canuel at the Virginia Institute of Marine Sciences allowed me to use her organic geochemistry lab to do analyses I could not have otherwise

completed. Her lab manager Beth Waterson answered many questions. Thank you to Noel Whittaker who manages the mass spectrometry facilities at the University of Maryland Department of Organic Chemistry. He was generous with his time and knowledge.

I had many conversations that helped me in understanding the subject matter of my thesis, and I think those people who took the time to talk with me: Philip Candela, Murray Hitzman, David T. Johnston and Roger Summons.

I thank all my fellow graduate and undergraduate students for sharing their time, knowledge and, most importantly, wonderful friendship. I give a particular thank you to Brendan Williams.

Thank you to *Geotimes* and the people at the American Geological Institute for helping me to discover the very cool, wonderful world of geology. A special thank you to David Applegate for his good word and his encouragement.

Lastly I want to thank my beautiful family: my husband Loren, daughter Eliana, and all my extended family. Thank you for your help, patience and support, without which I could not have made it to this point.

Table of Contents

List of Tables

List of Figures

Chapter 1: Introduction

1.1: Context: Biomarkers and Earth History

This study is a biomarker investigation supplemented by carbon and sulfur isotope analyses of a postglacial, organic-rich shale sequence. The hope is that these combined data sets can help in understanding the relationship between biogeochemistry and extreme climate events early in Earth history.

Biomarkers are carbon-based molecules formed only by biological processes. They have become a major tool in understanding the origin and evolution of life on the Earth, particularly during the Precambrian interval before the appearance of animals with hard parts that fossilize.

Biomarkers begin as the molecules synthesized by any of the organisms in the extant domains of life — Bacteria, Archaea, and Eukaryotes — and include the fats and other substances in cells, such as lipids (Fig. 1.1). When buried and preserved in sediments, these molecules retain their basic skeletal structures, which are unique to specific biosynthetic pathways. Studies have matched the molecules synthesized by extant bacteria and other organisms to the biomarkers preserved in the geological record (Ourisson *et al.*, 1979**;** Rohmer *et al.*, 1992), providing a template for using biomarkers as molecular fossils for the presence of specific types of organisms.

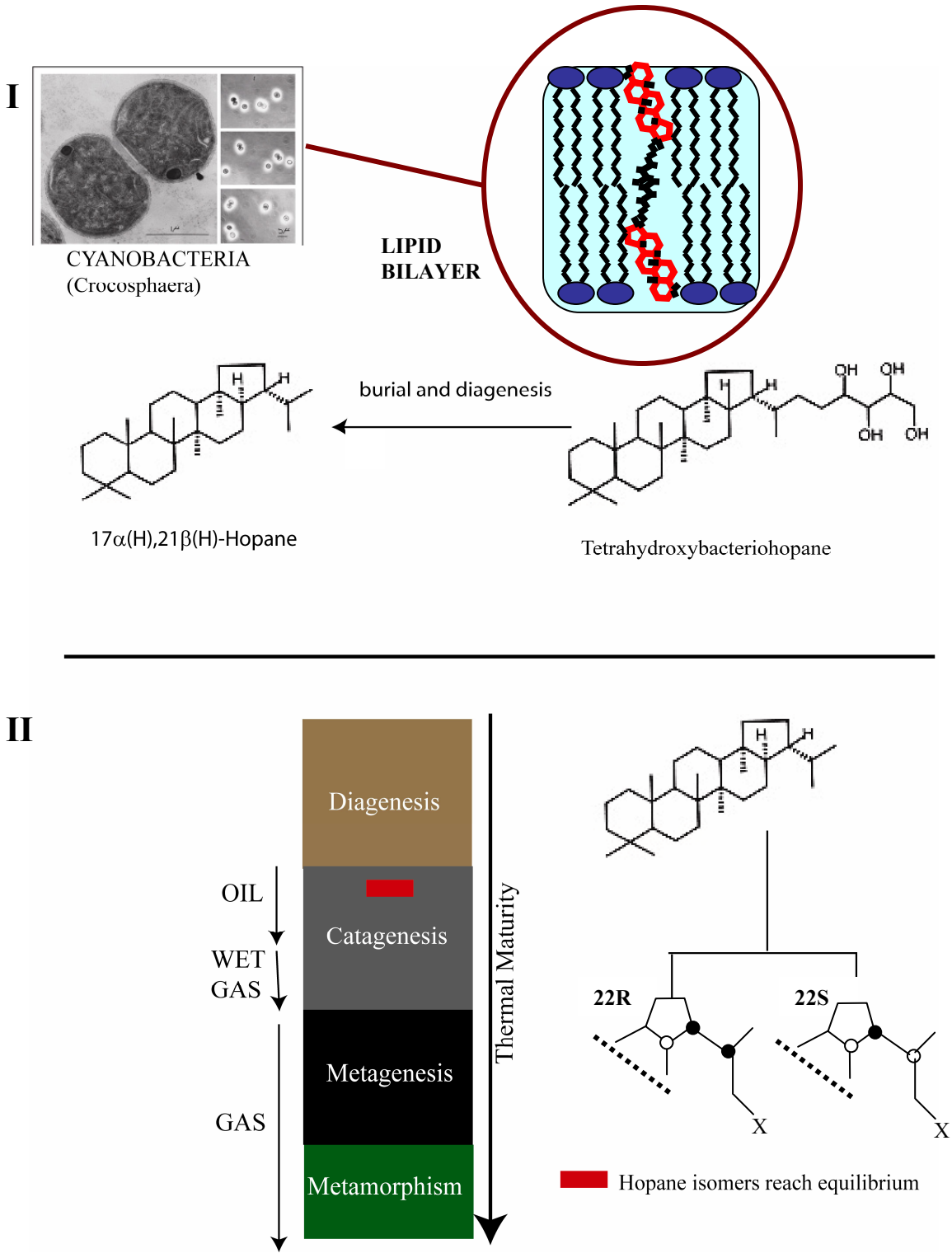

Figure 1.1: Illustration of processes leading to preservation of a hopane biomarker in sediments. I: A lipid synthesized by a cyanobacteria can be preserved and buried, losing its functional groups but retaining its characteristic skeleton. II: As time and temperature increase after deposition, the preserved geolipids undergo reactions that result in more thermally dynamic structures. The relative amounts of these different structures can indicate degree of thermal maturity.

For studies of the early Earth, a biomarker can serve as a record that a particular metabolism was active at a particular time in a specific environment. For example, Summons *et al.* (1999) identified high abundances of 2α-methylhopane in the 2.5 Ma Mt. McRae Formation of the Hamersley Basin in Western Australia. They showed that the presence and abundance of this molecule indicated the presence of cyanobacteria performing oxidative photosynthesis. Similarly, Brocks *et al.* (1999) identified steranes, thought to evolve from the sterols produced by eukaryotes, in the Mt. McRae Formation and in the 2.7 Ma Jeerinah Formation from the same sedimentary succession. This work showed that eukaryotes, more complex than Bacteria and most Archaea, were present much earlier than originally thought. These studies were unique not only for their findings but also because they described detailed methods establishing that the biomarkers preserved in the shales were indigenous to their host rocks.

1.2: Testing Glacial Hypotheses

Recently, Precambrian biomarker studies have been aimed at geological transitions, including tests of specific climate-related hypotheses. Olcott *et al.* (2005) used biomarkers extracted from organic-rich, synglacial shale from Brazil to test end-member, biological predictions of the "snowball Earth" hypothesis — that continental glaciers and thick sea-ice covered the planet for millions of years at least once during the Neoproterozoic (1000–543 Ma; Plumb, 1991; Bowring *et al.*, 1993).

The Olcott *et al.* (2005) study used samples from the Serra do Poço Verde Formation (hereafter called the Poço Verde Formation) that lies unconformably

beneath the Lapa Formation, the focus of this study. Notably, new Re-Os age dates from the Poço Verde Formation suggest the Vazante Group, which includes both formations, is Mesoproterozoic, rather than Neoproterozoic, in age (Geboy *et al.*, 2006), as earlier assumed by Azmy *et al.* (2001, 2006).

1.2.1: Low-latitude glaciation

Unique to the Neoproterozoic is a worldwide distribution (Hambrey and Harland, 1981; Evans, 2000) of marine diamictites (poorly sorted debris flow and mass wasting deposits) topped by enigmatic dolomites and limestones (thereafter known as "cap carbonates"), strata hosting unique textures and strong negative excursions in carbon isotopic compositions (Kaufman *et al.*, 1991; Kirschvink, 1992; Grotzinger and Knoll, 1995; Kennedy, 1996; Kaufman *et al.*, 1997; Hoffman *et al*., 1998; Schrag, 2002). In some places, the diamictites are associated with sedimentary iron deposits (Hoffman and Schrag, 2002).

Harland (1964) proposed that these unique deposits were glacial in origin and that their global distribution suggested a worldwide ice age in Earth's distant past. After data confirmed that late Neoproterozoic glacial diamictite of the Elantina Formation of Southern Australia was deposited close to the equator (Hoffman and Schrag, 2002), Kirschvink (1992) postulated that an unusual concentration of land masses at middle and tropical latitudes at that time would result in high albedo in the subtropics, increase the silicate weathering rate and thus the CO_2 sink, and thereby weaken heat transport by Hadley cells. The result would be large ice caps and enough ice cover to start a runaway ice-albedo effect (Erikkson, 1968; *cf.* Hoffman and

Schrag, 2002) with thick pack-ice covering tropical oceans (a "snowball Earth"; Kirschvink, 1992).

Using high-resolution sequence stratigraphy, carbonate carbon isotope and paleomagnetic data from the Congo craton in Namibia, Hoffman and co-authors (1998) revived the "snowball Earth" hypothesis, offering a model of at least one snowball Earth event lasting millions of years and followed by extreme greenhouse conditions during which cap carbonates were deposited rapidly due to extreme carbonate alkalinity in the glacial aftermath.

1.2.2: Testing biological postulates

The snowball Earth hypothesis predicts the virtual shutdown of surface processes due to high albedo and extreme cold. According to this hypothesis only the long-term buildup of volcanic CO_2 in the atmosphere would have ended the ice age. The CO_2 dissolved in torrential acid rain would have reacted with continental sediments, which were ground to powder by the overlying ice sheets. This extreme weathering delivered carbonate alkalinity to the oceans, resulting in widespread deposition of the texturally and isotopically enigmatic cap carbonates (Kaufman *et al.*, 1991; Kennedy, 2001; Kaufman *et al.*, 1997; Hoffman *et al.*, 1998; Hoffman and Schrag, 2002). Given the long-term buildup of nutrients in seawater and inputs from accumulated weathering, primary producers in the shallow marine environment engaged in oxidative photosynthesis would do well and the oxygen they produce would potentially accumulate.

Since the revival of this hypothesis in 1998, much debate has centered on the number, extent and extremity of all Neoproterozoic glaciations, and on the processes that would have taken Earth into and out of the extreme climate events. At present, all of the competing hypotheses for the geological and geochemical anomalies invoke changes in the carbon and, in some places, sulfur cycles, along with related changes in the oxidation of Earth's oceans and atmosphere. These hypotheses are largely based on explanations for the extreme carbon and sulfur isotope excursions recorded in carbonates deposited at the onset and the aftermath of the ice ages.

Many workers hypothesize that biological regulation of greenhouse gases (i.e. CO_2 and CH_4) at a time of lower solar luminosity initiated the Neoproterozoic ice ages (Kaufman *et al.*, 1997; Hoffman *et al.*, 1998; Schrag *et al.*, 2002; Pavlov *et al.*, 2003). Biomarker and paleontologic studies of organic-rich pre-glacial shale and carbonate could help to elucidate the sources of these gases by identifying the suite of microorganisms responsible for their buildup. Similar analysis of like lithologies deposited during post-glacial transgression should also explain whether the anomalous accumulations of unusually textured cap carbonates are: 1) the result of silicate weathering under a 10% CO_2 atmosphere (Hoffman *et al.*, 1998; Hoffman and Schrag, 2002), 2) a catastrophic methane release from permafrost and methane cold seeps (Kennedy *et al.*, 2001; Jacobsen, 2001), or 3) ice age bacterial sulfate reduction in the water column similar to the present day Black Sea (Gorjan *et al.*, 2000) coupled with extreme rates of primary productivity in the aftermath (Kaufman *et al.*, in preparation). All three scenarios can affect biological systems. A runaway greenhouse effect in which CO_2 is abundant could boost photosynthesis and primary productivity.

A sudden methane release could affect populations of sulfate reducing bacteria and in some periods of Earth history and some hypotheses suggest such methane "burps" are related to mass extinctions such as the end-Permian extinction (Dickens, 2004).

Another corollary of the snowball Earth hypothesis is that glacier-covered oceans were largely devoid of oxygen. The reappearance of iron-formations is often cited as evidence of such anoxia (Kaufman *et al.*, 1991; 1997; Hoffman *et al.*, 1998; Hoffman and Schrag, 2002). The biogeochemical carbon isotope anomalies associated with such events suggest that a glacier-covered ocean significantly decreased eukaryotic and prokaryotic diversity (Hoffman and Schrag, 2002). To test this end-member version of Neoproterozoic climate change, Olcott *et al.* (2005) investigated the syn-glacial shale of the Vazante Group in south-central Brazil. They identified 2α-methylhopanes within the Poço Verde Formation. Accepting that the diamictites represented the remains of a Sturtian (ca. 700-750 Ma) snowball Earth event, they maintained that the variety of biomarkers they identified in the shale is evidence that photosynthesis, as well as a diverse suite of other metabolic processes, was not attenuated during this ice age (Olcott *et al.*, 2005).

This study of the overlying Lapa Formation in the Vazante Group was also originally carried out to test biological corollaries of the snowball Earth hypothesis directly through the structural and isotopic identification of biomarkers in post-glacial shale and carbonate samples. Biomarkers indicating a diverse suite of life forms immediately after a glaciation would suggest that the end member corollary of the snowball Earth hypothesis is not robust. For this study, much of the Vazante Group is interpreted as glaciogenic. Based on stratigraphic, lithologic, and isotopic

observations, the Lapa Formation is interpreted as having accumulated in the immediate aftermath of a glaciation. The presence of the organic-rich shale at the base of this unit suggests enhanced primary productivity during post-glacial transgression. The presence and potential diversity of biomarkers in extracts of these organic-rich sediments provides clues about the diversity of the microbial community that thrived in the transition between extreme climate states.

1.3 Geologic Setting

The Vazante Group in the northwestern part of Minas Gerais state in Brazil (Fig. 1.2) hosts one of the world's most important carbonate-hosted non-sulfide zinc deposits (Vazante) and sulfide zinc deposits (Morro Agudo). Samples for this study were taken from unmineralized exploration drill cores of the Companhia Mineira de Metais from near Paracatú, Minas Gerais, Brazil, specifically from the Morro Agudo mine.

The focus of this study is the Serra da Lapa Formation (hereafter called the Lapa Formation), a marine and mostly siliciclastic unit that unconformably overlies the carbonate- and diamictite-dominated lower formations of the Vazante Group. These are part of the Meso- to Neoproterozoic sediments that overlie the Archean-Paleoproterozoic São Francisco craton.

The borders of the São Francisco craton are defined by three fold belts (Teixeira et al., 2000; Martins-Neto, 2001). Bordering the craton on the west is the Brasília Fold Belt, which likely formed about 600 Ma during closure of an oceanic basin during the Brasíliano orogeny (Pimentel *et al.*, 2001).

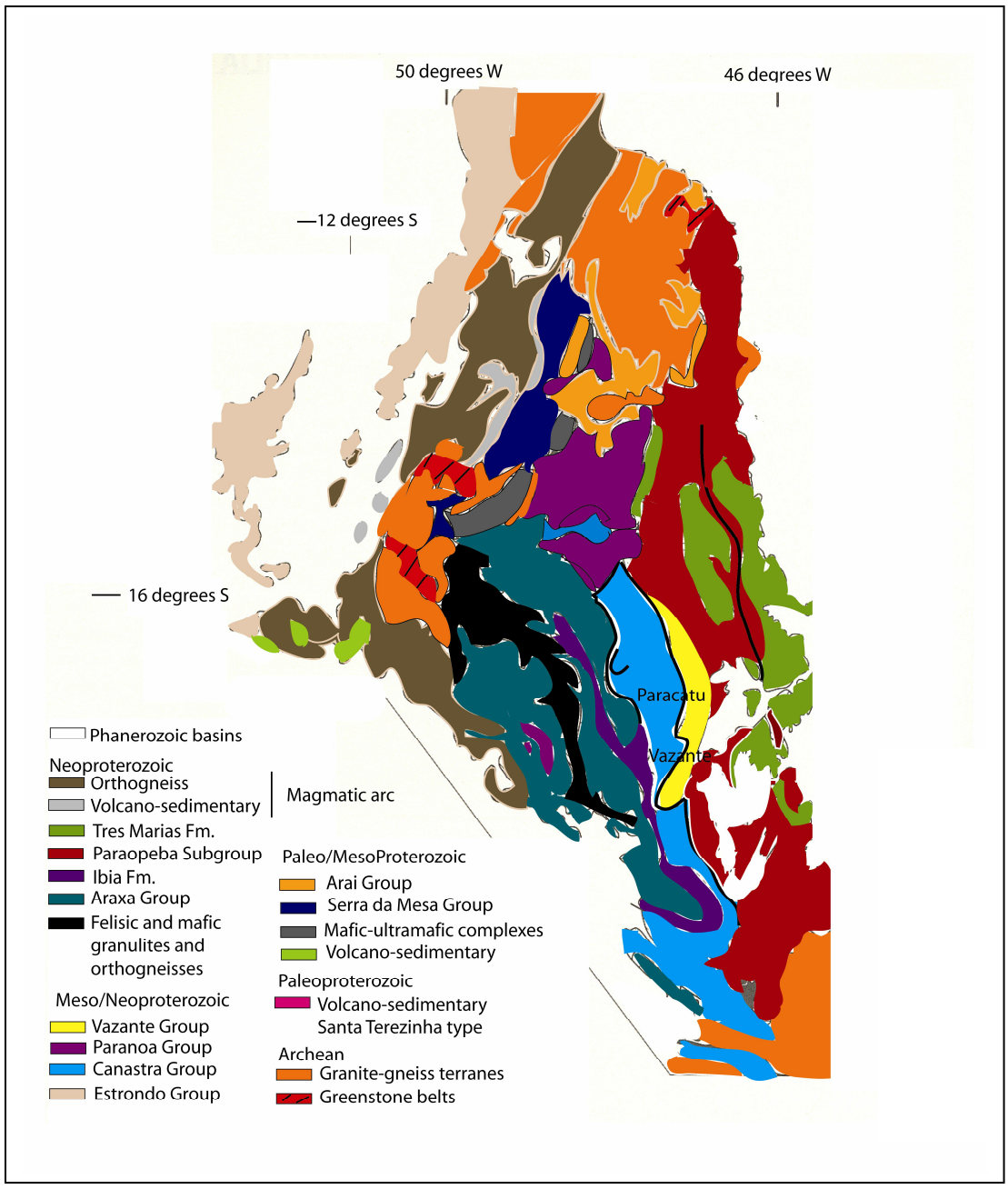

Figure 1.2: Map of the Vazante Formation and surrounding formations that constitute the Brasília Fold Belt. The Vazante Group sits atop the Archean-Paleoproterozoic São Francisco craton in central eastern Brazil. The Vazante likely experienced low-grade, possibly greenschist, metamorphism. This map is modified from Dardenne (2000).

Trending north-south for ~250 km, the Vazante Group is one of the outlying metasedimentary units of the Brasília Fold Belt (Babinksi *et al.*, 2005; Dardenne, 2000). The Vazante Group likely experienced sub-greenschist grade metamorphism (Moraes, pers. comm., 2005; Babinski *et al.*, 2005, Rostirolla, *et al.*, 2001); while innermost groups of the fold belt experienced amphibolite- to granulite-grade metamorphism (Fuck *et al.*, 1994).

The Lapa Formation is the uppermost of the seven Vazante Group formations (Fig. 1.3). Dardenne (2000) describes the Lapa succession as hosting carbonaceous phyllite, carbonate-bearing metasiltstone, dolomite lenses and quartzite layers. Azmy *et al*. (2006) additionally described the Lapa Formation as hosting rhythmically laminated argillaceous dolomites with shales in the uppermost reaches of the unit. The cores sampled for this study host organic-rich shale at the base of the Lapa Formation, transitioning to laminated dolomite and dolomitic marl upsection.

1.3.1: Age of the Lapa Formation

Radiometric age dates for the Lapa Formation are presently unavailable. A number of geochronological studies have focused on the Vazante Group in general, but these studies reach varying conclusions on the age of the succession.

Cloud and Dardenne (1973) were the first to assign the Vazante Group to the Proterozoic. Based primarily on the presence of *Conophyton metula Kirichenko* in the Lagamar Formation — one of the lowest in the Vazante Group — they suggested an age of between 1350 and 950 Ma for the lower Vazante Group. A shale Rb-Sr whole-rock isochron yielded an age for the Vazante Group of 600 ± 50 Ma, but this likely

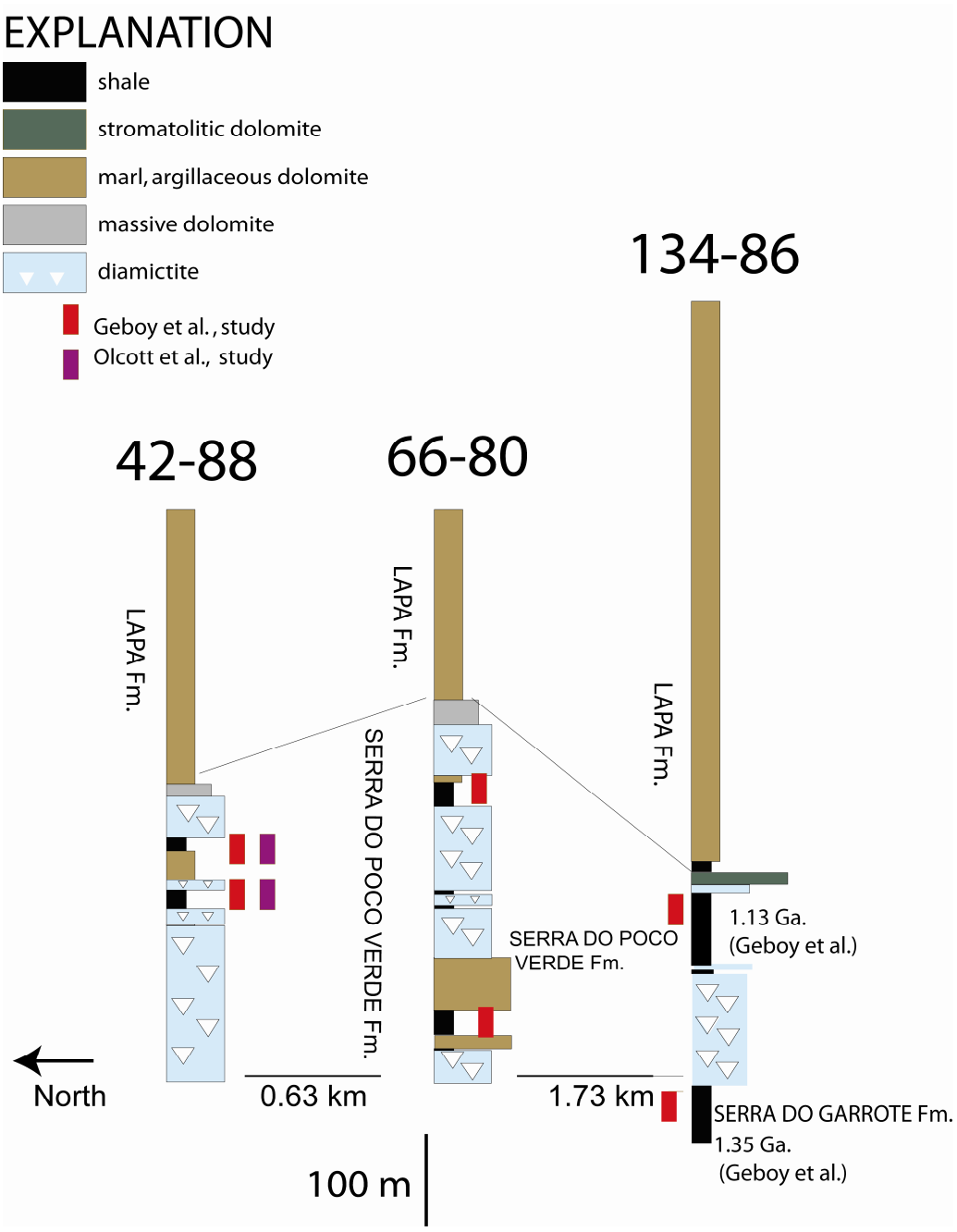

Figure 1.3: Stratigraphic columns of the three cores sampled, based on observations and core log data from the Vazante mine. Core MAF 134-86 was sampled continuously in order to obtain time-series carbonate isotope data and to conduct organic analyses of the organic shale horizons that occur within the carbonate and diamictite intervals. Cores MAF 42-88 and MAF 66-80 were sampled from the organic shale intervals. The Lapa Fm. lies unconformably above the Serra do Poço Verde Fm.

represents resetting of the isotopic system during the Brasíliano orogeny (*cf.* Babinski *et al.*, 2005). Lead model ages from galenas from different locations with the Vazante and Morro Agudo deposits suggest ages ranging from 930 to 600 Ma, but these have been considered as times of mineralization or remobilization (Babinsksi *et al.*, 2005).

Azmy *et al.* (2001) used strontium, carbon and sulfur isotopic variations in the Vazante sediments to suggest that the succession was older than 600 Ma. More recently, Azmy *et al*., (2006) focused on the Lapa Formation, and based on the regional recognition of a moderate negative carbon isotope excursion above basal shale and a single strontium isotope measurement (ca. 0.7068) correlate the Lapa Formation with the Sturtian (ca. 740 Ma) Rasthof Formation in Namibia (Hoffman *et al.*, 1998).

Geboy *et al.* (2006) used the Re-Os isotope system to assign ages to the Serra do Garrote and Serra do Poço Verde shales of the Vazante Group. Unfortunately, the Lapa Formation had the lowest concentrations of rhenium and osmium of the Vazante Group samples studied, and did not generate a precise isochron (Geboy *et al.*, 2006). On the other hand, shale in the Serra do Garrote Formation yielded an age of 1,353 ± 69 Ma and a similar shale in the Serra do Poço Verde at 1063 ± 190 Ma. Based on core log data, the Lapa Formation is shown to sit unconformably above the truncated Moro do Calcario Formation; in some cores Lapa strata lie directly on shale of the underlying Serra do Poço Verde Formation. Thus, the Lapa Formation is younger than 1.1 Ga, but how much younger is as yet undetermined.

The Vazante Group sediments are believed to have been deposited in a passive margin setting (Fuck et al., 1994) or in a foreland basin during the beginning

of the Brasíliano orogeny (Dardenne, 2000). Based on the new Re-Os ages, Geboy *et al*. (2006) suggest that deposition along a passive margin is a more likely model than active-margin deposition during the orogeny, which is thought to have occurred much later.

1.3.2: Paleolatitude of the Lapa Formation

The Saõ Francisco craton is conjugate to the Congo craton in Namibia, where data from the broadly equivalent Otavi Group was used to revive the snowball Earth hypothesis (Hoffman *et al.*, 1998). These cratons were joined during the 1200–500 Ma period in which the Rodinia supercontinent was assembled, fragmented, and then re-assembled as Gondwana during the Brasíliano orogeny (Tohver *et al.*, 2006).

In a reassessment of existing paleomagnetic data from Africa and new data from South America for this time period, Tohver *et al.* (2006) suggest that at about one billion years ago, the São Francisco-Congo cratons were likely at ~40º latitude. By about 600 Ma, the conjoined cratons had moved close to the equator.

If the Lapa Formation is a Neoproterozoic deposit, it may indeed have been located at the equator during this time, adding it to the list of snowball Earth successions recording tropical and equatorial glaciations. If the Lapa is a late Mesoproterozoic deposit, it may have been further south but would still have been at low-latitudes. Schrag *et al.* (2002) cite energy-balance models suggesting that a runaway ice albedo effect can occur when ice cover reaches critical latitudes (as low as 40º).

1.3.3: The Lapa Formation as a postglacial succession

Observations from core PMA04 suggest a depositional pattern in the upper Vazante Group (Fig. 1.4; Brody *et al.*, 2004) similar to those of other identified glacial transitions (Hoffman *et al.*, 1998; Hoffman and Schrag, 2002, Kaufman *et al.*, 1997). This includes the upsection transition from 1) glacial diamictite with dropstones (ice rafted debris) in the upper Poço Verde Formation, 2) sedimentary iron-formation (Derry *et al.*, 1992; Klein and Beukes, 1993; Kennedy, 1996); 3) a regional unconformity encompassing 10s to 100s of meters of section (de Oliveira, pers. comm., 2004; Misi *et al.*, 2005); 4) deep-water shale representing maximum post-glacial flooding; and 5) dolomite and marl. Based on lithologic observations of the Lapa Formation and on carbonate carbon isotopes in several cores, Azmy *et al.* (2006) similarly defined the basal part of the succession as a cap carbonate lithofacies.

1.3.4: Mineralization in the Vazante Group

The Vazante Group hosts one of the world's largest zinc deposits. It is largely classified as a hypogene nonsulfide zinc deposit (Babinski *et al.*, 2005; Hitzman, 2003), which is relatively rare. Notably, similar mineralization is found in the late Mesoproterozoic Franklin Mine of northern New Jersey, USA. Sulfide mineralization is also reported in the Vazante Group, and is the principle ore of the Morro Agudo mine close to where the cores from this study were drilled. The Vazante deposit is structurally confined and likely formed from the mixing of fluids of differing temperatures and chemical compositions (Hitzman, 2003). The dominant

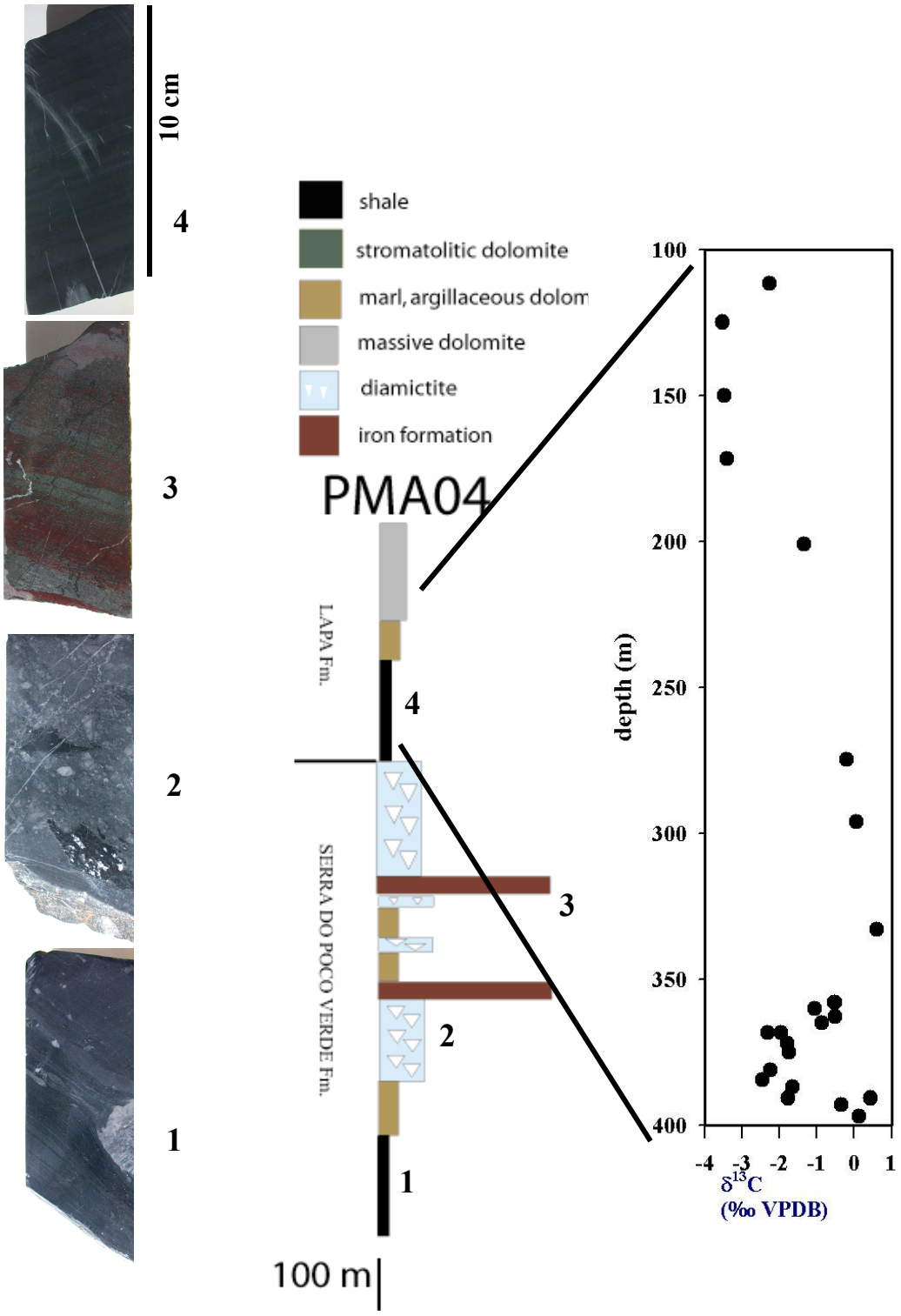

Figure 1.4: Lithologic and carbonate carbon isotopic observations similar to cap carbonate lithofacies. Middle: a stratigraphic column of core PMA4 based on observations and core log data from the Vazante mine. The column is pictured with photos (left) of selected samples from the core and with carbonate isotope data (right) reported by Azmy *et al.* (2006). The progression from 1) shale with dropstone to 2) breccia to 3) possible iron formation and then into 4) shale is consistent with observations of other facies determined to be post-glacial cap carbonate.

ore mineral in the Vazante mines is willemite (Babinski *et al.*, 2005; Hitzman, 2003), a characteristic of these types of zinc deposits (Candela, pers. comm., 2006). Deposits dominated by willemite tend to only form from relatively low-temperature fluids. Fluid inclusion studies suggest temperatures of mineralization in the Vazante ore deposit ranged from 65 to 150^{o}C (Hitzman, 2003). The Morro Agudo may be an Irish-type deposit (Monteiro *et al.*, 2006), with temperatures reaching 240^{o}C (Hitzman, 1996).

Chapter 2: Organic Matter in the Geological Record

2.1:Biomarkers: A Brief History

The modern study of biomarkers has its roots in petroleum geochemistry. As early as 1931, the American Chemical Society recognized the need for fundamental research into the organic molecules that characterize petroleum, and started the Petroleum Research Fund for basic research and education. By then, it was long recognized that petroleum was derived from the maturation of bulk organic matter deposited in sedimentary basins. But, in 1934, Alfred Treibs identified porphyrins in crude oil and showed that these molecular fossils were derivatives of chlorophyll from plants (*cf*. Hunt, 2002). A connection between the products of biological metabolism and geologically re-arranged organic molecules is the basis of biomarker research, and this study.

Early efforts in petroleum chemistry were aimed at developing methods for separating the various components of petroleum. Central to this goal were the techniques of gas chromatography and mass spectrometry, which allowed researchers to isolate components with high resolution into individual classes and molecules. With improvements in instrumentation and techniques, it became possible to characterize hydrocarbons from smaller and smaller quantities of ancient sediments. The primary focus of these studies is on source rocks, in which trace oil or bitumen (organic matter soluble in organic solvents such as dichloromethane) is indigenous to, rather than migrated into, the sediments (Hunt, 2002). As a result, the hydrocarbons in the source rocks likely derived from organic matter deposited at the same time as

the surrounding sediments, and thus may reflect dominant biological metabolisms in the environment of deposition.

Based on work by petroleum chemists to use biomarker suites as fingerprints that can track oil migration and identify source rocks, Abelson in 1954 (Hunt, 2002) suggested that "Precambrian fossil biochemicals" could yield clues about early life (*cf.* Brocks et al., 2003a). In 1964, Eglinton et al. identified simple alkanes, specifically phytane and pristane (see Table 2.1), in oil seeping from the Precambrian (~1 Ga) Nonesuch Formation in Michigan. They wrote that these hydrocarbons "show promise as biological markers since they are evidently stable for long periods of time under geologic conditions."

Even with early success, researchers recognized that both modern and ancient contaminants complicate any interpretation of these molecular fossils as indigenous to the host sediments. Many of these compounds may have been introduced by fluids that flowed through the rocks after deposition, or by crude sampling techniques. To avoid these obvious problems, geochemists have developed methods to test for both thermal maturity and secondary contamination (*cf.* Brocks et al., 2003a), in order to more clearly interpret biological signals of early life (for example, see Brocks *et al.*, 1999 and Summons *et al.*, 1999).

2.2: Preservation of Organic Matter

The processes that preserve biomarkers in sedimentary rocks are the same that preserve large oil and gas accumulations. Through burial and lithification, the preserved organic matter has escaped the short-term carbon cycle, which would have

Table 2.1: A basic overview of the organic molecules analyzed in this study. Pictures are example molecules. Many families have several structural variations. Molecules are shown as skeletal structures (see Discussion for detailed explanations and interpretations.

HOPANES

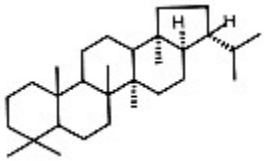

17α(H),21β(H)-Hopane

Likely precursor molecule(s): C_{35} tetrahydroxybacteriohopane (see Fig. 1.1)
Common biosynthetic pathway: by cyanobacteria (many types)
Clues for depositional environment: presence of photosynthesis and/or other processes performed by other types of cyanobacteria
Clues for thermal history: isomerization reaches equilibrium during early oil generation

STERANES

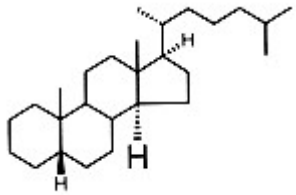

20R5β(H),14α(H),17α(H)-Cholestane

Likely precursor molecule(s): sterols
Common biosynthetic pathway: by eukaryotes, requiring oxygen
Clues for depositional environment: presence of oxygen, presence of complexity in life forms. Diasterane abundances are affected by clay content.
Clues for thermal history: isomerization equilibrium can extend well into oil generation

NORMAL ALKANES

n-Pentadecane

Likely precursor molecule(s): various
Common biosynthetic pathway: n/a
Clues for depositional environment: dominance of alkanes having either an odd or even number of carbons within an alkane family varies with organic source
Clues for thermal history: even- or odd-numbered dominance lost over time, with thermal

Table 2.1 (cont)

ISOPRENOIDS

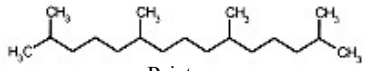

Pristane

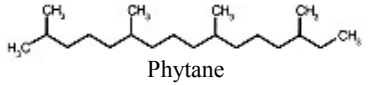

Phytane

Likely precursor molecule(s): various; pristane and phytane derive from the phytol side chain of chlorophyll.
Common biosynthetic pathway: Can indicate bacterial activity.
Clues for depositional environment: A pristane/phytane ratio above 1 is most likely in an oxidizing environment.
Clues for thermal history: the pristane/phytane ratio is also affected by thermal

NAPHTHALENES

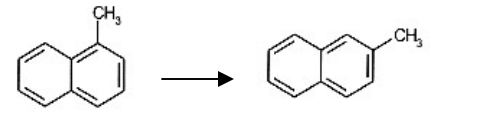

1-Methylnaphthalene 2-Methylnaphthalene

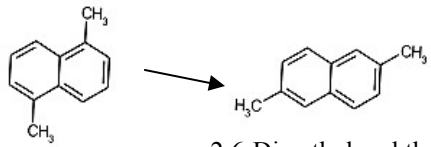

1,5-Dimethylnaphthalene 2,6-Dimethylnaphthalene

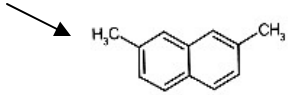

2,7-Dimethylnaphthalene

Likely precursor molecule(s): unknown
Common biosynthetic pathway: n/a
Clues for depositional environment: n/a
Clues for thermal history: Increases in the relative amounts of 2-Methylnaphthalene to 1-Methylnaphthalene, and of [2,6-Dimethylnaphthalene + 2,7-Dimethylnaphthalene] to 1,5-Dimethylnaphthalene, have been shown to correlate with increasing thermal maturity.

transformed it into CO_2, methane or the food or substrate for another organism. In biomarker studies of the early Earth, the volumes of preserved and/or remaining insoluble organic material (i.e., kerogen) in samples is extremely small, particularly for soluble organic constituents (i.e., bitumen).

Photosynthesis is the engine for mass production of organic matter, and aquatic sediments are the primary environments of preservation (Tissot and Welte, 1984). During the Archean and most of the Proterozoic eons, the main contributors of organic matter in sediments were autotrophic bacteria. In contrast, modern sediments host organic matter also synthesized not only by photosynthetic bacteria, but also by phytoplankton, zooplankton, and higher plants (Tissot and Welte, 1984).

For organic matter to be preserved in aquatic environments, primary productivity, water depth, rate of deposition, oxygen content and other factors must reach an equilibrium that allows a significant amount of organic matter to escape the short-term carbon cycle and to be buried. Fine-grained detrital sediments containing at least 0.5% organic matter and carbonates or evaporites containing at least 0.3% organic matter are good candidates for becoming petroleum source rocks (Tissot and Welte, 1984). Both transgressions and regressions of sea level can be favorable conditions for preserving organic matter (Tissot and Welte, 1984). Favorable environments include continental slopes, areas just beyond continental slopes, and deep, restricted basins (Tissot and Welte, 1984). In modern sediments, open ocean sediments tend to host much less organic carbon (< 2.5 mgC/g) than do coastal or continental margin sediments (200 mgC/g and greater), which tend to underlie anoxic bottom waters and sit in regions of coastal upwelling (Burdige, 2007).

The energy level in the water column must be high enough to supply ample sediment for deposition, but not too high that erosion wins out or grain size is too large for adsorption of organic matter. An inverse relationship between grain size and amount of organic matter has been observed because smaller particles have better adsorption capacities (Tissot and Welte, 1984).

Preserved organic matter can be autochthonous or allochthonous (local or transported, respectively), dissolved or particulate. Preservation is more likely where primary productivity is high, although anoxia in the water and sediment columns is a more powerful preservation factor (Peters and Moldowan, 1993; see Pederson and Calvert, 1990, for a different view). The presence of oxygen promotes oxidation of organic matter to CO_2 and the relatively more efficient aerobic use of organic matter by heterotrophs. The most ideal preservation scenario is high sedimentation rate (Derry *et al.*, 1992; Kaufman *et al.*, 1993) and high productivity, rapid deposition of organic matter, and low oxygen (Tissot and Welte, 1984).

High concentrations of organic matter in marine environments enhance rates of bacterial sulfate reduction because an adequate supply of organic carbon escapes oxidation, falls into sediments and is available to fermentative bacteria and sulfate reducers — in turn enhancing the production of H_2S and facilitating the combination of detrital, reactive iron with sulfide to form pyrite a the sediment-water interface.

The lipids that will become biomarkers are insoluble in water, increasing their chances of preservation. These molecules tend to be deposited with particulate organic matter (Tissot and Welte, 1984). Over time, most of the extractable organic matter is incorporated into the kerogen, enhancing its overall preservation potential

(Hayes, 1983). At the same time, the biomarkers tend to occur in very low concentrations and are very mobile. As a result, establishing that the biomarkers were deposited at the same time as the host rock, rather than migrated from elsewhere, is a primary consideration for Precambrian studies (Hayes, 1983; Summons et al., 1999; Brocks *et al.*, 2003).

Once buried, microbes in the sediment continue to rework organic matter as a carbon source for biosynthesis and energy (Tissot and Welte, 1984). Even after the organic matter is fossilized, modern bacteria can again rework it (Petsch *et al.*, 2005). The small portion of organic matter that is not recycled is preserved in sedimentary rock and becomes part of the long-term carbon cycle.

Studies of modern, subsurface petroleum reservoirs, as well as kinetic models of oil degradation, suggest that high-molecular weight hydrocarbons (15 or more carbon atoms) can survive under post-burial temperatures as high as 250º C (Brocks *et al.*, 2003 and references therein).

2.3: Kerogen and Bitumen

Kerogen is the organic portion of a sedimentary rock that is neither soluble in alkaline nor organic solvents (Tissot and Welte, 1984). Much of the preserved particulate organic matter is stored in kerogen, which also over time hosts degradation products of organic matter. Kerogen is bound with the host rock, promoting preservation of organic material. Bitumen, also termed extractable organic matter (Tissot and Welte, 1984), is dispersed within fine-grained sedimentary rocks (Peters and Moldowan, 1993) or within kerogen and is extractable with organic

solvents. Biomarkers exist free in bitumen and bound in kerogen, and also travel with migrating oils (Peters and Moldowan, 1993).

2.4: Stereochemistry and Isomerization

Biosynthesis imparts a specific structure to a molecule. In bonding with other molecules, the carbon atom can form single, covalent bonds in which one electron is shared, or double and triple bonds involving two or three electrons at a bonding site. When a carbon atom is surrounded by four single bonds, it is very stable and said to be saturated. It joins with the other molecules in a tetrahedron with one carbon atom at the center. When the four molecules connected to the central carbon atom vary in size, the tetrahedron achieves an asymmetry or, more specifically, chirality. Transposing any of the two molecules bonded to the central carbon can create a mirror image of the tetrahedron. Depending on the makeup of the rest of the organic molecule, changes in this stereochemistry result in molecules that, while they have the same molecular formula, differ in structure and behavior.

The biosynthesis of a hopane precursor lipid (see Fig. 1.1) and a sterane precursor sterol imparts a specific chirality to the saturated carbon bonds. In a hopane precursor, the carbon at position 22 has the right-handed, or R, configuration, as does the carbon at position 20 in a sterol. During thermal maturation, the molecule undergoes reactions that give it a more thermally stable overall structure, and the carbon at position 22 in a hopane and 20 in a sterane tends to invert to the S configuration. A similar process takes place in hopanes at positions 14 and 17, which are on rings (see illustrations in Table 2.1). Here, reactions leave hydrogen molecules

attached either above the plane of the molecule (β; shown by a closed circle in Fig. 1.1)) or below it (α, shown by an open circle). Biosynthesis results in sterols having the 14(α),17(α),20R configuration. Over time, molecules react to more thermally stable configurations, and reach an equilibrium ratio of 14(α),17(α),20(S) : αα20R : ββ20R : ββ20S of 1:1:3:3. In hopanes, the biological structure has carbon atoms at positions 17 and 21 with β configurations. Over time, they assume the more thermally stable 17(α), 21(β) structure.

The end results of these primary and diagenetic processes are steranes (Mackenzie *et al.*, 1980) and hopanes with varying mixtures of isomers. For the S and R isomers, the relative amounts reach equilibrium at 1:1 at various points during thermal maturation. The different isomers can be distinguished using a gas chromatograph-mass spectrometer (GCMS, see Chapter 3). As a result, it is possible to calculate the relative abundances of hopane and sterane isomers as an important tool for determining the thermal history of the molecules and sediments.

2.5 Carbon and Sulfur Isotopes

Two of the most important biological processes throughout Earth history are photosynthesis and bacterial sulfate reduction. Primary producers use sunlight (photosynthesis) or chemical energy to synthesize organic carbon, converting carbon in its oxidized form, mainly CO_2, into organic carbon, a more reduced form. The main photosynthesis process is the Calvin cycle. An overall equation for photosynthesis is:

$$6CO_2 + 12H_2O \longrightarrow C_6H_{12}O_6 + 6O_2 + 6H_2O$$

The fixation of CO_2 is mediated primarily by the enzyme Rubisco, or ribulose-1,5-bisphosphate carboxylase/oxygenase, which imparts a significant isotopic fractionation on carbon (up to 27‰, Hayes *et al.*, 1992), by selecting the lighter ^{12}C isotope and leaving the heavier ^{13}C isotope behind. As a result, the isotopic composition of both carbonate carbon and organic carbon preserved in sedimentary rocks can be used to understand whether photosynthesis was significant in the depositional environment. The main primary producers during the Archean and Precambrian are thought to be cyanobacteria, a large family of extant Bacteria conducting a variety of metabolisms, the Calvin cycle being the most common. It is thought that a hopane having an extra CH_3 group attached to its first ring in the α position (see Table 2.1) is a molecular fossil for photosynthesizing cyanobacteria (Summons *et al.*, 1999).

Secondary producers or heterotrophs in turn use the organic carbon synthesized by primary producers, and one of the most important families of these microorganisms are sulfate reducing bacteria (several studies suggest that sulfate reduction was in fact one of the first metabolisms on Earth). The organisms conducting sulfate reduction are diverse and occupy positions on both the Archaea and Bacteria limbs of the biological tree of life. Sulfate reduction is either dissimilatory because it uses organic carbon as an electron donor (oxidizing it) and sulfate as an electron acceptor (reducing it), or assimilatory, using the organic carbon and sulfate for cell synthesis.

$$2CH_2O + SO_4^{2-} \longrightarrow H_2S + 2HCO_3^-$$

Assimilatory reduction is more common, but dissimilatory reduction has a larger effect on the sulfur cycle (Widdel and Hansen, 1992). The process also imposes large isotopic fractionations (although fractionations can vary depending on sulfate concentrations, Habicht *et al.*, 2002), making the isotopic compositions of preserved sulfate and sulfide (often preserved as pyrite) excellent tools for understanding the organic sulfur cycle through time.

Recent studies have proposed hypotheses about Archean and Proterozoic ocean and atmospheric chemistry based on sulfur isotopic compositions resulting from photolytic and biologic fractionations in both the major isotope (^{34}S) and minor isotope (^{33}S and ^{36}S) systems. This study analyzes the major and minor fractionations recorded in sulfide preserved as disseminated pyrite in the Lapa samples to help understand changing depositional environments of the postglacial Lapa Formation.

Chapter 3: Methods

3.1: Sampling Strategy

With guidance from Tolentio Flavio de Oliveira — then the chief geologist of the Vazante mine of Companhia Mineira de Metais, Votorantim Metais, Minas Gerais, Brazil — samples for this study were taken from four unmineralized exploration drill cores located within kilometers of each other (see Fig. 3.1). Core MAF 134-86 was sampled continuously to conduct time-series isotopic analyses of the diamictite, siliciclastic and dolomite facies as well as biomarker analyses of organic shale. The organic shale portions of cores MAF 42-88 and MAF 66-80 were also sampled for biomarker analyses. These intervals were relatively thick for the Serra do Poço Verde Formation, but only one or two samples of organic-rich shale were collected from the Lapa Formation in these cores for this study.

3.2: Time-series Analyses

3.2.1: Percent carbonate

To determine percent carbonate carbon by weight, bulk powdered sample was accurately weighed and carbonate carbon eliminated by reaction with concentrated 12M HCl until no reaction was observed. The samples were centrifuged and decanted and then reacidified to assure quantitative removal of carbonate. Samples were then rinsed with MilliQ water, centrifuged and decanted multiple times. After samples

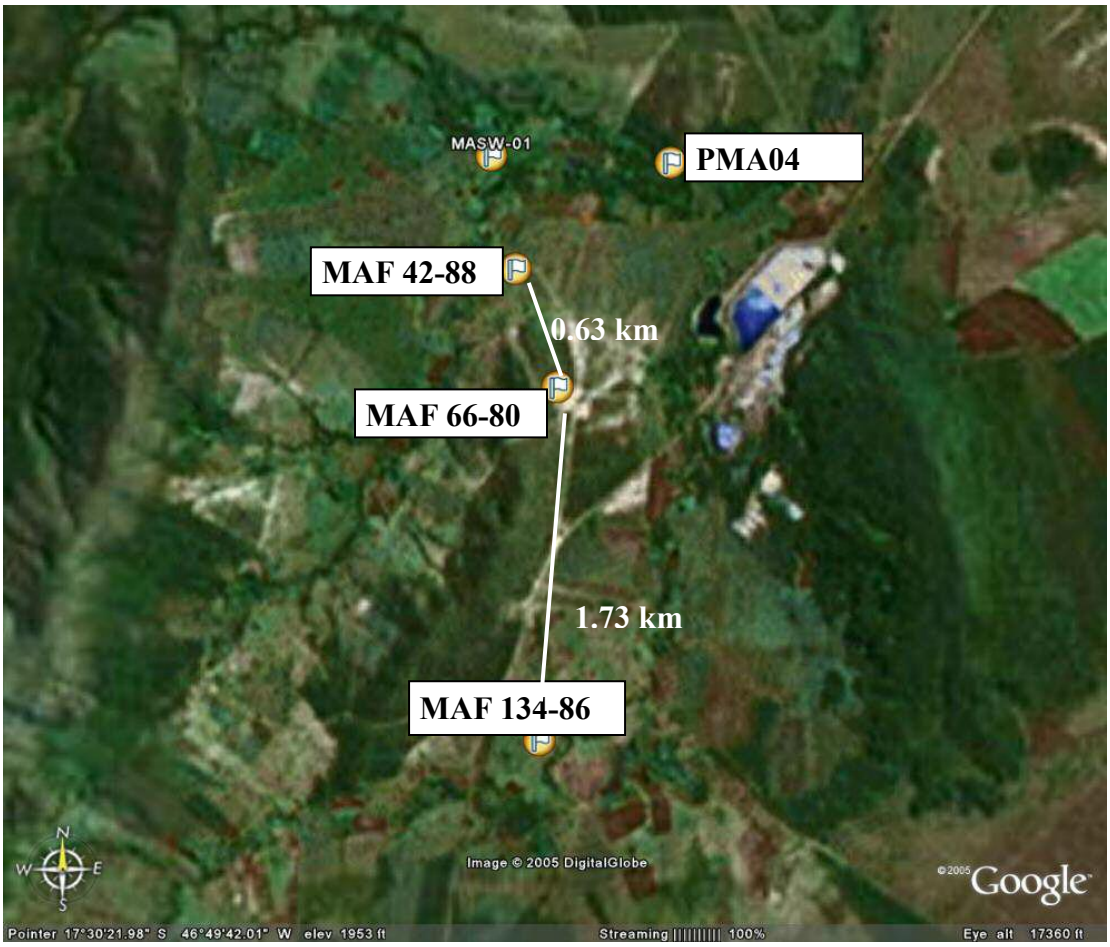

Figure 3.1: The relative locations of and distances between the four cores sampled for this study. The Google Earth map was assembled using GPS coordinates.

were dry, they were weighed again and the weight difference used to determine percent carbonate.

3.2.2: Total organic carbon

Total organic carbon (TOC) was determined by Dumas combustion of the organic carbon into CO_2 and then quantification of the gas volume with a cryogenic distillation line. Bulk rock powder was accurately weighed and the carbonate removed using 12M HCl (see above). Between ~30 and ~130 mg of rock powder (depending on color) was combined with 1 g cupric oxide and sealed under vacuum in annealed Vycor tubing. The powder/cupric oxide mixture was combusted at 850^{o}C for two hours, and the carbon oxidized to CO_2 while the cupric oxide reduced to elemental copper. The samples were cooled, attached to the distillation line, and the sealed tubes cracked to expand the gas through a water trap of ethanol/dry ice slurry to capture any non-CO_2 gases and then through a liquid nitrogen trap to capture CO_2. The CO_2 was warmed and its internal pressure shown on a Baratron readout. This pressure is converted to μmols using a calibration curve and then TOC abundances calculated and reported as wt. percent carbon.

3.2.3: Percent sulfide

Finely disseminated pyrite and bedding parallel accumulations of pyrite, as well as some secondary crosscutting veins with quartz, were observed in the Lapa Formation samples. Sulfides were extracted by a chromium reduction technique

modified from Hsieh and Shieh (1997). Care was taken to sample only portions of each sample hosting disseminated pyrite.

A reduced chromium mixture was prepared with 500 ml 5N HCl, 120 g Zn metal granules, and 208 g $CrCl_3 \bullet 6H_2O$ and left overnight in a vacuum-sealed container. A separate solution of zinc acetate ($ZnC_4H_6O_4$) was prepared with 432 ml MilliQ, 68 ml 50% w/w NaOH, and 5 g zinc acetate dihydrate powder ($ZnC_4H_6O_4 \bullet 2H_2O$).

Between 0.5 and 1 g of bulk powder was weighed into a small beaker and vacuum-sealed with a separate beaker containing a zinc acetate (ZnAc) trapping solution. The powder was then reacted with 15 ml each of 5M HCl and the reduced chromium solution. The reaction releases H_2S gas, which reacts with the ZnAc solution and precipitates out as ZnS. The ZnS mixture is taken from the vacuum atmosphere and rinsed over a filter with $AgNO_3$. Ion exchange results in the formation of Ag_2S onto the filter, which is dried, quantified, and used for isotopic analysis. The mass of extracted sulfide is calculated from the mass of Ag_2S and then compared with the starting bulk powder weight to determine percent sulfide in the original sample. A maximum and minimum yield of Ag2S was used to determine whether too little sulfide was present for a successful Cr extraction, or too much such that not all sulfide was extracted. Samples with values falling outside of this range may have experienced isotopic fractionation during extraction (Wing, pers. comm.). The Lapa values all fall within this range.

Percent sulfide was also determined by running about 1 mg of bulk powder through the Eurovector elemental analyzer (see below for details). Results for weight

percent sulfide are reported from both methods, as the weight of Ag_2S was not available for all samples.

3.2.4: $\delta^{13}C$ and $\delta^{18}O$ of carbonate

Carbonate carbon isotopes were analyzed only samples hosting relatively high percentages of carbonate. Analyses were conducted on a dual inlet gas source Isoprime mass spectrometer. For relatively pure carbonate samples about 100 μg of powder was weighed into Wheaton V-vial, placed into a Multi-prep inlet system and reacted online for 10 minutes with 102% H_3PO_4 at 90º C. Evolved CO_2 was separated from water vapor by cryogenic distillation, and then measured for isotope abundances by dual inlet mass spectrometry. Carbon and oxygen isotopic compositions were reported using the δ-notation as per mil (‰) deviations. For example:

$$\delta^{13}C = [(({}^{13}C/{}^{12}C)_{sa}/({}^{13}C/{}^{12}C)_{PDB})\text{-}1] \text{ X } 10^3 \text{ [‰,PDB]}$$

where *sa* is the sample and *PDB* is the Peedee belemnite standard. Uncertainties of these measurements were determined by multiple analysis of a standard carbonate (NBS 19) interspersed with the samples. These values ranged between ±0.09 and ±0.36 ‰.

3.2.5: $\delta^{13}C$ of organic carbon

Residues of acidifications were directly combusted in a Eurovector elemental analyzer on-line with a continuous flow gas source Isoprime mass spectrometer. Samples were weighed and folded into tin capsules that were sequentially dropped into the analyzer with a pulsed O_2 purge of 15 ml into a catalytic combustion furnace

operating at 1040°C. The quartz combustion tube was packed with chromium oxide and silvered cobaltous oxide separated with quartz chips. Water was removed from the combustion products with a 10-cm magnesium perchlorate column, and the resulting CO_2 was separated from other gases with a GC column. The cycle time for these analyses was 320 seconds with reference gas injection as a 30-second pulse beginning at 20 seconds. Sample CO_2 pulses began at 110 seconds and returned to baseline values between 150 and 180 seconds, depending on sample size and column conditions. The effluent from the EA was introduced in a flow of He (65 kPa) to the IRMS through a SGE splitter valve that controls the variable open split. Timed pulses of CO_2 reference gas (99.9% purity, ~ 8nA) were introduced at the beginning of the run using an injector connected to the IRMS with a fixed open ratio split. The isotope ratios of reference and sample peaks are determined by monitoring ion beam intensities relative to background values. Isotope ratios were determined by comparing integrated peak areas of *m/z* 44, 45, and 46 for the reference and sample CO_2 pulses, relative to the baseline of ~1 x 10^{-11}A. Uncertainties of these measurements (± 0.2‰) were determined by multiple analysis of a urea standard ($\delta^{13}C$ = -29.39‰) interspersed with the samples.

3.2.6: $\delta^{34}S$ of sulfide

To determine the isotopic composition of extracted sulfide, approximately 100 µg of resulting Ag_2S from the chromium reduction method (see above) was weighed and folded into tin capsules that were sequentially dropped into a Eurovector elemental analyzer with a pulsed O_2 purge of 12 ml into a catalytic combustion

furnace operating at 1030°C. The frosted quartz reaction tube was packed with high purity reduced copper wire for quantitative oxidation and O_2 resorption. Water was removed from the combustion products with a 10-cm magnesium perchlorate column, and the SO_2 was separated from other gases with a 0.8-m PTFE GC column packed with Porapak 50-80 mesh heated to 90°C. The cycle time for these analyses was 210 seconds with reference gas injection as a 30-second pulse beginning at 20 seconds. Sample SO_2 pulses begin at 110 seconds and return to baseline values between 150 and 180 seconds, depending on sample size and column conditions. The effluent from the EA was introduced in a flow of He (80-120 ml/min) to the IRMS through a SGE splitter valve that controls the variable open split. Timed pulses of SO_2 reference gas (99.9% purity, ~ 3nA) were introduced at the beginning of the run using an injector connected to the IRMS with a fixed open ratio split. The isotope ratios of reference and sample peaks were determined by monitoring ion beam intensities relative to background values. Isotope ratios were determined by comparing integrated peak areas of *m/z* 66 and 64 for the reference and sample SO_2 pulses, relative to the baseline of ~1 x 10^{-11}A.

Isotopic results were expressed in the δ notation as per mil (‰) deviations from the Canyon Diablo Meteorite (CDM) standard. Uncertainties of these measurements (± 0.3‰) were determined by multiple analysis of a standard barite (NBS 127) interspersed with the samples.

3.2.7: Minor sulfur isotopes

David Johnston from James Farquhar's stable isotope lab conducted measurements to determine minor isotopic compositions of the extracted sulfide by converting extracted Ag_2S to SF_6 by fluorination with a 10x excess of F_2. Resulting SF_6 was purified cryogenically (distilled at -110^{o}C) and chromatograhically (on a 12' molecular sieve 5Å Haseq Q column with a TCD), and then measured as SF_5^+ (m/e of 127-129) on a Thermofinnigan MAT 253. Isotopic data are reported relative to V-CDT. Data are reported in ‰ as $\delta^{34}S = (({}^{34}R_{sample} - {}^{34}R_{standard})/ {}^{34}R_{standard})*1000)$ and $\Delta^{33}S = (\delta^{33}S - ((\delta^{34}S/1000+1)^{0.515} - 1)*1000)$ relative to V-CDT assuming that the standard IAEA-S1 has a composition on the V-CDT scale of $\delta^{33}S$ = -0.05‰ and $\delta^{34}S$ = -0.3‰.

Analytical uncertainties on minor sulfur isotope measurements are estimated from long-term reproducibility of Ag_2S fluorinations of the IAEA S1, S2, and S3 standards; these are 0.14, 0.008, and 0.20‰ (1σ) for $\delta^{34}S$, $\Delta^{33}S$, and $\Delta^{36}S$, respectively.

3.3: Characterizing the source rock

Methods used by petroleum geologists for assessing the petroleum potential of a source rock were used as a first-order determination of the organic carbon content and characteristics of the Lapa samples.

3.3.1: Pyrolysis

Source-rock analyses, similar to Rock-Eval pyrolysis, were conducted on all six biomarker samples and, for comparison, several samples from cores MAF 66-80 and MAF 42-88. Rock-Eval pyrolysis helps to determine the type and maturity of preserved organic matter. The maximum temperature the organic matter could have experienced is indicated at T_{max}, which is delineated by the S2 peak, which can be integrated to indicate volume of organic matter volatilized. Thus, the S2 peak represents the relative abundance of material thermally released at this temperature, which is equivalent to the quantity of hydrocarbons the rock could produce under present conditions (Strauss *et al.*, 1992**)**. The amount of organic matter detected in the Lapa samples was extremely small and the S2 integrations were not used directly to determine an exact mass of organic matter because error was significant in analyzing such trace amounts of organic matter. Instead, the presence or absence of an S2 peak was used for making interpretations.

To determine T_{max}, about 100 mg of each sample was heated gradually in an inert atmosphere, starting at 300ºC and rising at 25ºC/minute to 600ºC. Any volatilized hydrocarbons were detected by a flame-ionization detector, yielding two temperature peaks: S1 (at 300º C) records the amount of free hydrocarbons that had been present in the rock; S2, or T_{max}, is the point at which nonvolatile and heavy hydrocarbons are released, and is unique to organic matter of different types and maturities.

3.3.2: H/C ratios

Because hydrogen atoms are expelled during thermal maturation, the ratio of hydrogen to carbon atoms (H/C ratio) in bulk kerogen is another measure of thermal maturity. Following established methods (Strauss *et al.*, 1992), rock powders were treated with HF, HCl, and $LiAlH_4$ at Laola Party Ltd., Australia, to quantitatively remove the silicate, carbonate, and sulfide minerals from the bulk, acid-insoluble organic matter of the rock. Elemental analyses were done on vacuum-dried kerogens by Huffman Laboratories, Inc. in Colorado.

3.4: Biomarkers

3.4.1: Sample preparation

Throughout the preparation, extraction and analysis of the extractable organic matter and biomarkers, contamination is a major concern and steps must be taken to minimize it. All materials used for preparation, extraction and analysis were cleaned, heated and rinsed with dichloromethane to remove any organic material.

To remove contaminants potentially coating the exterior of the core and extending into it through occasional fractures, selected portions were broken into pebble-sized pieces, placed into an ashed beaker, rinsed with 18MΩ MilliQ water, sonicated for 15 minutes, decanted, and then rinsed again in MilliQ water. This process was repeated three times for each sample. Samples were dried overnight or longer if needed, and then each piece was dipped into dichloromethane so that any

soluble contaminants were removed. All materials used were cleaned, ashed and then rinsed with dichloromethane.

A blank of non-activated silica gel was prepared along with each group of samples. At the end of the extraction the blank solution was concentrated and then analyzed in the gas chromatographer-mass spectrometer (GCMS, see below). Cleaned samples were powdered, with the blank running through all steps ahead of the sample and all materials being rinsed with dichloromethane before powdering.

3.4.2: Extracting soluble organic matter

Attempts to extract bitumen — extractable organic matter (EOM) — from samples using the traditional Soxhlet reflux technique were unsuccessful. Despite considerable effort, it was not possible to develop a system for maintaining an ideal temperature balance during the 48-hour extraction that would both maintain the heat necessary for extraction while also preventing any extracted sample, which occurs in trace amounts, from being vaporized and lost from the Soxhlet system. Contamination was also difficult to minimize.

As a result, EOM was isolated from the powdered samples using an accelerated solvent extractor (Calvo *et al.*, 2003) at the organic geochemistry lab run by Elizabeth Canuel at the College of William and Mary Virginia Institute of Marine Sciences (VIMS) in Gloucester Point, Virginia. Samples were weighed and then loaded into stainless steel extraction cells of a Dionex ASE 200 Accelerated Solvent Extractor. Extractions were carried out at 1000 p.s.i. and 100°C as follows: (1) Preheating of the cell to the selected temperature for 2 minutes and pumping of 9:1

dichloromethane:methanol into the cell; (2) pressurization of the cell to 1000 p.s.i. with 5 min thermal equilibration; (3) static extraction for 2 min; (4) flushing of the extract from the sample into the collection vials; and finally (5) purging of the solvent residue with pressurized nitrogen. Steps 3 and 4 were repeated five times for each extraction cell with the introduction of fresh solvent after each static phase. The solvent was then combined in one collection vial. (Calvo *et al.*, 2003). The entire process was then repeated for each sample.

Samples were then concentrated from about 100 ml to 1 ml using a TurboVap at the VIMS lab, and then further concentrated down to 50 µl under a pure nitrogen stream traveling through Teflon tubing. From this amount, 25 µl was taken and used for GC analyses, and the remaining 25 µl archived in cold storage.

3.4.3: Determining percent EOM

Extracted organic matter was quantified by placing concentrated sample in a preweighed, ashed 5-mL vial. The vial with sample was placed on the scale and the dichloromethane solvent allowed to evaporate until a stable weight was reached, but before sample began to evaporate. This weight was recorded and the vial weight subtracted to determine the weight of the extracted organic matter. This method appears to overestimate abundances of bitumen by 30-50% relative to concentrations determined by GC-MS analysis of spiked samples (Brocks *et al.*, 2003). Evaporation of solvent also results in loss of lighter hydrocarbons, and residual solvent may add weight. Nonetheless, the weights of EOM in the Lapa Formation samples were extremely low, regardless of TOC present (see Discussion). For this study, only the

archived portion was weighed. This weight was doubled to provide a rough percentage of extractable organic matter in bulk powder.

3.4.4: Separating EOM components

The remaining 25 µl of concentrated EOM was mixed with silica gel that had been extracted (submerged in dichloromethane and sonicated for 15 minutes) and activated (water removed by heating overnight at 200ºC in a combustion oven) in preparation for column chromatography. The sample was allowed to dry on the silica gel so that component parts — saturated, aromatic and polar, in order of increasing polarity — could be re-extracted from the gel as follows: 1) an ashed portion of quartz wool was inserted near the opening of an ashed Pasteur pipette, 2) 0.6 g activated silica gel was poured into pipette and an ashed, 5-mL vial having a Teflon lid placed beneath it, 3) the pipette, silica and wool were rinsed with dichloromethane, 4) the silica-EOM mixture was added to the pipette, 5) saturated hydrocarbons were re-extracted from the silica column with 1.2 mL hexane, 6) once the saturated fraction had passed through the column into the vial, aromatic hydrocarbons were re-extracted with 3 mL of a hexane:dichloromethane mixture and collected in a new vial, 7) then polar hydrocarbons were re-extracted with 4 mL of a dichloromethane:methanol mixture. The saturated and aromatic fractions were each concentrated down to 50µL in dichloromethane under a pure nitrogen stream passing through Teflon tubing. The polar fraction was stored.

3.4.5: Identifying EOM molecules

From each concentrated portion of saturated and aromatic fractions, 1 μL was injected into an HP 6890 gas chromatograph using a 50% phenyl-50% dimethylsilicon column using He as a carrier gas. The GC was interfaced with a 5972 MSD (Mass Selective Detector) mass spectrometer, both run by George Cody at the Geophysical Lab of the Carnegie Institution of Washington.

Analyses were conducted for the saturate and aromatic portions of each sample both in full-scan mode and also in selected ion monitoring (SIM) mode.

Full-scan mode: For a first, overview inventory of molecules present, samples were put in 100 μL of dichloromethane, and 1 μL injected in splitless mode with the injector at 300ºC, pressure at 9.5 psi, total flow of 23.9 mL/min, the purge flow to the split vent at 20 mL/min and gas saver at 20 mL/min. The oven starting temperature was 50ºC and set to increase to 300ºC at a rate of 4ºC/min, holding at 300ºC for 15 min. with a run time of 78.5 min. To see hopanes more clearly, samples were then concentrated to 25 μL and 1 μL injected in splitless mode with the injector at 300ºC, pressure at 9.5 psi, total flow of 23.9 mL/min, the purge flow to the split vent at 20 mL/min and gas saver at 20 mL/min. The oven starting temperature was 50ºC and set to increase to 300ºC at a rate of 4ºC/min, holding at 300ºC for 35 min. with a run time of 129.33 min.

SIM mode: For selected ion monitoring of the saturated fraction, samples were concentrated to 25 μL and 1 μL injected in pulsed splitless mode with the injector at 300ºC, pressure at 9.5 psi, total flow of 23.9 mL/min, the purge flow to the split vent at 20 mL/min, gas saver at 20 mL/min, and the injection pulse pressure at

12 psi until 0.50 min. The oven starting temperature was 50ºC and set to increase to 300ºC at a rate of 3ºC/min, holding at 300ºC for 25 min. with a run time of 112.67 min.

For SIM analysis of the aromatic fractions, samples were concentrated to 25 µL and 1 µL injected in pulsed splitless mode with the injector at 300ºC, pressure at 9.5 psi, total flow of 23.9 mL/min, the purge flow to the split vent at 20 mL/min, gas saver at 20 mL/min, and the injection pulse pressure at 12 psi until 0.50 min. The oven starting temperature was 50ºC and set to increase to 300ºC at a rate of 3ºC/min, holding at 300ºC for 35 min. with a run time of 129.33 min.

The extract is vaporized upon injection and the various molecules separated in the GC column based largely on their size and polarity differences. The fractionated sample and He carrier gas enter the ion source of the mass spectrometer simultaneously. Sequentially, purified molecules are emitted and ionized and the mass of charged molecules quantified: these include the parent molecule and unique fragment molecules that identify the molecular species. Identification depends on comparing GC retention times with characteristic ions having a specific mass. The ionic mass is reported as a mass to charge ratio, or *m/z*.

Samples were run through the GCMS several times in order to first identify molecules. Hopanes and steranes occur in trace amounts, and SIM analyses were conducted to better detect these molecules by programming the mass spectrometer to spend longer periods of time looking for specific ions. Table 3.1 shows the ions scanned during SIM (see also Table 2.1 for characteristic structures). A scan for *m/z* = 369 was conducted on sample at depth 596.33m to test for the presence of oleanane, a

plant-derived biomarker that can also appear at *m/z* = 191; and for m/z = 205, a tentative test for 2αmethylhopane.

Table 3.1: Ions scanned during SIM analyses.

	Saturate fraction			Aromatic fraction			
	n-alkanes	hopanes	steranes	Aryl isoprenoids	phenanthrenes	dibenzothiphene	naphthalenes
m/z	85	191	217,218, 259	133	178,192,206	184	128,142,156, 170,184

3.4.6: Biomarker ratios

A GCMS chromatogram was generated that records the presence of specific ions by their elution times and as peaks having areas that correlate to the relative abundance of each ion. Chromatograms are generated with MSD ChemStation software by Hewlett Packard, which is also used for peak integrations.

The peak areas within a sample were integrated in order to compare the relative amounts of different molecules within a sample. Baseline integration points for individual peaks were done by visual inspection and manual manipulation in order to fully evaluate and compensate for coelution of peaks, or to avoid misidentification. Because the baseline for peak integrations can be difficult to determine for some molecules, a single standardized technique was used for all peak integrations (see Fig. 3.2). The peak of each molecule is integrated three separate times. Final peak areas were reported as the average of these three calculations, and the error reported as standard deviation. The error typically ranged between 1 and 5%, but was as high as

20% in cases where coelution of molecules complicated integrations. The primary aim here was to ensure consistency among calculations of ratios, so each type of analysis — the saturate fractions, the SIM analyses of the steranes, and the SIM analyses of aromatic fractions — were completed in single analytical sessions. Absolute concentrations of molecules were not determined in this study, so interpretations are based primarily on the strength of relative abundances and the biomarker ratios.

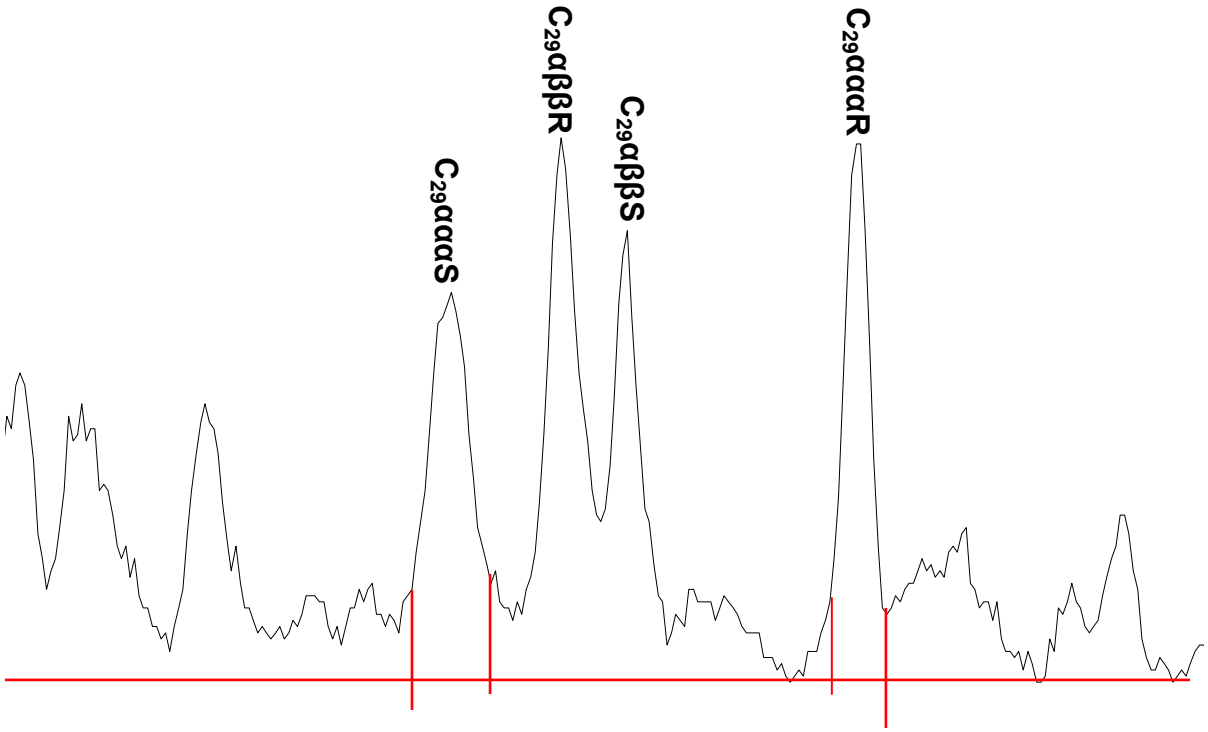

Figure 3.2: An example of peaks from a GCMS ion chromatogram generated for sample at depth 589.90m. Each peak represents a different isomer of C_{29} sterane, as indicated. The red lines show how the baseline was determined to integrate peak areas. A lowest point for the group of peaks was determined, and the baseline defined from that point. This method of determining the baseline was used for all the peak integrations in this study.

Chapter 4: Results

4.1: Sampling Strategy

The selection of samples from which organic material was extracted were based on lithologic observations and elemental and isotopic data (see Table 4.1).

Table 4.1: Lithologic and elemental characteristics of samples selected for biomarker analysis. n.d.= not determined.

Sample depth(m)	Lithology	% carbonate	TOC (wt. %)	EOM (ppm)	δ^{13}Ccarb (‰ VPDB)	δ^{13}Corg (‰ VPDB)
560.70	Marl	75	0.16	0.05	-0.48	-28.8
572.64	Marl	70	0.23	0.43	-1.67	-24.4
586.20	Shale Hosts quartz vein	7	0.22	0.13	n.d.	-23.2
589.90	Shale; disseminated pyrite visible	0	1.45	0.21	n.d.	-25.7
591.34	Black shale, disseminated pyrite visible; Hosts dropstone	3	3.7	0.93	n.d.	-24.8
596.20	Shale, disseminated pyrite visible	3	0.4	0.21	n.d.	-24.9

4.2: Time-series Analyses

4.2.1: Percent carbonate

Overall, the percentage of rock that is carbonate carbon increases upsection (Fig. 4.1c), although some of the samples closer to the base of the Lapa host relatively high percentages of carbonate carbon. The samples that are 50% or more carbonate

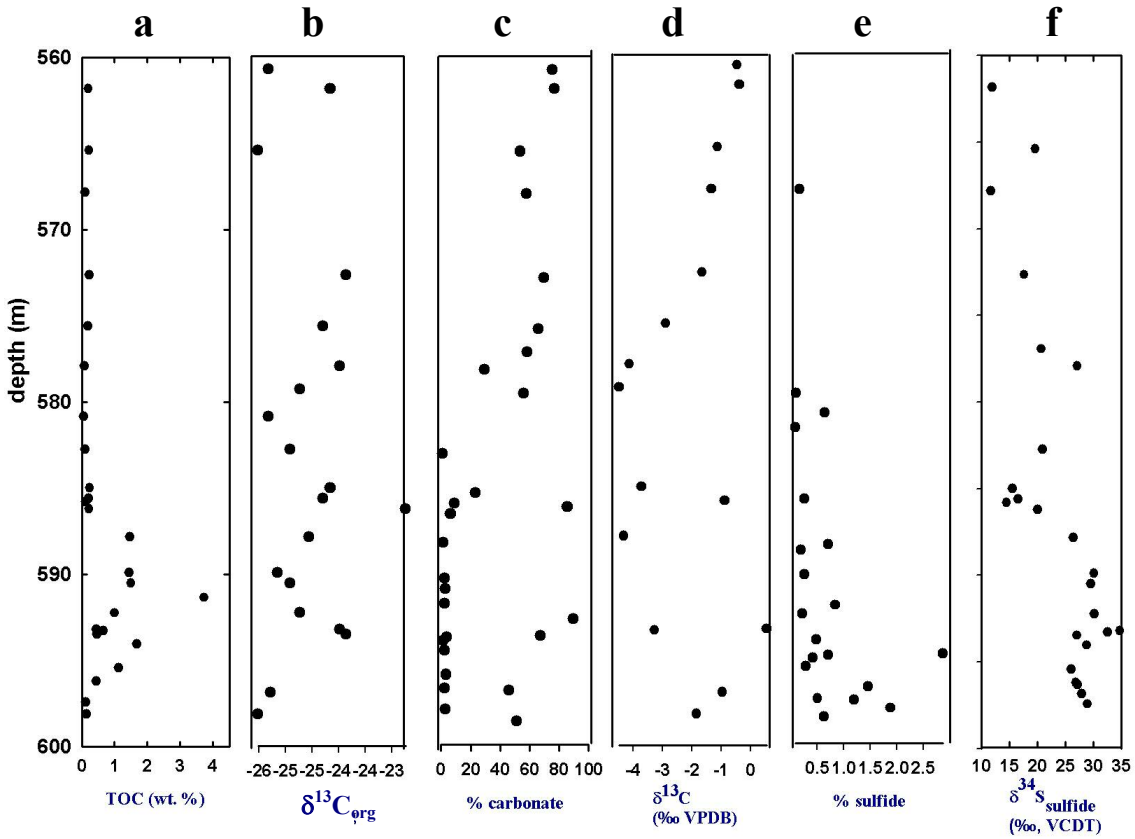

Figure 4.1: The elemental and isotopic composition of 40 meters of the Lapa in core MAF 134-86, as shown by total organic carbon by wt. % (TOC), the isotopic signature of the bulk organic carbon, the percent of each sample by weight that is carbonate, the isotopic signature of the carbonate, the percent of each sample that is sulfide, and the isotopic composition of extracted sulfide.

Table 4.2 Abundances and isotopic compositions of C, S and O in the 40m of Serra da Lapa samples from core MAF 134-86 analyzed. Abundances are reported as wt.%. Isotopic compositions for C and O are reported as ‰ vs. VPDB, and for S as ‰ vs. VCDT. --- indicates no data were collected.

Sample	Total organic carbon	Total sulfide	Total carbonate	$\delta^{13}C_{org}$	$\delta^{13}C_{carb}$	$\delta^{18}O_{carb}$	$\delta^{34}S_{sulfide}$
560.70	---	---	75	-25.8	-0.5	-6.3	---
561.82	0.20	0.16	77	-24.7	-0.4	-6.1	11.9
565.40	0.22	---	54	-26.0	-1.1	-7.7	19.6
567.83	0.10	---	58	---	-1.3	-7.3	11.7
572.64	0.23	---	70	-24.4	-1.7	-6.2	17.6
575.60	0.19	0.09	66	-24.8	-2.9	-6.2	9.6
576.93	---	0.64	58	---	---	---	20.7
577.92	0.08	0.08	30	-24.5	-4.1	-9.3	27.1
579.27	---	---	56	-25.2	-4.5	-8.9	---
580.83	0.07	---	---	-25.8	---	---	---
582.74	0.10	0.26	0.8	-25.4	---	---	20.9
585.00	0.24	---	23	-24.7	-3.7	-10.1	15.5
585.60	0.21	---	9	-24.8	---	---	16.5
585.80	0.12	0.7	86		-0.9	-5.0	14.5
586.20*	0.22	0.19	7	-23.2	---	---	20.0
587.84	1.47	0.26	2	-25.1	-4.3	---	26.4
589.90	1.45	0.83	0	-25.7	---	---	30.1
590.50	1.50	0.21	2	-25.4	---	---	29.5
591.34	3.73	---	3	---	---	---	---
592.23	1.0	0.48	2	-25.2	---	---	30.1
593.20	0.44	2.87	90	-24.5	0.5	-6.3	34.7
593.28	0.65	0.71	67	---	-3.2	-10.1	32.5
593.47	0.46	0.41	4	-24.4	---	---	27.0
594.04	1.68	0.28	1	---	---	---	28.8
595.42	1.12	1.46	2	---	---	---	26.0
596.20	0.44	0.50	3	---	---	---	26.9
596.33	---	1.20	3	---	---	---	27.2
596.85	---	1.88	45	-25.8	-1.0	-7.4	27.9
597.43	0.13	0.63	3	---	---	---	28.9
598.10	0.15	---	51	-26.0	-1.8	-5.3	---

by weight also tend to have lower TOC values (Fig. 4.1a). The shallower samples in the core tend to have, as a group, higher carbonate concentrations, including the interval from 560.70 to 579.27 meters. The lower half of the Lapa Formation shale interval in the MAF 134-86 core is far lower in carbonate abundance, except for the samples at (specifically at 585.80, 593.20, 596.85 and 598.10 meter depths).

4.2.2: Total organic carbon (TOC)

The wt. % of organic carbon (TOC, or total organic carbon) for all the Lapa samples collected from MAF 134-86 ranges between just above zero and just below 2, with one sample at 3.7 wt.% (the sample hosting a dropstone). Overall, organic concentrations are very low near the top of the core. TOC abundance and variability is much greater in the lower half of the Lapa Formation in the sampled core.

4.2.3: Percent sulfide

The percent of each sample that was sulfide, hosted as finely disseminated pyrite, increases down the core to as great as 2 wt.% (Fig. 4.1e). Care was taken to extract only portions of samples hosting disseminated sulfide. Remobilized pyrite veins and nodules were not sampled.

4.2.4: $\delta^{13}C$ carbonate

Isotopic compositions of carbonate carbon in the Lapa Formation samples are consistently negative and range between -4.5‰ to -0.4‰ (Fig. 4.1d). Values tend to scatter in the lower portion of the core, which contains ice-rafted debris, but show a steady increase in the upper half broadly coincident with an increase in carbonate, from a nadir of -4‰ at 580.83 m to near zero at 560.70m.

4.2.5: $\delta^{13}C$ of organic carbon

The $\delta^{13}C_{org}$ values for the Lapa samples of MAF 134-86 range between -26.0‰ and -23.2‰ (Fig. 4.1b). While no striking trend is discernable by depth, the two lowermost samples near the base of the core are the most ^{13}C depleted of the data set.

4.2.6: $\delta^{34}S$ of sulfide

The strong negative $\delta^{34}S$ excursion starting from remarkably positive extremes near the base of the Lapa Formation then following an overall decline (with variation in $\delta^{34}S$ as discussed below) of nearly 20‰ over less than 40 meters is one of the most striking trends of the time series data set (Fig. 4.1f). Sulfide is heaviest in the lower half of the core reaching values as high as +30.1‰. These generally decrease upsection to as low as +11.9‰. Values appear to make a slight drop going into the unconformity at the very base of the Lapa Formation.

4.2.7: Minor sulfur isotopes

The minor sulfur isotopes do not show any signals of mass-independent fractionation. All the $\Delta^{33}S$ values are below 0.05 ‰ from 0 (see Fig. 4.2). Samples for $\delta^{33}S$ and $\delta^{36}S$ measurements were selected to represent the widest range of $\delta^{34}S$ values. The $\delta^{34}S$ vs. $\Delta^{33}S$ plot reveals a stratigraphic trend that takes a parabolic path from right to left as samples become shallower in the core.

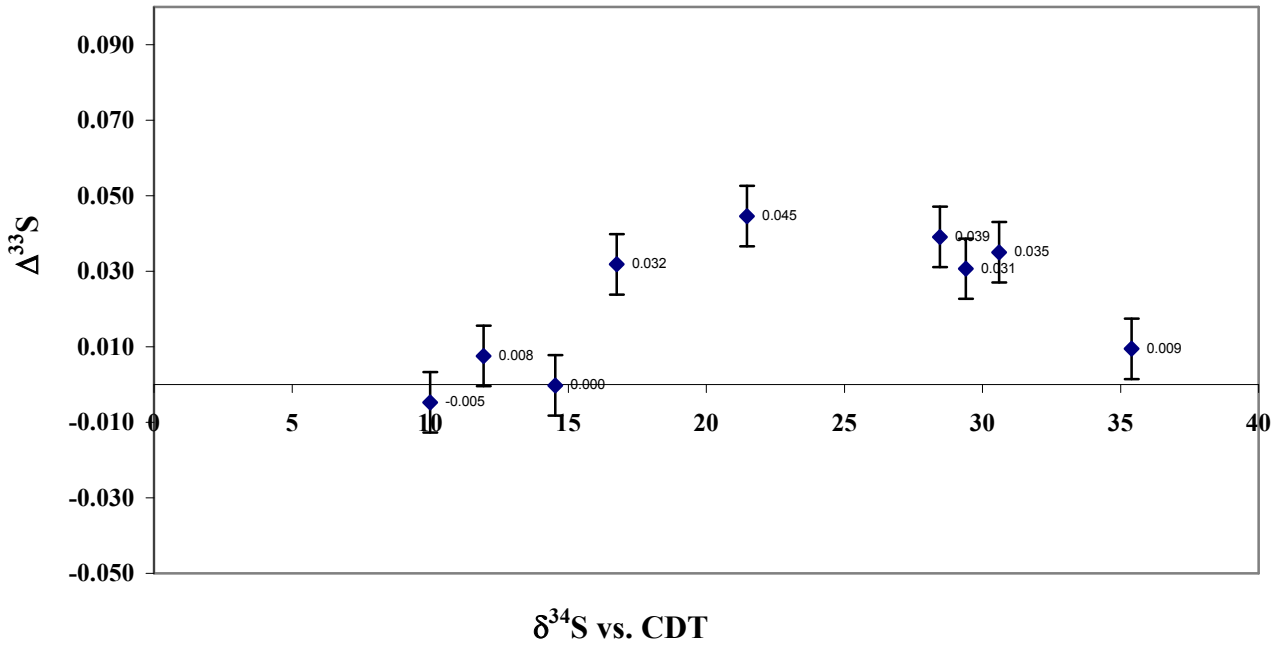

Figure 4.2: A plot $\delta^{34}S$‰ VCDT (x-axis) as $\Delta^{33}S$ VCDT (y-axis) for nine of the Lapa samples. The depth of each sample is indicated on the graph. Data were collected and plotted by David T. Johnston.

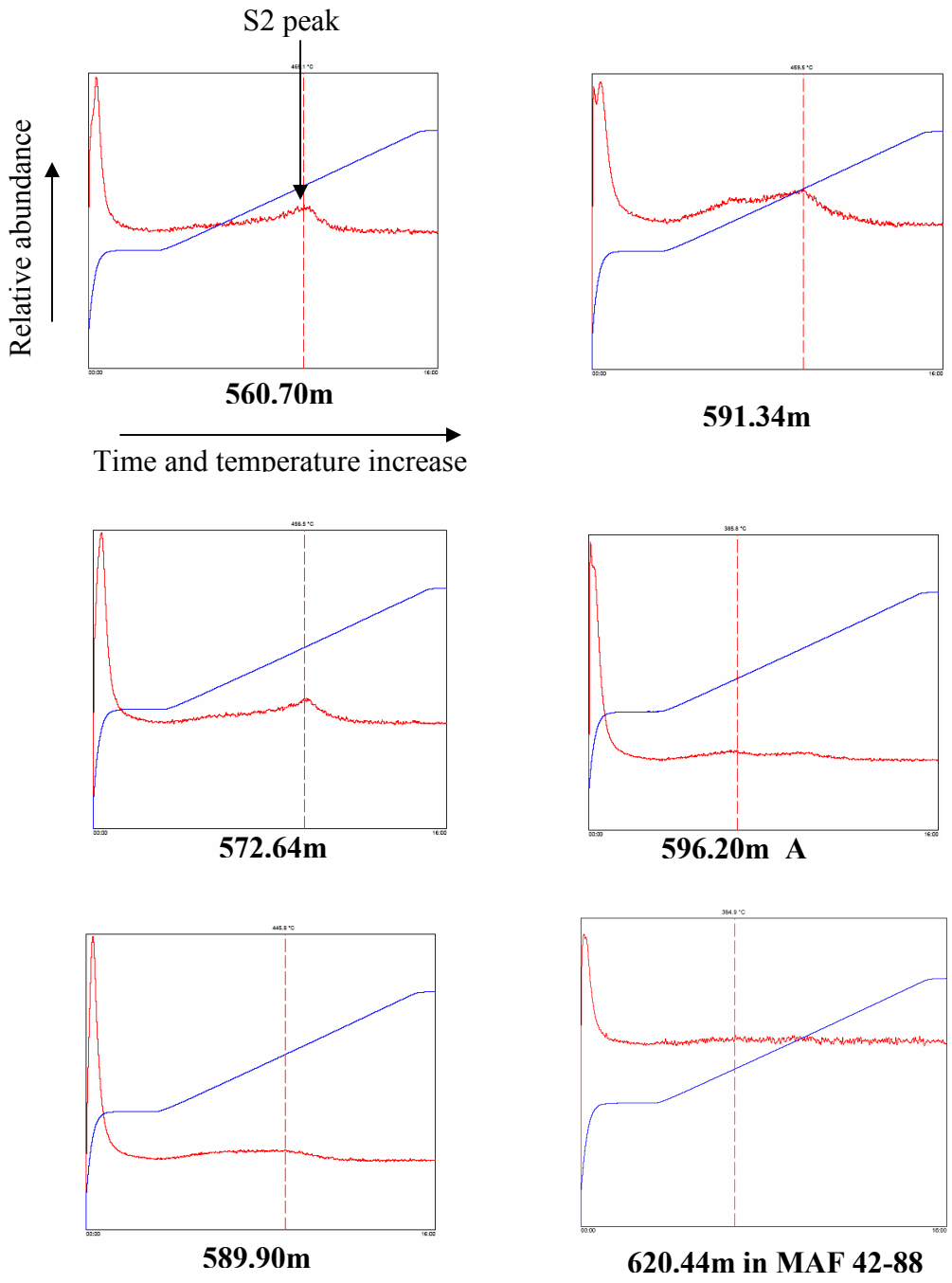

Figure 4.3: Pyrograms generated during source-rock analysis for Lapa Formation samples from core MAF 134-86. T increases from 300ºC to 600ºC at 25ºC /min. The blue lines show the programmed increase of oven temperature during the analysis. A sample from core MAF 42-88 is shown for comparison.

4.3. Characterizing the Source Rock

4.3.1: Pyrolysis

Pyrograms generated from the Lapa samples (see Fig. 4.3) show that trace amounts of volatile organic material remain in the samples as represented by the small and broad S2 peaks. The shape and amplitude of these peaks vary among the samples. The peak in sample 591.34 m is the largest and most complex. The T_{max} values are relatively consistent for the sample set ranging between 458º C and 461º C.

By comparison, samples from the Lapa in cores MAF 42-88 and MAF 66-80 showed no visible S2 peak and T_{max} could not be determined (see Table 4.2), which indicates that little or no volatile organic matter was preserved.

4.3.2: H/C ratios

The ratio of hydrogen to carbon in the kerogen can also supply information about maturity and alteration as hydrogen atoms are lost from the hydrocarbon structures over time. Atomic H/C ratios in two Lapa Formation kerogen isolates were determined and both have a common value of 0.21 (Table 4.2).

Table 4.3: Ratio of hydrogen to carbon in kerogen isolated from whole rock.

Sample	% carbon	% hydrogen	H/C ratio (molar)
MAF 134-86/589.90m	43.11	0.77	0.21
MAF 134-86/596.33m	29.24	0.51	0.21

4.3.3: Percent EOM

All the samples host low percentages of EOM (see Table 4.1). The end members are the sample at 560.70 m, having 0.05 ppm EOM and also hosting the most carbonate; and at 591.34 m, having 0.93 ppm EOM and also hosting a dropstone and the highest TOC content. The other four samples range between 0.13 ppm and 0.43 ppm. There is no clear trend of percent EOM with depth, percent carbonate or percent TOC.

4.4: Identifying Biomarkers and other Molecules

4.4.1: Saturated fraction: Normal alkanes

The normal alkane fraction in each sample (see Fig. 4.4) closely matches that of the total ion concentration of the saturate fraction. Most evident is that each sample reveals a biomodal pattern of *n*-alkane distribution (Fig. 4.4 and 4.5). While the shape of this pattern varies slightly among the samples, at least two peaks are obvious in both shale and carbonate lithologies. This biomodal distribution is notably less obvious in the sample from 586.20 m depth, which was selected because it hosts a large quartz vein.

Overall, the most abundant molecule in the first mode of peaks is at $C_{18,}$ which is dominant in four of the samples, and at C_{19} for the samples at depth 560.70m and 586.20m. The most abundant molecule in the second mode of peaks is C_{26} for sample 572.64 m, C_{25} for sample 596.20 m and 591.34 m, and at C_{27} for sample 586.20 m. The bimodal pattern is not as obvious for the samples at 560.70 and 589.90 m.

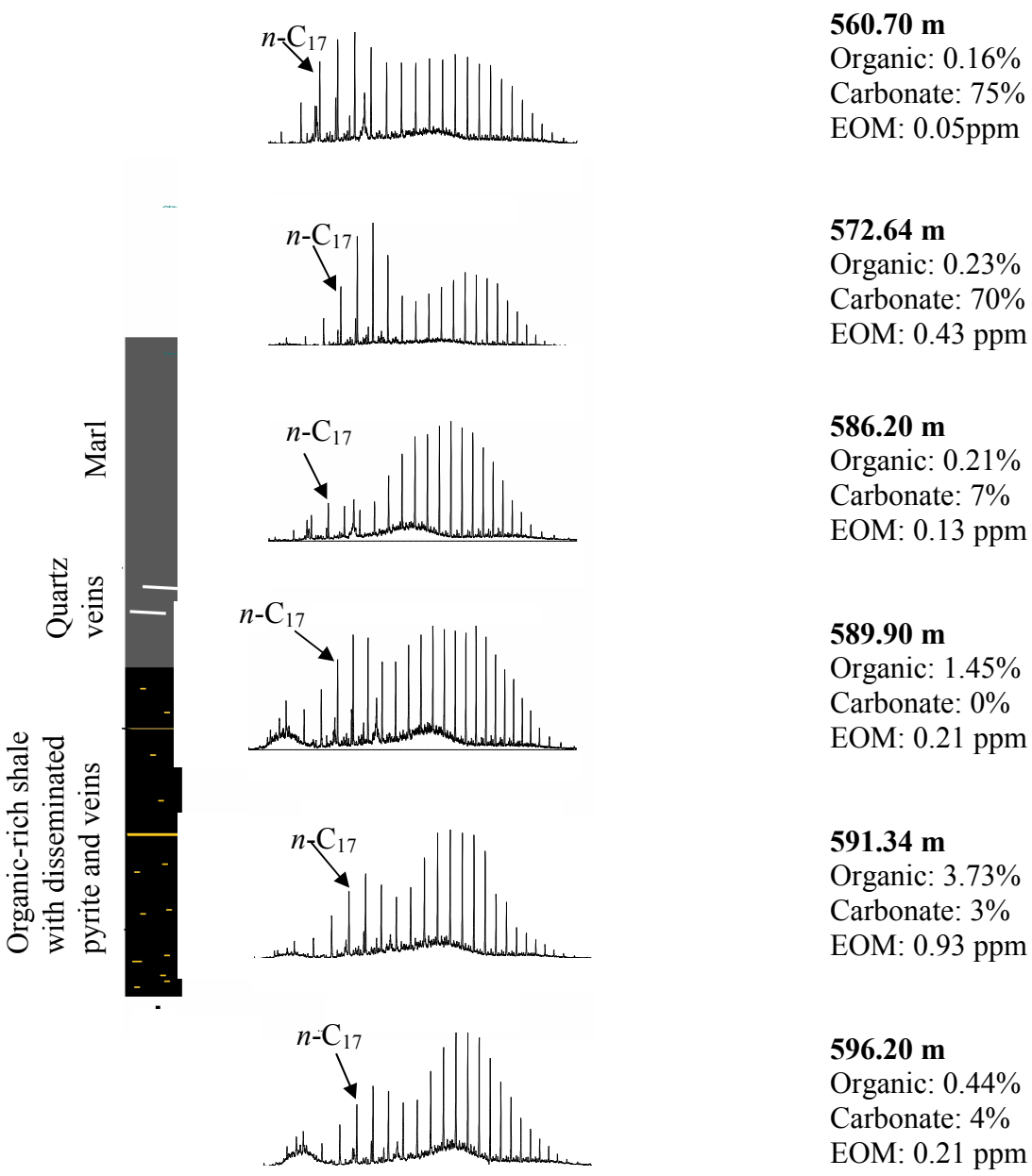

Figure 4.4: Ion chromatograms of the normal alkane fractions for each sample analyzed in the Lapa Formation MAF 134-86 drill core. Unique to this study is that each sample shows a bimodal normal alkane distribution. Listed with the chromatograms are the percentages of organic carbon, carbonate carbon, and extractable organic matter (EOM). On the column used for this particular GCMS run, pristane and phytane elute just before the C_{17} and C_{18} homologues.

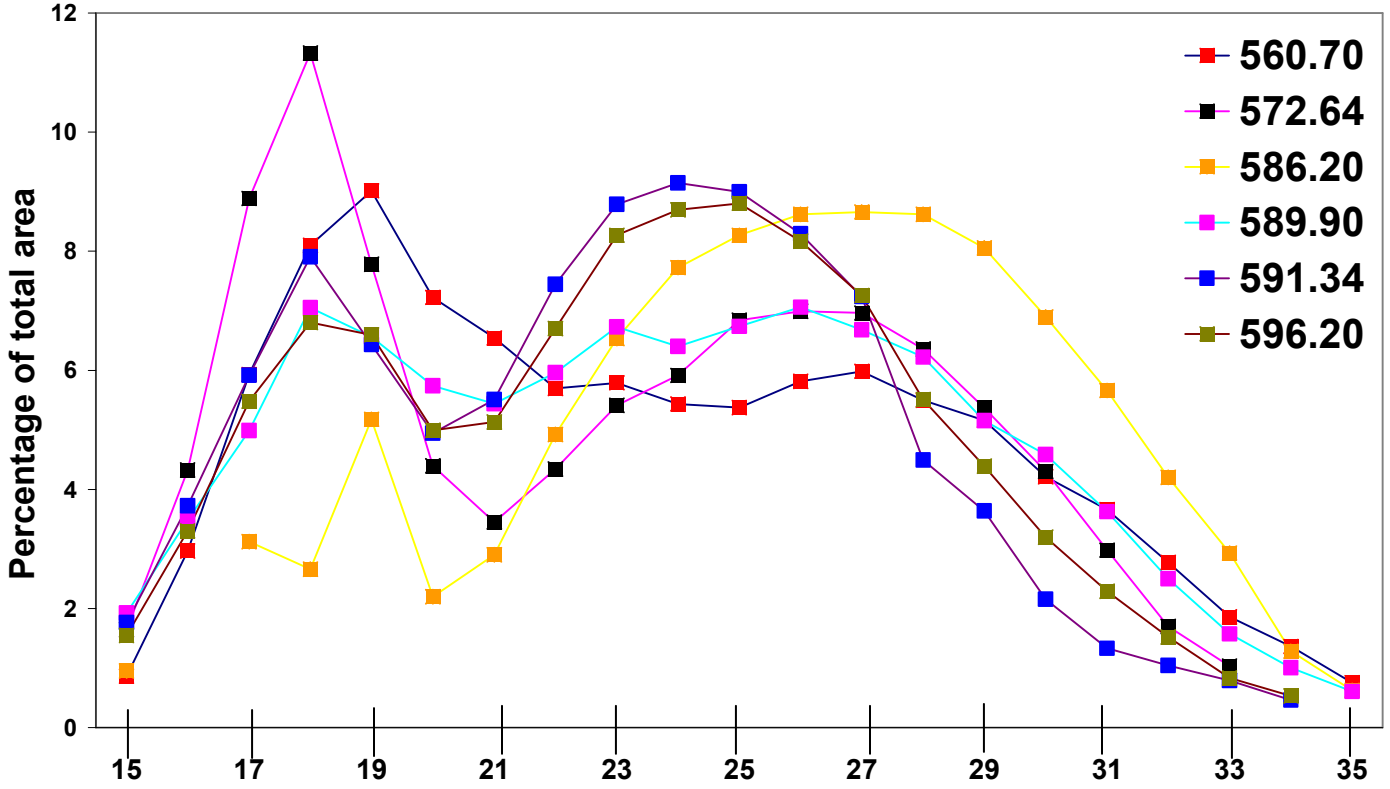

Figure 4.5: In core MAF 134-86, the relative abundances of *n*-alkanes from C_{15} to $C_{35,}$ with one data point for each *n*-alkane on the x-axis. The chart shows abundances as a percentage of individual peak area relative to the total of all peak areas, which was calculated from integrated peak areas in the GCMS chromatogram of the *m/z*=85 fraction. Note the absence of any odd-over-even or even-over-odd pattern. The appearance of a clear bimodal pattern in every sample is unique to this study. The colored lines delineate samples, which are not listed in order of decreasing depth.

In three of the samples, the alkanes with more than 20 carbon atoms dominate. In the sample at depth 572.64 m, the C_{18} alkane dominates; at 560.70m, C_{19} dominates. These samples are also the most carbonate-rich of the six samples. At 589.90 m the sample reveals a relatively more uniform distribution, with a small peak at C_{18}. All the samples show a sudden decrease in abundance starting at about C_{30}.

4.4.2: Saturated fraction: Pristane and phytane

Pristane and phytane, are isoprenoids that are homologues of the *n*-alkanes C_{17} and C_{18} and, in the column used for the GCMS scan of the saturated fraction, elute just before each homologue. These isoprenoids showed strong peaks in all samples. The ratio of pristane/phytane is less than 1 for all the samples, with the widest observed range occurring between the two shallowest and carbonate-rich samples from the core (0.78 at depth 560.70 m and 0.51 at depth 572.64 m). The deepest shale samples are very close in composition with values around 0.58. These pristine/phytane abundance patterns observed in these samples are similar to that of phytane/C_{18} *n*-alkane.

4.4.3: Saturated fraction: Hopanes

Hopanes were detected in all shale and carbonate samples (Fig. 4.6 and 4.7). A characteristic peak also appeared at *m/z*=205, the primary fragment of the 2-αmethylhopane thought to indicate the presence of photosynthesizing cyanobacteria (Summons et al., 1999). This identification is tentative, as higher resolution analyses are required to identify that the methyl group is at the second carbon and in the alpha

position. The hopanes appear least abundant in the sample from 572.64 m. For all samples, the hopanes with 29 and 30 carbons dominate. Each sample, except that at 572.64 m, contains detectable amounts of C_{31} and C_{32} hopanes. The amounts of C_{34} and C_{35} are generally too small to integrate or too small to detect. In some samples, C_{35} is either below detection levels or no longer present.

4.4.4: Saturated fraction: Steranes

All three types of steranes — those with 27 carbon atoms, 28 and 29 — occur in every sample and in roughly equal amounts; that is, no one type of sterane is dominant (Fig. 4.6 and 4.8). The SIM analyses for ions 217, 218 and 259 were used to more accurately distinguish the sterane types and construct a ternary diagram showing their relative distributions, which has been shown to correlate with source of the original organic material (Huang and Meinschein, 1979; Fig. 4.9).

The ternary diagram shows possible groupings among the samples. Samples at 560.70, 572.64 and 589.90 m tend to have more C_{27} and C_{29} steranes than do samples from 586.20, 591.34, and 596.20 m. The diagram was primarily constructed to discern whether groupings correlated with percent carbonate abundances. There appears to be no systematic relationship, although the three samples with relatively low carbonate concentrations do tend to group together. The two shale samples near the base of the Lapa Formation, one of which contains ice-rafted debris, have very similar sterane distributions, and also demonstrate a similar pattern of sterane isomerization (see below).

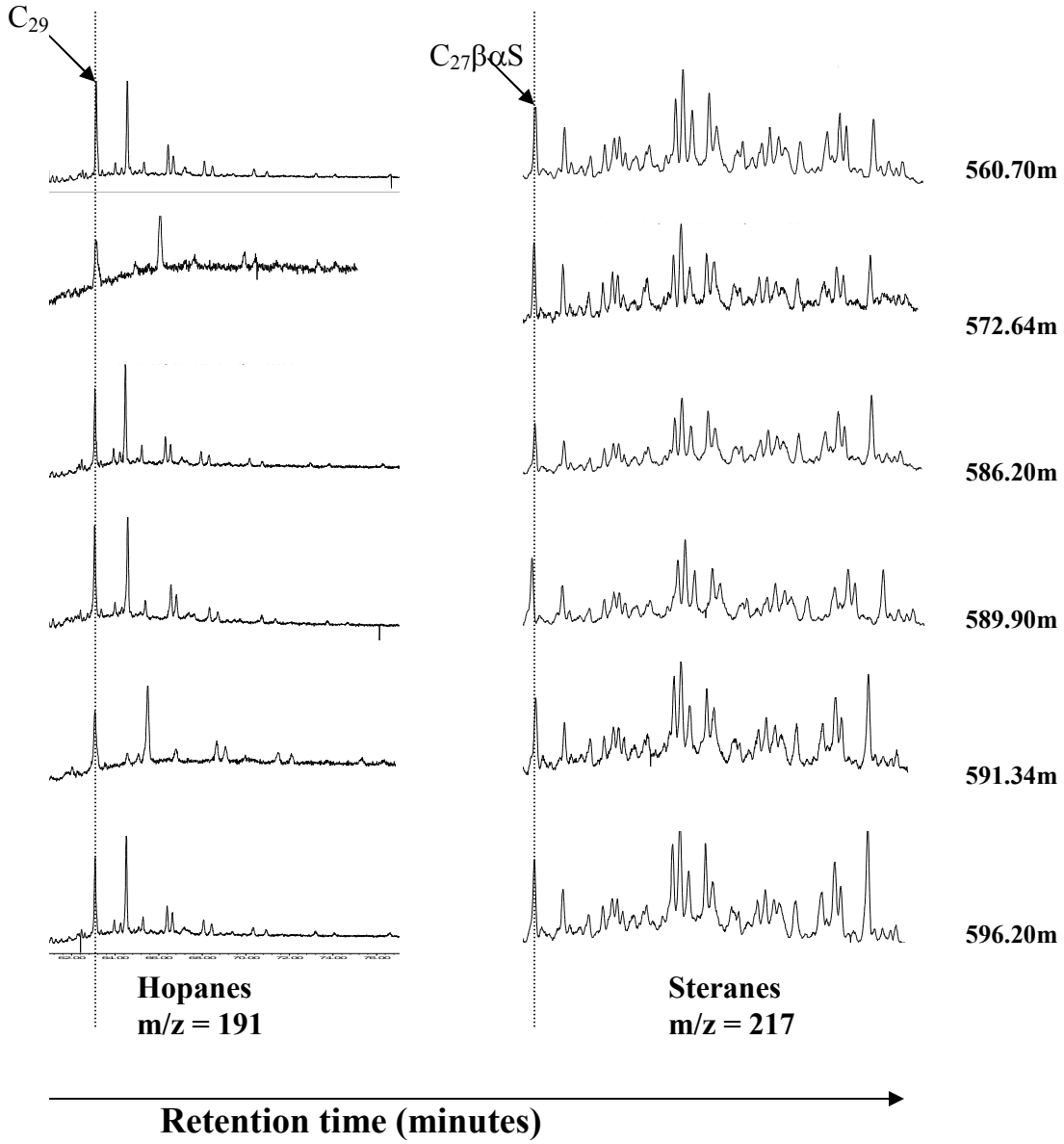

Figure 4.6: Ion chromatograms showing I) hopanes and II) steranes were identified in all samples. Abundances are relative within each sample and cannot be compared among samples (see Table 4.2 for calculations of relative abundances among samples).

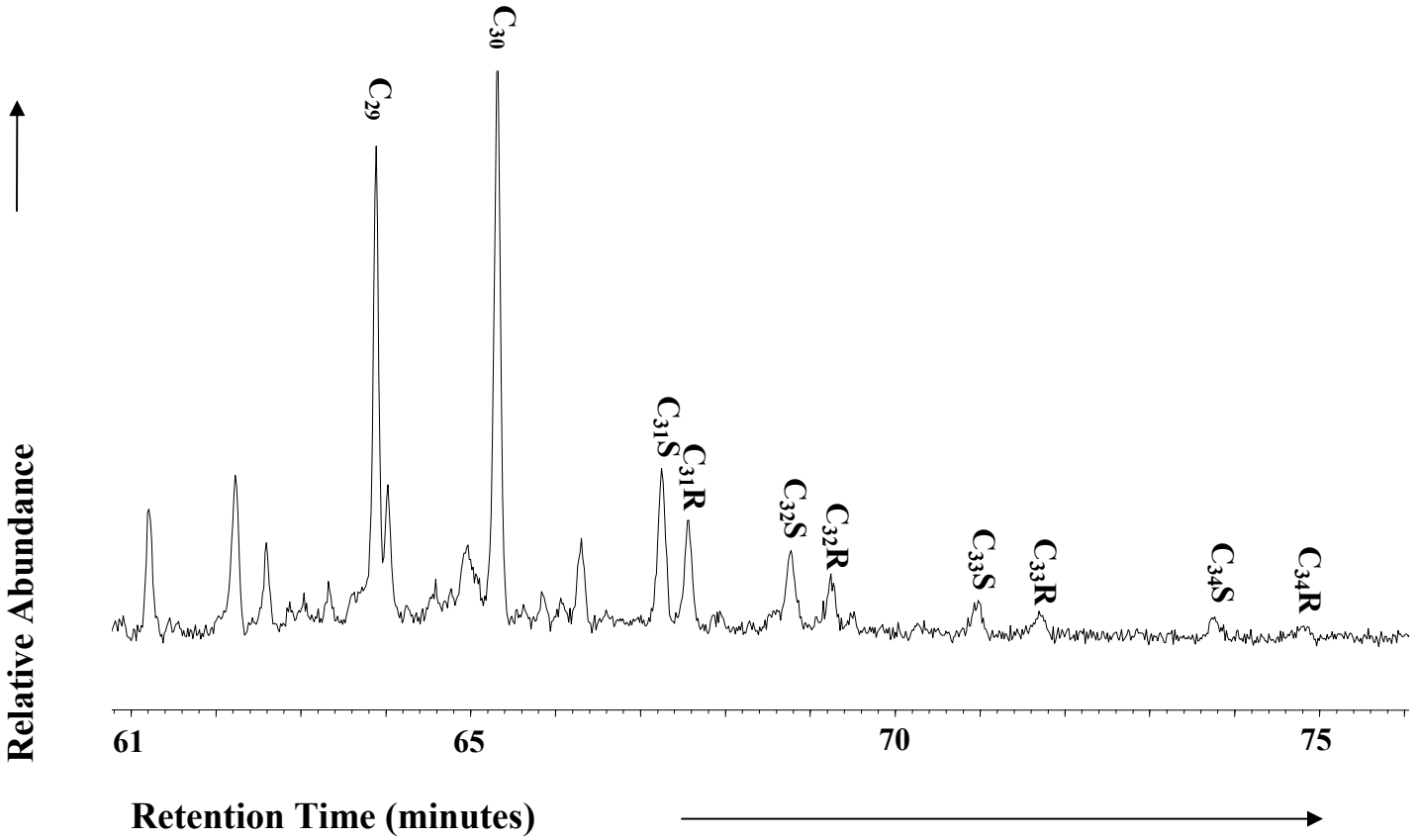

Figure 4.7: Ion chromatogram of hopanes from a sample at depth 591.34 m. The stereoisomer pairs are indicated.

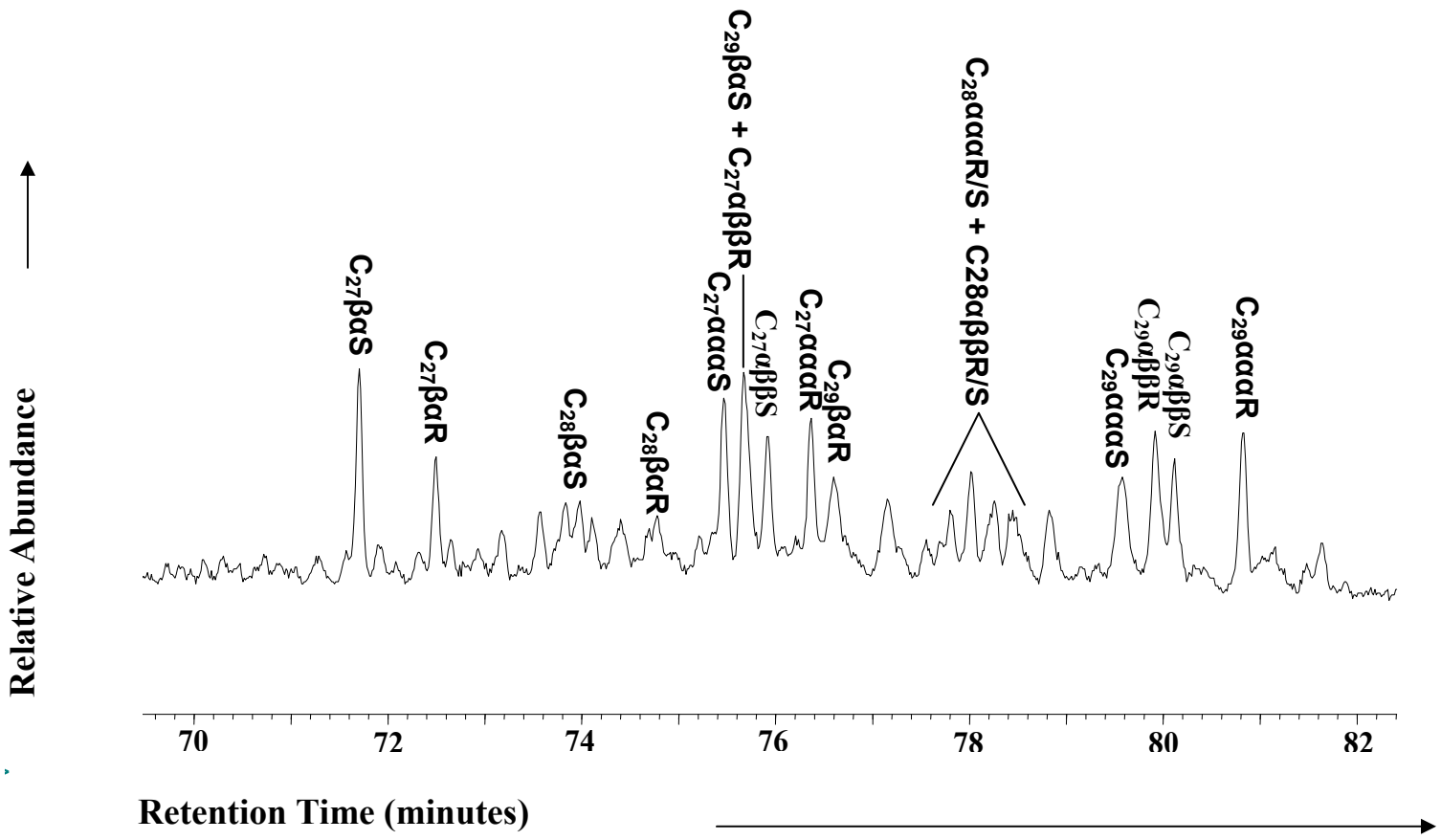

Figure 4.8: Ion chromatogram of steranes from a sample at depth 589.90 m. The three different sterane types are indicated.

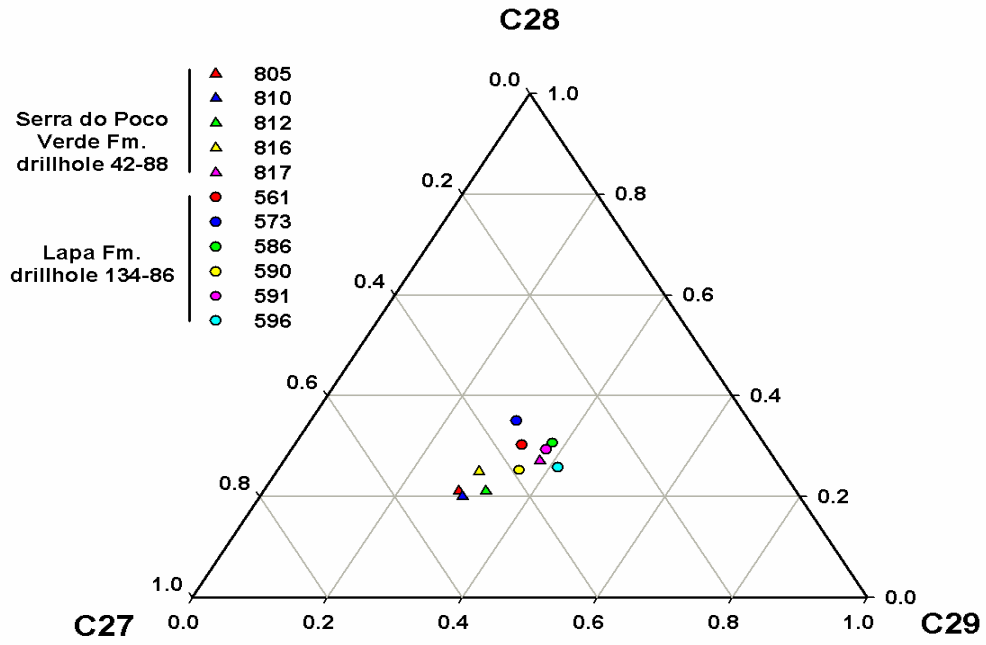

Figure 4.9: A ternary diagram showing the relative abundances of the C_{27}, C_{28}, and C_{29} steranes in the Lapa Formation samples from core MAF 134-86 and the Serra do Poço Verde Formation in core MAF 42-88. The steranes are categorized by number of carbon atoms. The distribution pattern of biosynthesized sterols is retained as these are transformed into geological steranes (Huang and Meinschein, 1979; Peters and Moldowan, 1993). A dominance of C_{29} steranes has been shown to correlate with organic matter originating from a source rich in terrestrial plant material (Huang and Meinschein, 1979). No one sterane type is dominant in these samples.

4.4.5: Aromatic fraction

SIM analyses scanned for aryl isoprenoids, thought to be biomarkers for green sulfur bacteria (Summons, 1987), and for phenanthrenes and naphthalenes, which are widely used maturity parameters. Aryl isoprenoids were either below detection limits or not present in the Lapa Formation samples, as was dibenzothiophene, which can also be used to measure thermal maturity. Phenanthrenes were present in relatively small amounts, but a contaminant molecule that co-eluted with these compounds prevented integrating their peak areas (see Appendix).

Naphthalene, methylnaphthalenes and dimethylnaphthalenes (see Table 2.1) eluted well in the samples, particularly in the sample from a depth of 596.20 m (see Fig. 4.10). Naphthalene is dominant, consistent with findings that methyl groups are lost over time.

4.5: Maturity Parameters

4.5.1: Hopane isomerization

The relative abundance of hopane isomers are thought to reach an equilibrium of 1:1 corresponding to early oil generation (Peters and Moldowan, 1993; Tissot and Welte, 1984). All the Lapa samples have hopane isomerization ratios within a range considered equilibrium (Fig. 4.11), although error bars extend beyond this range.

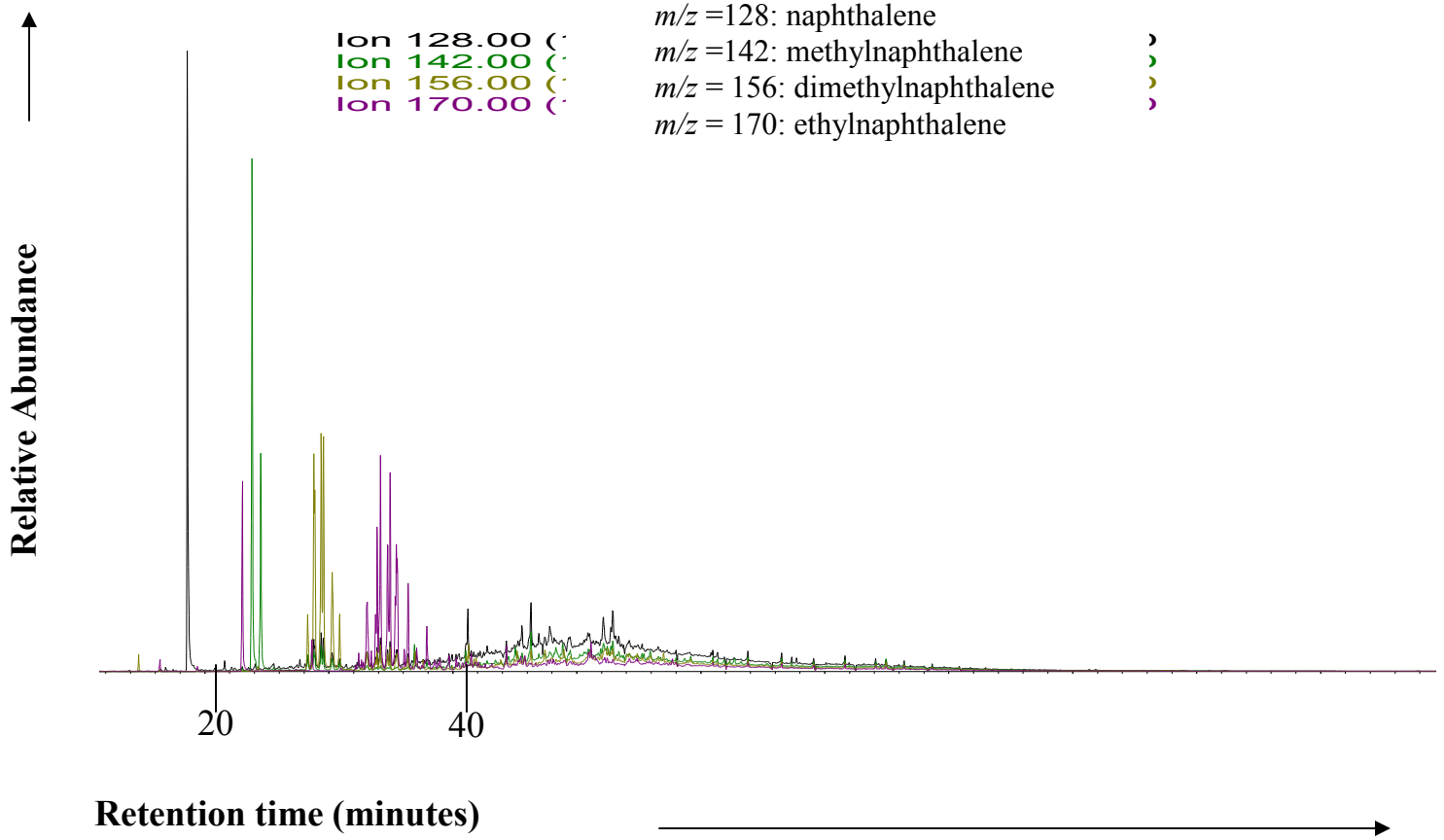

Figure 4.10: Ion chromatogram showing naphthalenes identified in the sample at depth 596.20 m. Labeled are the naphthalenes used to calculate the methylnaphthalene ratio and dimethylnaphthalene ratio (see Table 2.1).

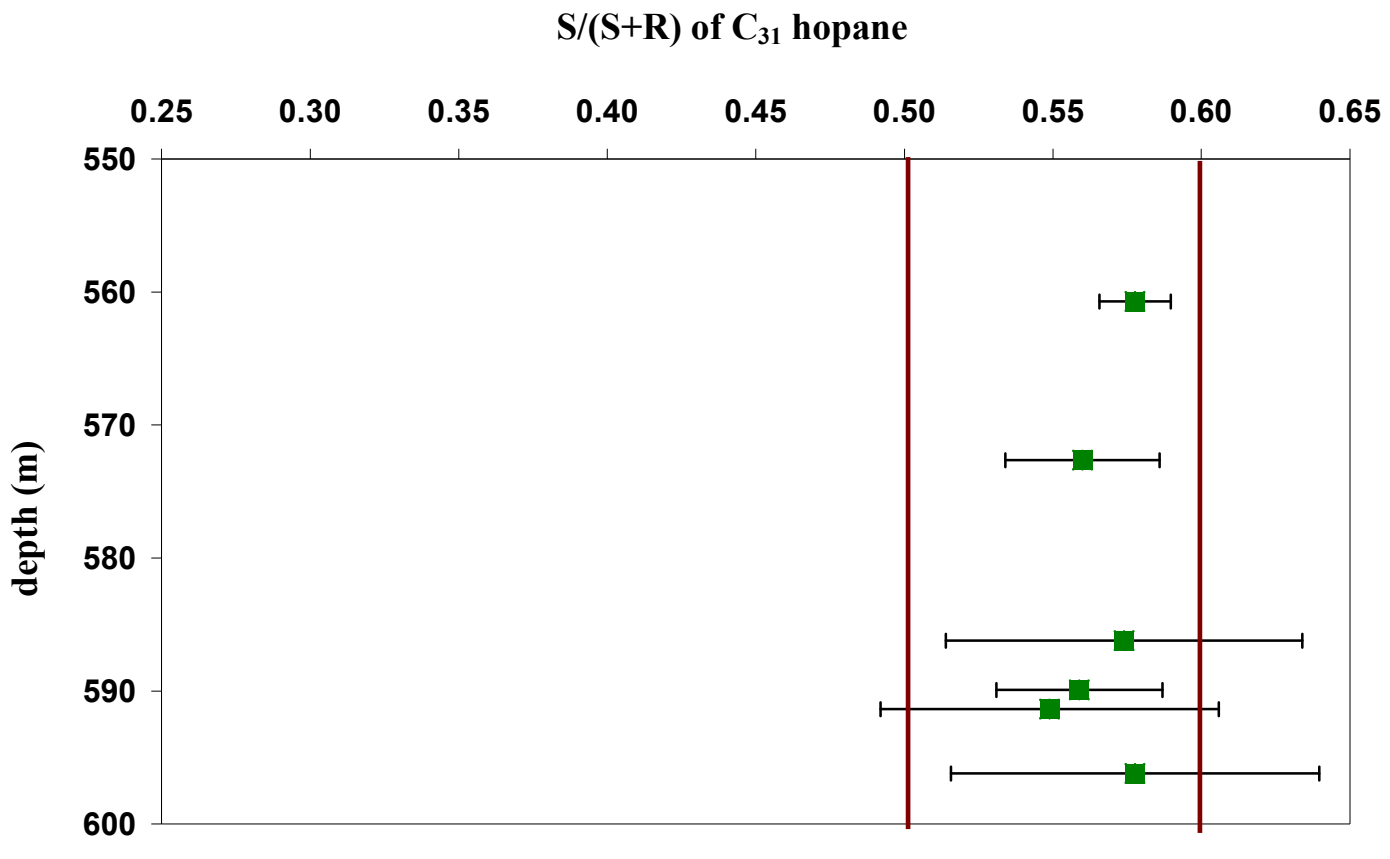

Figure 4.11: Isomerization ratios of the C_{31} hopanes in each Lapa Formation sample. Shown is the standard ratio of the relative amount of C_{31} hopanes having the S configuration vs. the sum of all C_{31} hopanes: S/(S+R). The red lines approximate the equilibrium ratio isomers reach, which for hopanes occurs during early oil generation (Peters and Moldowan, 1993). See Table 4.5 for a complete list of all ratios calculated.

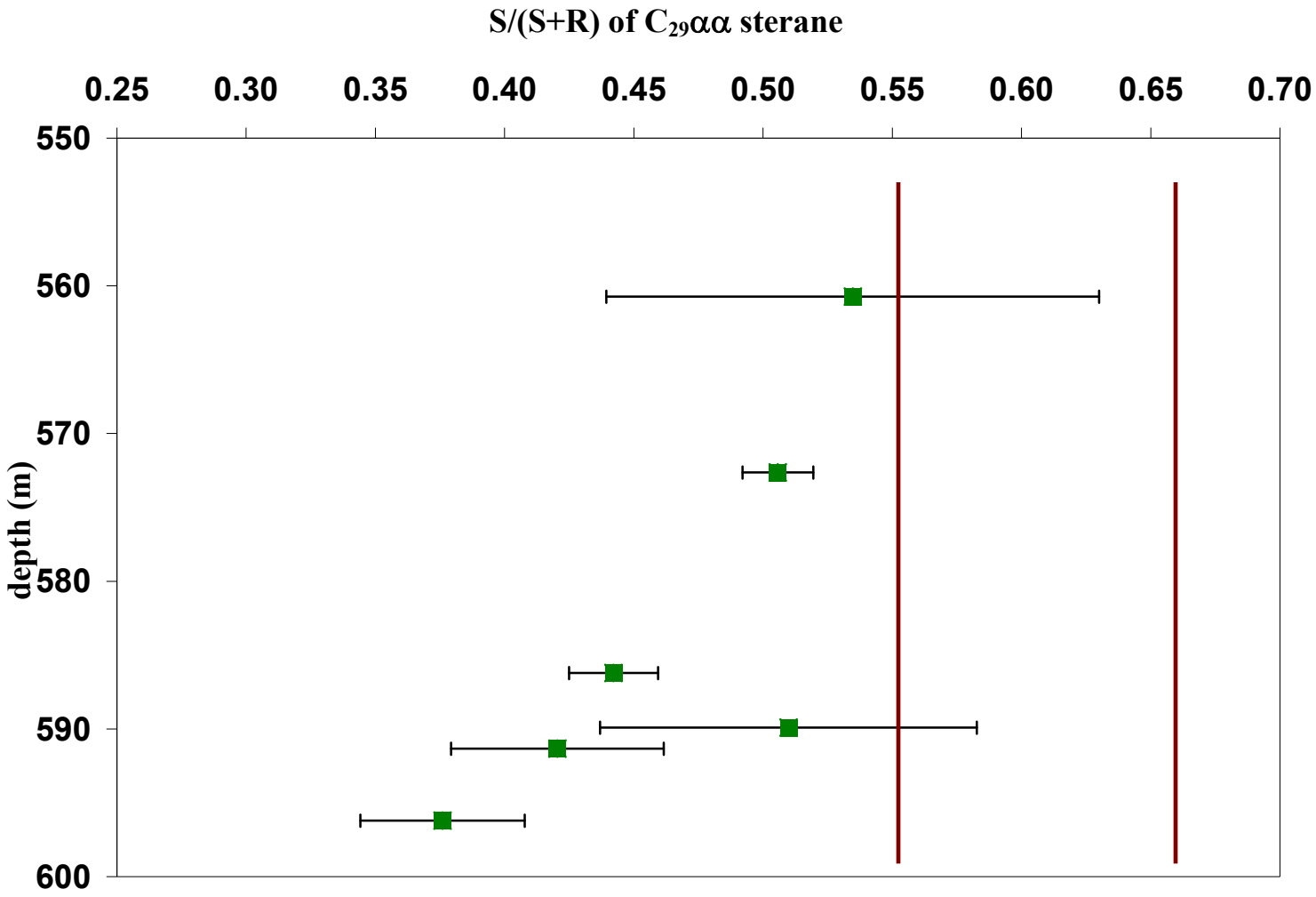

Figure 4.12: Isomerization ratios of the C_{29} steranes in each Lapa Formation sample. Shown is the standard ratio of the relative amount of C_{29} αα steranes having the S configuration vs. the sum of all C_{29} αα steranes: S/(S+R). The red line approximates the range at which isomers reach equilibrium, which for steranes can stretch well into oil generation (Peters and Moldowan, 1993, Tissot and Welte, 1984).

None of the samples is obviously immature. Unlike with the sterane isomerization ratios (see below), the hopane isomerization ratios are consistent among the samples.

The C_{32} hopane ratios are similar to C_{31}, except for the sample at 596.20 m.

The ratios of the rearranged hopane Ts to the rearranged hopane Tm, another measure of maturity, plot close to 1. In the Lapa samples, they are comparable to the C_{31} S/(S+R) ratio (the Ts/(Ts+Tm) ratio would be around 0.5 as well). Interestingly, the sample hosting the quartz intrusion (586.20m) plots consistently with the other samples.

4.5.2: Sterane isomerization

The $C_{29}\alpha\alpha$ isomerization ratio follows a clear trend of decreasing maturity with depth (Fig. 4.12). Even with error considered, samples at 586.20, 591.34 and 596.20 m have $C_{29}\alpha\alpha$ isomerization ratios that are under equilibrium.

None of the diasterane ratios indicate that the samples have reached equilibrium (see Appendix for how C29$\beta\alpha$ was integrated). No obvious trend is visible, except perhaps the same dichotomy seen in other ratios: higher values in the two upper samples (which host the most carbonate) and lower values in the two bottom samples. The sample with the lowest ratio is also the sample that hosts a quartz vein.

4.5.3: Naphthalene ratios

Both the methylnaphthalene ratio (MNR) and dimethylnaphthalene ratio (DNR) (Table 4.3) have been shown to increase with increasing thermal maturity (Radke et al., 1982). All samples except for one at a depth of 596.20 m had naphthalene peaks that also coeluted with peaks of an unknown molecule.

An interesting contrast emerges (Table 4.3). The MNR (1-methylnaphthalene to the rearrangement product 2-methylnaphthalene) has reched equilibrium in all samples and exceeded it in the sample for which elution was cleanest (sample at 596.20 m). The DNR (1,5-dimethynaphthalene to its rearrangement products 2,6-dimethylnaphthalene and 2,7-napthalene) — a slower reaction (Radke, 1982) — is very low for all samples, not even close to equilibrium.

Table 4.4: The methylnaphthalene ratio (MNR) and dimethylnaphthalene ratio (DNR) for all Lapa Formation samples from the MAF 134-86 drill core. --- indicates not determined; n.d. indicates none detected.

Sample	MNR	DNR
560.70m	nd	nd
572.64m	1.35 +/- 0.11	0.30 +/- 0.03
586.20m	1.08 +/- 0.17	0.34 +/- 0.02
589.90m	---	---
591.34m	0.92 +/- 0.11	0.22 +/- 0.01
596.20m	2.33 +/- 0.09	0.28 +/-0.03

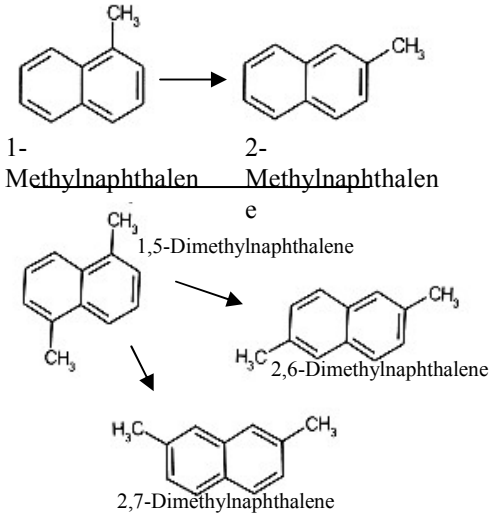

Table 4.5: All biomarker ratios calculated in this study. n.d. indicates none detected.

	Elemental analyses			Isomerization ratios				Rearrangement ratios			Mixed source/maturity ratios		
	TOC (wt. %)	Bitumen (ppm)	%carbonate	C_{29} sterane ααα S/S+R	C_{29} sterane αββ S/S+R	C_{29} sterane αββ/(ααα+αββ)	C_{31} hopane S/S+R	C_{32} hopane S/S+R	Ts/Tm	C_{27} diasteranes/ all C_{27} steranes	Pristane/ Phytane	Phytane/ n-C_{18}	Homohopane index (%C_{35})
560.70m	-----	0.05	75.37%	0.54	0.47	0.47	0.58	0.57	0.90	0.35	0.78	0.54	No C_{35} detected
572.64m	0.23	0.43	69.58%	0.51	0.67	0.49	n.d	n.d	0.79	0.44	0.51	0.30	No C_{35} detected
586.20m	0.22	0.13	6.46%	0.44	0.47	0.46	0.57	0.58	0.85	0.31	n.d	n.d	1%
589.90m	1.45	0.21	n.d	0.51	0.47	0.50	0.56	0.56	0.89	0.36	0.66	0.43	No C_{35} detected
591.34m	3.73	0.93	2.98%	0.42	0.63	0.46	0.55	0.54	0.89	0.36	0.59	0.34	No C_{35} detected
596.20m	0.44	0.21	3.45%	0.38	0.62	0.42	0.58	0.53	0.99	0.30	0.57	0.34	1%

Chapter 5: Discussion

Lacking radiometric age constraints for the Lapa Formation, it is difficult to correlate the time series isotopic compositions of carbon and sulfur and the biomarker distributions determined in this study with any broad Proterozoic interval. However, the general lithologic and isotopic patterns are comparable with known post-glacial phenomena recognized throughout the Neoproterozoic Era. However, given the Re-Os ages older than 1 Ga for the underlying shales of the Serra do Poço Verde and Serra do Garrote formations in the Vazante Group (Geboy *et al.*, 2006), it is possible that the Lapa Formation is also late Mesoproterozoic in age. The discussions below will consider both possibilities.

5.1 Elemental Abundances, Stable Isotopes and Environmental Change

In general, the upper and lower halves of the Lapa Formation sampled in this study from drill core MAF 134-86 differ in lithologic, isotopic, and biomarker compositions. This dichotomy is primarily related to the transition from samples low in carbonate — but high in organic matter and sulfur — at the base of the unit to those having 30% or more carbonate and proportionally lesser amounts of organic carbon and pyrite at the top. Similarly, the bottom half of the formation shows significant variability in carbon and sulfur isotopes, while those in the upper half are relatively stable. The one notable exception is a gradual increase in carbonate carbon isotopes through the top of the measured section.

5.1.1 Glacial implications of carbonate carbon isotopes

In this study, the lithologic transition in the PMA-04 drill core from the Serra do Poço Verde Formation into the Lapa Formation (carbonate diamictite to iron-formation to dropstone-laden organic rich shale to marl and carbonate) is interpreted to be related to glacial and immediate post-glacial processes. Support for the interpretation of the basal Lapa Formation as an unusual cap carbonate lithofacies (organic-rich shales are not commonly found prior to capping dolomites) comes from the regional recognition of a progressive stratigraphic cutout of pre-Lapa sediments derived from drill core data (Brody *et al.*, 2004).

Azmy *et al.* (2006) similarly interpreted the basal Lapa Formation in other cores to be a cap carbonate lithofacies, and suggested a Sturtian (750 Ma) age for this unit. Those authors compared the Lapa succession with the microbial-dominated cap carbonate of the < 748 Ma Rasthof Formation in the Otavi Group in northern Namibia (Hoffman *et al.*, 1996; 1998). In this Rasthof, however, there is no basal organic-rich shale. TOC contents in the Rasthof carbonates are similar to the Lapa carbonates, which are much lower than the basal Lapa Formation shales. Carbon isotope variations through the two post-glacial successions are however similar. The Lapa carbonate carbon isotopes are generally negative, with values as low as -4‰ at the base and middle of the unit. In the lower half the $\delta^{13}C$ values are variable, likely associated with the sources of carbonate ice-rafted debris in these samples. In the upper half, starting with the sample at 579.27 meters, there is a monotonic trend upward to values near zero at the top of the section. Coupled with time series data

from pre-Lapa carbonates (Azmy *et al.*, 2001) there appears to be a ca. 8‰ drop in $\delta^{13}C$ values (from +4 to -4‰) across this glacial divide. These patterns of isotopic variability are similar to those reported for the Rasthof Formation, and many other equivalent pre- and post-glacial deposits of the Neoproterozoic Era (Hoffman and Schrag, 2002; Hoffman *et al.*, 1998).

While the carbon isotope correlation proposed by Azmy et al. (2006) is possible it is a non-unique solution given that the $\delta^{13}C$ composition of seawater proxies oscillated throughout the Neoproterozoic glacial epoch. The specific correlation is supported by the similarity of Sr isotope compositions of well-preserved limestone in the Rasthof Formation and a single dolomitic rim cement from a Lapa Formation dolomite. This evidence is viewed as tenuous, however, given the likelihood of alteration during dolomitization and subsequent exchange of radiogenic fluids with the host rock in the Brazilian example.

If the Lapa carbonates are late Mesoproterozoic in age, the time series $\delta^{13}C$ trends should be comparable with recorded events. In Summarizing Mesoproterozoic carbonate isotopic trends, Kah *et al.* (1999) and Frank *et al.* (2003) show that $\delta^{13}C$ values of seawater proxies shift upward starting around 1250 Ma from near 0‰ to as high as +3.5‰ near to the boundary with Neoproterozoic sediments. This increase in values is viewed as gradual over the late Mesoproterozic because it is punctuated with excursions to negative values. These shifts have been interpreted in light of changing crustal inventories of organic carbon (Kah *et al.*, 2004), but have not previously been related to glacial phenomenon. Frank *et al.* (2003) suggest increased tectonic activity may have affected burial of organic carbon leading to the overall increase in $\delta^{13}C$

values through the interval, but that eukaryotic diversification and the increased preservation of organic carbon in anoxic deep marine environments may also have been factors.

5.1.2 Abundance and isotopic composition of organic carbon

If the basal Lapa Formation is a cap carbonate lithofacies, then the shale samples from the lower half of the formation analyzed in this study are unusual in their organic contents as well as the presence of ice rafted debris. These observations support the idea of high primary productivity and/or preservation of organic carbon in the immediate aftermath of this glaciation. These samples are significantly enriched in organic matter relative to a global survey of Mesoproterozoic and Neoproterozoic shales, which most typically have less than 1 wt.% organic carbon contents (Strauss *et al.*, 1992). The range of $\delta^{13}C$ values in Lapa Formation organic carbon (between -22 and -26‰) is consistent with the overall range of values in late Proterozoic sediments (Hayes *et al*., 1992), in that they are slightly more enriched in ^{13}C than expected for normal photosynthetic inputs. This may be the result of thermal maturation and associated loss of hydrogen from preserved kerogen (H/C ~0.21 in the Lapa), or from some degree of carbon limitation in the depositional environment. In contrast, Rasthof Formation organic matter is significantly enriched in ^{13}C, which suggests clear differences in depositional environments or thermal histories, even if the units are laterally equivalent.

Some possibility remains that organic carbon isotopic compositions were affected by thermal processes. It is also possible that the organic carbon isotopes are

relatively heavy because access to CO_2 was relatively limited and, as with enriched sulfide isotope values, the resulting organic carbon formed from primary production was heavy relative to that formed when CO_2 supply is abundant (Kaufman, pers. comm.). The difference between the carbonate carbon isotopes and organic carbon isotopes can be used to infer the volume of organic carbon buried (Hayes *et al.*, 1992). Given that the isotopes may have been affected by thermal processes, this difference was not calculated for the Lapa samples.

It is interesting to note that the carbonate carbon and organic carbon isotopic compositions do not co-vary. The organic carbon isotopic trends do not show any obvious trend with depth as the carbonate carbon isotopes do.

5.1.3. Trend in the sulfur isotopes

Two striking trends emerge in the sulfide sulfur isotopic compositions of the 40 sampled meters of the Lapa Formation. First, sulfides in the basal half of the formation are unusually enriched in the heavy ^{34}S isotope, with values ranging from +10 to +30‰. Pyrite formed from sulfide produced by bacterial sulfate reduction is expected to have negative values, as bacterial sulfate reduction selects the lighter ^{32}S isotope and can result in fractionation of the product sulfide (relative to that of the starting reactant sulfate pool) as large as 46‰. These anomalously enriched $\delta^{34}S$ values have been noted in several studies of sulfides in cap carbonate lithofacies (Hoffman and Schrag, 2002). Several recent studies suggest that the sulfate concentration in the ocean remained low during the Mesoproterozoic and early Neoproterozoic (Canfield, 2004; Kah *et al.*, 2004; Johnston *et al.*, 2005; Kaufman et

al., 2007), leaving the oceanic sulfate reservoir vulnerable to changes in the isotopic composition of sulfate entering the system during the Neoproterozoic (Kah *et al.*, 2004), with isotopic variation highest by the Neoproterozoic (Canfield, 2004). Postglacial oceans may have been even more vulnerable to rapid sulfur isotope changes because the oceanic sulfate pool may have been largely reduced by bacterial processes under an ice-covered, and hence anoxic, ocean (Hurtgen *et al.*, 2002).

The second striking trend in Lapa sulfide isotopic compositions is the profound (~20‰) upsection decrease in $\delta^{34}S$ values (see Fig. 4.1) over the 40 meters of sampled section. If primary, this trend suggests significant changes in the sulfur cycle, either global or regional, at this time. Models proposed to explain enrichments and extreme stratigraphic variations in $\delta^{34}S$ in other sections generally suggest factors such as environmental stresses caused by oscillations in the chemocline or sea level, variable access to sulfate from weathering, changes in the oxidation state of shallow seawater, or physical changes in a basin restricting access to the open ocean.

Given the wide range of possibilities, and our lack of understanding of sulfur isotope fractionation in this system, it is difficult to point to any one set of events leading to the extreme enrichments in pyrite from the basal Lapa Formation. At the same time, we can compare these results with other formations having similar sulfide isotopic compositions, and discuss the likelihood of different depositional models.

5.1.4 Glacial implications of sulfide sulfur isotopes

Bacterial sulfate reduction requires organic carbon (usually acetate or lactate formed by fermentative processes) as a substrate (see equation in Chapter 2). It has

thus been suggested that increased concentrations of dissolved or particulate organic carbon in the water column can enhance the rate of bacterial sulfate reduction (Logan *et al.*, 1995). If sulfate supply is limited, higher rates of bacterial sulfate reduction quickly remove ^{32}S depleted sulfur from the system resulting in progressive ^{34}S enrichment of residual seawater sulfate. Through this process the isotopic composition of sulfides may, over time, approach that of beginning sulfate. Thus, in the Lapa Formation, the higher concentrations and sulfur isotope compositions of sulfides in the lower half of the formation are consistent with a limited sulfate pool in the immediate glacial aftermath. Lower sulfate concentrations are likely if high rates of primary productivity during post-glacial transgression increased the supply of organic carbon and thereby enhanced the rate of bacterial sulfate reduction. In this model, the upsection decline in $\delta^{34}S$ values may simply be related to a general increase in oceanic sulfate concentrations.

Bacterial sulfate reduction in an ice-covered ocean during a long-lived snowball Earth event could result in quantitative reduction of sulfate so that resulting sulfide would have $\delta^{34}S$ values matching those of beginning oceanic sulfate (Gorjan *et al.*, 2000; Hurtgen *et al.*, 2002). This is possible if the terrestrial flux of weathered sulfur was cut off from the ice-covered ocean. Alternatively, the observed sulfur isotope compositions might reflect the influence of different sulfur bearing pools in the Proterozoic ocean associated with shallowing or deepening of a chemocline separating oxidized and reduced forms of sulfur.

The isotopic compositions of the minor sulfur isotopes ^{33}S and ^{36}S were analyzed to help determine whether the Lapa samples fit any of the published models

for evolution of sulfur isotope values under varying conditions. We make a rough comparison of $\delta^{34}S$ vs. $\Delta^{33}S$ data of the Lapa with one model proposed by Johnston *et al.* (2006) for projecting sulfate isotopic values during the Paleoproterozoic, tested against measured sulfide values. It is a steady-state model that uses experimentally determined sulfate reduction fractionations and assumes that the main sulfide sink is pyrite. We propose that the parabola defined by Lapa sulfides is similar to the curve for sulfides in the Johnston *et al.* (2006) model, if starting sulfate is already highly enriched, as it could be after a glaciation, rather than 0‰ as assumed in the Johnston *et al.* model. This reasoning matches the explanation Johnston *et al.* (2006) give for the enriched sulfide values recorded in the Paleoproterozoic sediments they discuss. Given this assumption, we suggest that the Lapa $\delta^{34}S$ vs. $\Delta^{33}S$ values correlate with decreasing rates of pyrite burial moving upsection, with the most enriched $\delta^{34}S$ values in the lower shale samples representing a high proportion of reduced sulfate preserved as pyrite.

Possible changes that could result in less pyrite burial are 1) oxidation of sulfide as the chemocline moves up in shallowing water (Hurtgen *et al.*, 2002); a 2) decreased rate of bacterial sulfate reduction if the supply of organic carbon decreased, as suggested by the lower TOC values in the carbonate portion of the Lapa; 3) higher levels of primary productivity changing the water column from sulfidic to oxic; or 4) slowing of bacterial sulfate reduction as the water column became more oxic and bacterial sulfate reduction moved into sediments. These changes are consistent with the suggestion that the Lapa shale horizon was deposited during glacial transgression, accessing a limited pool of sulfate enriched in an ice-covered ocean, and that water

chemistry changed to a shallower, carbonate-saturated environment over time. Because the $\delta^{34}S$ sulfide values started at such enriched values, even the extreme change in isotopic composition of preserved sulfides moves to values that are still positive and enriched.

5.1.5. Mixing of sulfate reservoirs

Although the relationship between $\delta^{34}S$ and $\Delta^{33}S$ moving upsection forms a parabola, the values of $\delta^{34}S$ from sample-to-sample vary considerably. The $\delta^{34}S$ values over the 40m sampled decrease from $\delta^{34}S$ values of ~30 ‰ down to values of ~10 ‰, but not in a monotonic fashion (Fig. 5.2) Linear plots of $\Delta^{33}S$ vs. $\delta^{34}S$ (Fig. 5.1) and $\delta^{36}S$ vs. $\delta^{34}S$ suggest this variability signals that sulfate reduction accessed two different sulfate pools that mixed. One pool retains a constant $\delta^{34}S$ value over time resulting in $\Delta^{33}S$ vs. $\delta^{34}S$ values that retain the smooth parabola over time even as $\delta^{34}S$ values vary on shorter time scales, from sample to sample (Fig. 5.2). The second pool could be more restricted because sulfate reduction is occurring in a partially closed basin or in the sediments. This second pool may have had continued but relatively restricted access to the first pool, lending short-term variability to the resulting $\delta^{34}S$ values in the sulfides. The third pool would be the sulfide pool that is sampled here.

Modeling of this mixing model best fits the $\Delta^{33}S$ vs. $\delta^{34}S$ values (Fig. 5.2) when the fractionation factor for sulfate reduction is relatively high at 0.963. This value is feasible based on sulfate reduction rates observed in recent experiments (Farquhar, pers. comm.). It implies that resulting sulfide is relatively heavy for

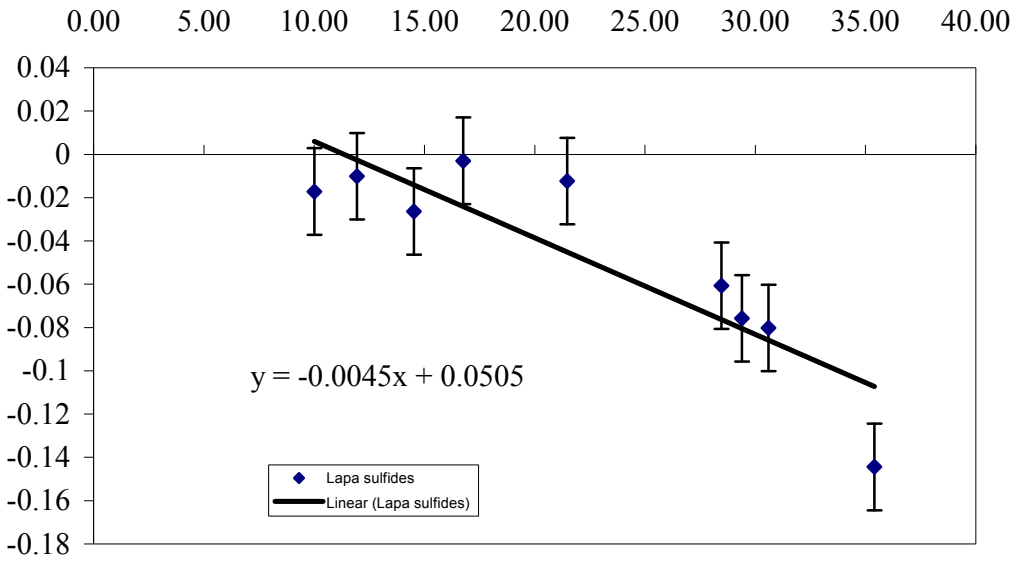

Fig. 5.1: A plot showing the linear relationship of $\delta^{34}S$ vs. $\Delta^{33}S$, where $\Delta^{33}S = \delta^{33}S - (0.5155)\delta^{34}S$. The sulfide values in the Lapa plot close to a line consistent with mixing of two different sulfate reservoirs. Graph supplied courtesy of J. Farquhar.

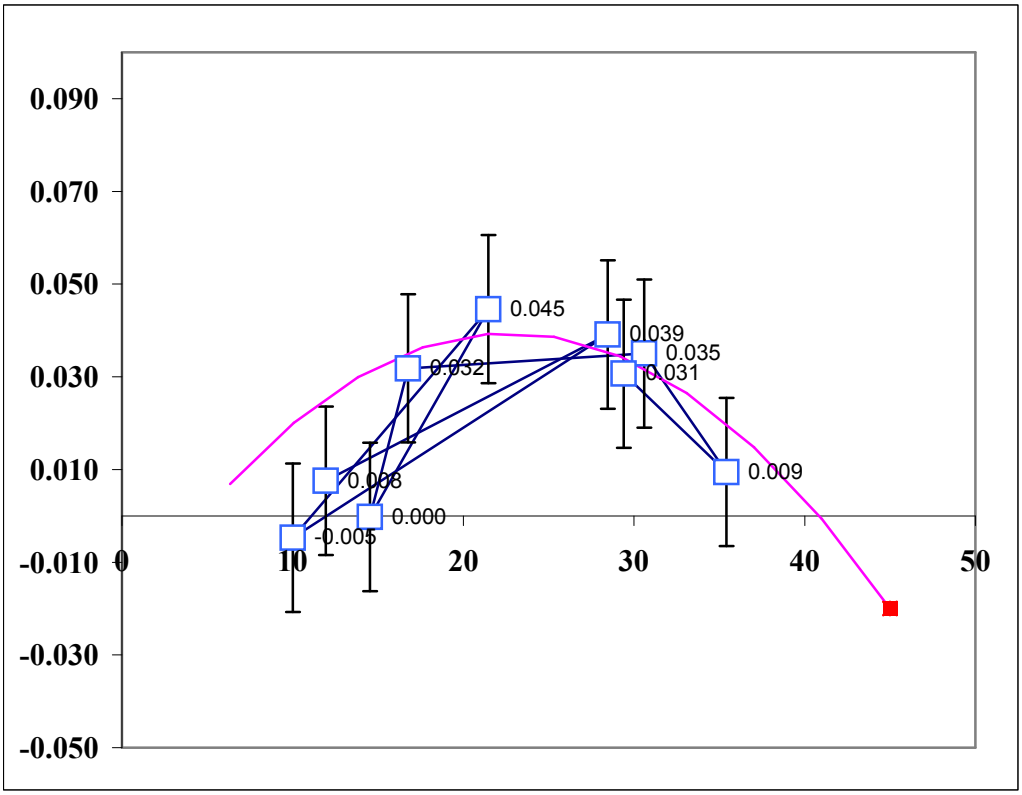

Fig. 5.2: Plot of $\delta^{34}S$ vs. $\Delta^{33}S$ with blue lines connecting $\delta^{34}S$ values, which show significant variation as samples move upsection (right to left on plot). A model of mixing sulfate reservoirs (see Fig. 5.1) is shown by the pink parabola and fits best with a relatively high fractionation factor and starting sulfate $\delta^{34}S$ value of 45 ‰. Blue lines connecting data points show the oscillation of $\delta^{34}S$ values moving from deeper samples (right) to shallower (left). Plot provided courtesy of J. Farquhar.

bacterial sulfate reduction. The model also fits best with a suggested starting $\delta^{34}S$ sulfate value of 45 ‰, within the range of possible sulfate values for this time period as modeled by Johnston *et al.* (2005).

5.2 Basic Characteristics of the Organic Carbon

Brocks *et al.* (2003) established a protocol for showing that extractable organic matter was deposited at the same time as a host rock. Such a protocol is important because the extractable organic matter in which biomarkers are found is mobile and can migrate from its source rock into other facies or even across large lateral distances (Tissot and Welte, 1984). Meteoric waters and hydrothermal fluids can also carry extractable organic matter into a rock. Based on petroleum geochemical methods for matching oils with their source rocks, the Brocks *et al.* (2003) method combines elemental analyses of organic matter (source-rock analyses, TOC and H/C discussed below) with the relative abundances and distributions of as many types of organic molecules and their isomers as possible (essentially, biomarker analyses). It compares what these results, taken together, imply about depositional environment and thermal maturity to what is already known about the depositional and metamorphic history of the host rock. Because organic matter stored in sedimentary rock is not necessarily indigenous to the host rock, analyses of the organic matter cannot be used to determine thermal history of the source rock; the comparison must work in the other direction.

Overall, the source-rock, elementary and isotopic analyses of the organic matter in the Lapa Formation are consistent with other Precambrian samples in that

they match the values seen in mature rocks. It is likely the Vazante Group in the drill core region experienced some level of metamorphism, particularly during the ca. 600 Ma Brasília Orogeny. Even though the samples show characteristics of thermally mature rocks, biomarkers are still present, in concentrations that, like other rocks similar in lithology and thermal maturity, are very low (Brocks *et al.*, 2003). Differences between the Lapa and Serra do Poço Verde formations suggest vertical heterogeneity in the Vazante Group, and reported differences in the Serra do Poço Verde between two cores suggest lateral heterogeneity.

5.3.1: Pyrolysis

Source-rock analyses subject preserved organic matter to pyrolysis to constrain an upper temperature limit for thermal maturity. During the progressive increase in temperature two notable peaks (S_1 and S_2) are monitored. The S_1 peak records the pyrolysis of any hydrocarbons present in a free or adsorbed state. These tend to pyrolyze at about 200 to 250ºC (Tissot and Welte, 1984; note that pyrolysis for the Lapa samples began at 300ºC). The S_2 peak records the pyrolysis of kerogen, which occurs at higher temperatures and mimics the generation of hydrocarbons that would have occurred naturally during burial metamorphism. The failure to detect the S_2 peak during source-rock pyrolysis implies that the organic matter still present in the rock already reached temperatures high enough to generate hydrocarbons, or that the amounts of organic matter were too small for detection.

None of the Lapa Formation samples analyzed revealed an obvious S_1 peak, indicating that there are no free hydrocarbons or too few to detect above 300ºC. This observation is consistent with the extremely low percentages of extractable organic matter in the Lapa (see below), and supports the idea that the extractable organic matter is bound in the kerogen and more likely indigenous to the host rock.

On the other hand, all Lapa Formation samples had a definable S_2 peak, suggesting that the kerogen did not experience temperatures (T_{max}) above 465^{o}C. The S_2 peak is not sharp, and in some samples two small peaks are discernable. The small concentrations of organic matter in the rocks made analyses difficult. As a comparison, samples from the Lapa portion of core MAF 42-88 were also analyzed. None showed an S_2 peak. The differences between the two cores most likely reflect the composition of the samples rather than analytical error. The appearance of an S_2 peak suggests the organic matter in the kerogen may not have reached lower greenschist metamorphic temperatures. This contrast may suggest that a nonnative, less mature oil migrated into the samples. At the same time, temperatures for lower greenschist metamorphism are not absolutely defined, so it is not possible to conclude that the volatilized organic matter is foreign.

Alternatively, what has been defined as an S2 peak could in fact be an S1. The very low concentrations of free hydrocarbons in the samples may have naturally exceeded 300ºC and remained to be volatilized. Biomarker molecules, which can exist in the free or adsorbed hydrocarbon fraction, remain intact at temperatures above 200ºC (Brocks *et al*., 2003). This explanation could provide a reason for why some "S2" peaks appear bimodal (see Fig 4.1).

Pyrolysis during Source-Rock analysis suggests the presence of organic matter in the Lapa that did not reach greenschist temperatures, although interpretations of Source-Rock data on such low concentrations of organic material must be made with caution. The source-rock analyses results suggest that organic matter in the Lapa Formation samples experienced temperatures above 300^{o}C but below 465^{o}C. Greenschist facies rocks are believed to have experienced temperatures between 400 and 500^{o}C. It is difficult to say from the source-rock pyrolysis whether the organic matter clearly experienced (sub-)greenschist levels of metamorphism.

5.3.2: H/C ratios

Elemental ratios in kerogen may also be used to estimate thermal histories. The H/C ratio in modern, unaltered sedimentary organic material is generally 1.4 or higher. Hydrogen atoms are expelled during thermal maturation resulting in lower H/C. Ratios lower than 0.7 tend to correlate with kerogen that has progressed beyond gas generation (Peters and Moldowan, 1993), but kerogens with values down to 0.2 are believed to retain depositional carbon isotopic signatures (Strauss *et al.*, 1992).

The two analyzed Lapa Formation kerogens had identical H/C ratios of 0.21 suggesting that carbon isotope compositions of the bulk organic matter can be interpreted as depositional in origin. Nonetheless, the kerogen has experienced significant hydrogen loss. Published H/C values for the underlying Serra do Poço Verde in core MAF 42-88 range between 0.04 and 0.97 (Olcott *et al.*, 2005). This wide range of values is difficult to understand in metamorphic terms, but perhaps not in terms of mineralization fluids. In pyrolysis experiments, free hydrocarbons

volatalize between 200º and 250º. Mineralization temperatures may have reached 240ºC in the Morro Agudo mine (Hitzman et al., 1996) if it is an Irish-type deposit (Monteiro *et al*., 2006). The paths of these fluids can vary, and some of the Poço Verde samples may have been affected differently than others. It is possible that some samples originally hosted low concentrations of organic matter vs. others, and the H/C ratios were difficult to detect and thus unusually low. This interpretation is less likely, though, because most of the lowest H/C values occur in samples with the higher EOM values, and shales and carbonates alike can show low H/C values.

5.3.3: Percent EOM

Concentrations of extractable organic matter in the Lapa Formation samples were very low with all samples less than 1 ppm. These concentrations generally vary with TOC contents and are extremely low (they are all less than 0.05% of the TOC), consistent with the interpretation that the EOM is directly associated with the kerogen and likely indigenous to the host rock and (Tissot and Welte, 1984; Peters and Moldowan, 1993).

Bitumen was not extracted from Serra do Poço Verde Formation samples from core MAF 134-86. In core MAF 42-88 of the same interval, Olcott *et al.* (2005) report EOM concentrations ranging between 2.4 and 10.8 ppm. These concentrations in the synglacial shale are an order of magnitude greater than in samples from the post-glacial shale of the Lapa Formation. Olcott *et al.* (2006) suggest that the correlation of TOC and EOM in their samples across various lithofacies (shale, carbonate, and diamictite) indicates that the organic matter was indigenous to the host

rock. EOM concentrations in this study are likely too low to make an equivalent assessment of environmental gradients, although the time-series isotopic compositions suggest a strong environmental control on sediment chemistry. The relatively small EOM values compared with those for the Serra do Poço Verde Formation in core 42-88 suggest that 1) relatively little soluble organic matter was preserved in the Lapa and/or 2) most of the preserved soluble organic matter was lost during thermal maturity and/or 3) most of the original soluble organic matter was lost and much of the organic matter extracted represents soluble, mobile, less mature hydrocarbons that were introduced after burial and mixed with remaining bitumen.

Given the low H/C ratios and poorly defined S2 peaks in the Lapa samples, it is possible that much EOM could have been lost during thermal maturation. However, the contrast of some higher H/C ratios and more EOM in the underlying Poço Verde shales is difficult to reconcile with regional metamorphism of the Vazante Group. Thermal gradients can vary vertically over hundreds of meters, but only by tens of degrees (Tissot and Welte, 1984), so the units would never have experienced strongly different temperatures. Furthermore, temperature should have increased with depth, causing more alteration in the older units (Tissot and Welte, 1984). There is no evidence for igneous intrusions in any of the cores sampled or in the Vazante Group. Mineralization fluids may have caused differential heating, but these fluids likely only reached temperatures as high as 240ºC in the Morro Agudo mine (Hitzman *et al.*, 1996 and Monteiro *et al*., 2006).

On the other hand, the elemental contrast between the shales might reflect depositional differences in the original amount of organic carbon preserved, assuming

the units are broadly equivalent in age. The presence of a regional unconformity beneath the Lapa Formation makes it possible that the Vazante succession is diachronous: capturing two glacial events, with each age interval experiencing different degrees of alteration. It is more likely that both the Lapa and Serra do Poço Verde shales experienced similar temperatures and similar relative losses of organic matter, but that the Serra do Poço Verde was the more organic rich interval initially. Notably, H/C and organic extractions from the Serra do Poço Verde in core MAF 134-86 were much different from the same formation in core MAF 42-88 (Olcott, pers. comm.), hinting at lateral heterogeneity.

5.3.4 Contamination

EOM is vulnerable to contamination by migrating hydrocarbons, drilling fluids, contamination during core storage, biodegradation, migrating fluids, and organic materials in lab supplies.

The laboratory blank for the Lapa samples as well as those from the Olcott *et al.* (2005) study showed no identifiable modern contaminants (see Appendix), suggesting that significant amounts of contaminants were not introduced during preparation and analysis of the samples. Key differences in the biomarker suites from the two intervals further reduce the possibility of contamination by drilling fluids.

Most notable, however, is the relative distribution of the three main types of steranes. The organic matter shows roughly equal amounts of all three types, and not a dominance of the C_{29} steranes, which is considered a signature of terrestrial plant material. This observation indicates that the preserved EOM in these sediments did

not migrate from Phanerozoic-aged successions, and that modern meteoric waters have not contaminated the samples.

The sample at depth 586.20m hosts a quartz grain and was selected to test whether fluid infiltration altered the organic matter in this horizon in discernable ways. The elemental data for this sample are not clearly different than for the other samples, but this similarity does not imply that all the samples were affected by fluid infiltration. Processes affecting the elemental characteristics of the organic matter could have occurred after fluid infiltration.

5.4 Biomarker Analyses

Relative abundances of biomarkers and biomarker isomers have been used to understand the degree of thermal maturity the organic matter experienced as well as characteristics of its source. The Lapa Formation biomarker data are interpreted with both perspectives, first focusing on thermal maturity and then discussing trends in the biomarker abundances that correlate with lithologic differences in the host rock. Discussions of thermal maturity are based on the idea that the Vazante Group experienced lower greenschist metamorphism, although a detailed metamorphic history of the drilled area is not available. The abundances are also discussed in relation to interpretations made in this study about depositional environment.

5.4.1: Normal alkanes

Compared to other Precambrian biomarker studies, the Lapa Formation samples of core MAF 134-86 are unusual in that every sample studied hosts a

bimodal pattern of normal alkane (*n*-alkane) abundance (see Fig. 4.10), and a key indicator of thermal maturity shows a decrease in maturity with depth (see below).

The distribution of the *n*-alkanes in the Lapa Formation samples spans the range of expected molecular weights, however, the bimodal distribution of these molecules is recorded in both shale and carbonate lithologies. In addition, the *n*-alkane fraction no longer retains an odd- or even-carbon number predominance, a biological feature lost with thermal maturity (Peters and Moldown, 1993; Tissot and Welte, 1984). Bimodal patterns are also lost with thermal maturity beyond early to middle oil generation (Peters and Moldowan, 1993; but see Amijaya *et al.*, 2006 who report the retention of *n*-alkane bimodal patterns in coals of high maturity).

Distributions of normal alkanes can be affected by fluid infiltration (called "water washing"; Mauk and Burruss, 2002), biodegradation, and source (Peters and Moldown, 2005). The Lapa *n*-alkanes are likely not showing a signature of biodegradation, which preferentially depletes the C_{17} and C_{18} homologues before it does pristane and phytane (Peters *et al*., 2005). The phytane/C_{18} ratio is generally at or below 0.5 in the Lapa. The ratio of rearranged steranes (diasteranes) to all steranes, which are low, also does not support an interpretation of biodegradation. Seifert and Moldowan (1979) show that regular steranes are consumed before diasteranes.

In four of the six Lapa Formation extracts, the distribution of *n*-alkanes shows a general predominance of the heavier alkanes relative to the lighter. (The sample at 572.64 m is an exception insofar as it has a spike in the amount of C_{15} relative to the other *n*-alkanes below C_{21}.) This overall predominance of heavier alkanes could reflect either the preferential loss of lighter alkanes when the samples were

evaporated during evaporation, or it could reflect the preferential loss of the lighter alkanes during water washing (Mauk and Burress, 2002).

A bimodal pattern of normal alkanes was recorded in only one of the Serra do Poço Verde Formation samples (from a "transitional" marl lithology) analyzed by Olcott *et al.* (2005; Olcott, pers. comm.), making less likely that the unusual biomarker signature represents contamination by drilling fluids, which would similarly affect all samples in the drill core regardless of age.

That every sample has two peaks can also indicate the presence of more than one oil, and that the characteristic *n*-alkane patterns of each oil are overlapping.

5.4.2: Pristane and phytane

Pristane and phytane are isoprenoids (see Chapter 2) thought to form from phytol ($C_{20}H_{40}O_2$), a side chain of chlorophyll, either via decarboxylation, which results in loss of a carbon and formation of pristane ($C_{19}H_{40}$); or by reduction, which results in phytane ($C_{20}H_{42}$; loss of the very electronegative O_2 in essence reduces the terminal carbon). Welte and Waples (1973) show that reduction of phytol is more likely under reducing conditions. As a result, the relative abundance of pristane to phytane in preserved organic matter can be an indicator of the redox level of the source environment.

All of the pristane/phytane ratios in the Lapa Formation samples are lower than 1, suggesting reducing conditions. The ratio can increase with thermal maturity to values greater than 1, but the low values found in the study suggest that the ratio

was not greatly affected by heating of the sediments. Thus, we interpret the pristane/phytane ratios in terms of environment of the source of the organic matter.

As with every other biomarker ratio analyzed, the two lower shale samples have similar pristane/phytane ratios. Except for the sample at depth 572.64m, the ratios gradually increase, even with error considered, which could suggest increasing oxygen concentrations, although still within predominantly reducing conditions. Peaks could not be integrated for the sample at depth 586.20m. Either the sample at 572.64m falls out of the trend of increasing values, or all the remaining values are variable without any trend; samples are too few to tell. Either way, the variability suggests different source conditions.

5.4.3: Regular hopanes and rearranged hopanes

Hopane isomerization ratios in all of the Lapa Formation samples in this study tell a consistent story about thermal maturity; these include 1) the homohopane index, which is the ratio of the C_{35} hopane to all other hopanes (the heavier hopanes are thought to degrade over time); 2) the isomerization of the C_{31} hopane and 3) the ratio of rearranged, thermally stable hopane Ts to the less stable Tm.

All the samples have homohopane contents of 1% or less. The C_{31} hopane isomerization ratio for these samples reached thermal equilibrium at a value around 0.5, which is within the oil generation window (Peters and Moldowan, 1993). Work has shown that C_{31} isomerization ratios do not increase beyond 0.5 even if thermal maturation continues (until the point where some molecules disappear altogether)

(Peters *et al.*, 2005, Tissot and Welte, 1984), so this must be considered a minimum estimate of thermal maturity.

The Ts/Tm values are also close to unity with the exception of the sample at 572.64 m (0.79), which is much lower than values for the other samples. These ratios support the interpretation that the organic matter in these post-glacial sediments reached temperatures of at least early oil generation (Peters and Moldowan, 1993).

The hopane isomerization ratios Olcott *et al.* (2005) report for the underlying Poço Verde Formation are also consistent among samples and fall within equilibrium values, suggesting that the organic matter in this horizon also reached early oil generation maturity.

5.4.4: Steranes

The isomerization of the $C_{29}\alpha\alpha$ sterane is considered an ideal indicator of thermal maturity because it may not attain equilibrium until well into the oil generation window (Tissot and Welte, 1984). Thus it provides information the hopane isomerization ratio does not.

In strong contrast with the consistency of hopane and rearranged hopane ratios, significant variations are recorded in the Lapa Formation sterane ratios, which appear to increase upsection through the 40 sampled meters (see Fig. 4.12). This trend suggests that the relative maturity of the organic matter decreases with depth. The reverse is expected, as lower, older samples should host older organic matter and also experience higher burial temperatures. This unusual trend in the sterane isomerization ratios suggests complexity. It also suggests that organic matter in the

lower samples reached temperatures high enough for hopane isomerization to hit equilibrium, but not high enough for sterane isomerization. The sterane isomerization ratios Olcott *et al.* (2005) report for the underlying Poço Verde Formation are consistent among the samples and within equilibrium values (Fig. 5.3).

5.4.5 Uneven heating?

Raymond and Murchison (1986) show that maturity parameters of saturated and aromatic hydrocarbons can reverse or fail to reach equilibrium under the rapid heating of igneous intrusions, vs. the slow heating of burial metamorphism. Also, Peters *et al.* (1990) show that the $C_{29}\alpha\alpha$ S/(S+R) and the C_{29} $\beta\beta/(\alpha\alpha+\beta\beta)$ ratios inverted in pyrolysis experiments at temperatures above 300ºC. No evidence for igneous intrusions is seen in the Lapa Formation in the examined core. On the other hand, mineralization fluids may have reached temperatures as high as 240ºC (see Chapter 1). Thus, it is possible that hydrothermal fluids were high enough to cause inversions of isomerization ratios.

5.4.6 Evidence of a migrated oil?

The ratio of $C_{29}\beta\beta$ steranes to the sum of $C_{29}\beta\beta$ and $C_{29}\alpha\alpha$ steranes reaches 0.75 at equilibrium (Peters and Moldowan, 1993; Chiron, 2005 and references therein). Paradoxically, the shale samples having the lower $C_{29}\alpha\alpha$ isomerization

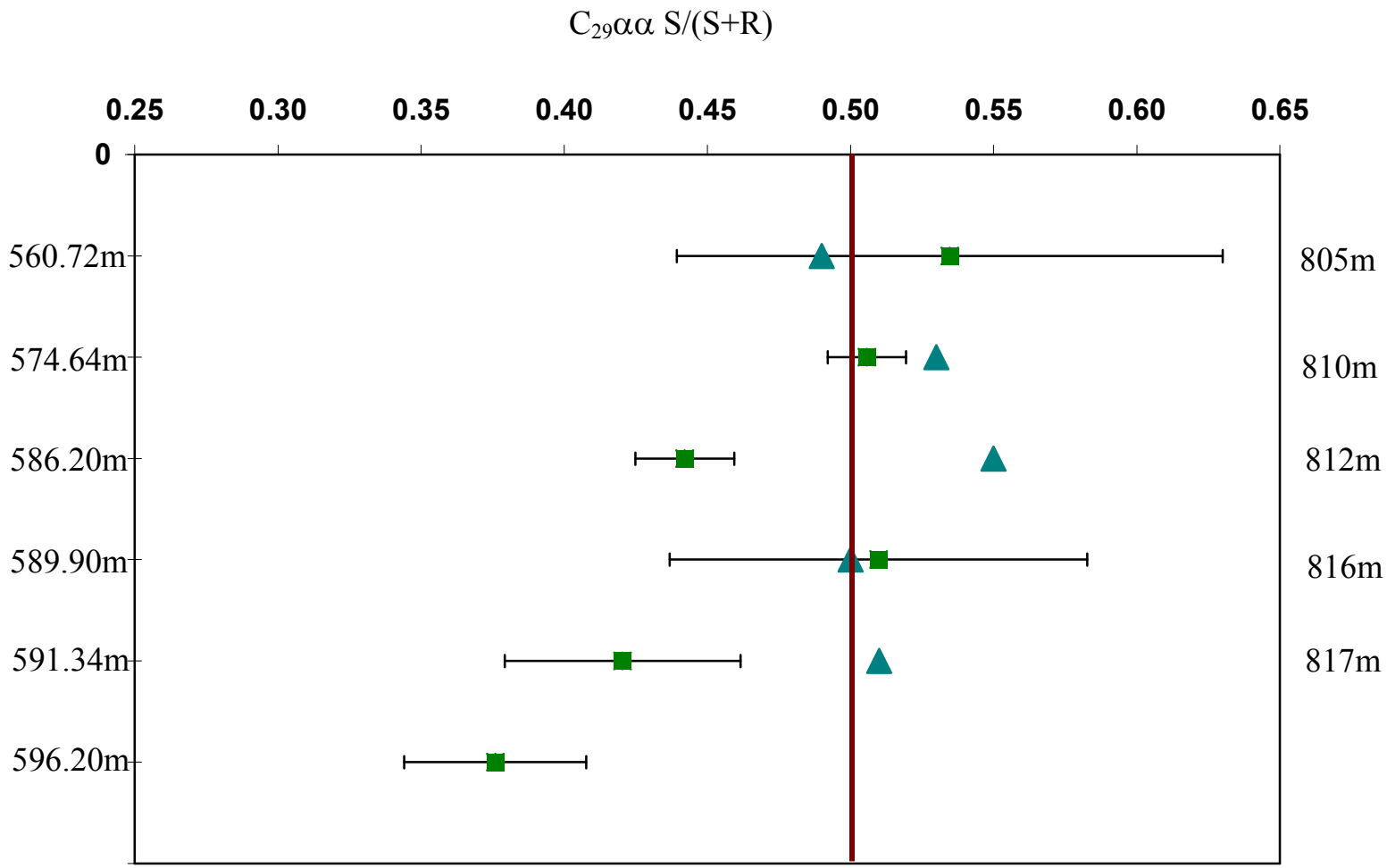

Fig. 5.3: A comparison of C_{29}aa isomerization ratios for the Serra do Lapa Formation (green squares) and those reported by Olcott *et al.* (2005) for the Serra da Poço Verde Formation (blue triangles). The Serra do Poço Verde values do not show the marked trend of decreasing maturity with depth.

ratios have the higher $C_{29}\beta\beta/(C_{29}\beta\beta + C_{29}\alpha\alpha)$, and the sample at depth 572.64m groups with them, while the other three share a value of 0.47.

It is better to make thermal maturity interpretations based on the $C_{29}\alpha\alpha$ isomerization ratios because their elution through GCMS is more reliable and less prone to interference (Eigenbrode and Summons, pers. comm.). Nonetheless, the discrepancies between these two ratios within each of the lower shale samples could suggest a mixing pattern, particularly when considered with other evidence for possible mixing, as discussed above. Zhusheng *et al.* (1988) performed lab experiments that suggested that ββ-steranes are preferentially removed during expulsion of oil from a source rock, and that αα-(20S) steranes could be removed before αα-(20R). In this light, the dominance $C_{29}\beta\beta$ steranes in the lower two shale samples could indicate that an expulsed oil enriched in these isomers migrated in to these horizons. At the same time, these samples are relatively depleted in $C_{29}\alpha\alpha$-20(S). Given the better resolution of $C_{29}\alpha\alpha$ steranes in GCMS, it is better to focus on the $C_{29}\alpha\alpha$ trend discussed above.

If migration occurred, the less mature oil did not rise above the sample at 589.90 m depth, perhaps because the shale and diamictite lithofacies are more permeable than carbonate. The bimodal pattern of the *n*-alkanes also supports the interpretation of mixing, except that this pattern, unlike the $C_{29}\alpha\alpha$ sterane pattern, is seen in all the analyzed samples. There is variation among the *n*-alkane biomodal patterns, as described above, which can be interpreted in terms of lithology and/or the suggestion that a migrated oil only entered the bottom three samples, bringing a

relatively larger volume of higher-chain *n*-alkanes (and the $C_{29}\alpha\alpha$-20(S) and $C_{29}\beta\beta$ sterane isomers) with it.

The Vazante Group lies in the southern portion of the Brasilia Fold Belt, which has been deformed into an imbricated series of nappes (Dardenne, 2000) that has left many conduits and fractures for oil migration over large and small scales. The presence of an unconformity at the base of the Lapa Formation is suggested by well log data from exploration drill cores. (de Oliveira, pers. comm.) Unconformities can allow oil to migrate from one basin to another, as in the case of the Athabasca tar sand in Canada, which hosts an oil deposit covering several hundred square kilometers that could have migrated there via the Cretaceous-Paleozoic unconformity in Western Canada (Tissot and Welte, 1984).

The varying flow of mineralization fluids reaching possible temperatures of 240ºC could also have affected the organic matter, or introduced new organic matter.

5.4.7: Aromatics: naphthalenes

When heated, 1-methylnaphthalene can convert to 2-methylnaphthalene, and 1,5-dimethylnaphthalane can convert to 2,6-dimethylnaphthalene and 2,7-dimethylnaphthalene (see Table 2.1). Thus, the methylnaphthalene ratio (MNR) and dimethylnaphthalene ratio (DNR) can be used as additional tools for determining degree thermal maturity. In the Lapa, MNR is 1 or higher for all the samples, but DNR is well below 0.5 (Table 4.4). The DNR conversion is relatively slower (Radke *et al.*, 1986).

If maturity only reached the early oil generation window, as suggested by the samples in the lower part of the Lapa, maturity was perhaps high enough for the MNR conversion but not for the DNR conversion.

5.5 Lithologic Trends

Most of the samples in the lower portion of the Lapa are relatively carbonate free, while all the samples in the upper 20 m host at least 30% carbonate. A similar dichotomy is seen in the concentration of organic carbon and sulfide, as discussed above, and also in the relative abundances of some of the analyzed biomarkers.

The biomodal pattern in the *n*-alkane fraction is seen in all samples, but is slightly different in the two carbonate samples than in the shale samples. These two host a relatively higher amount of smaller-chain hydrocarbons, while the lower shale samples host a relatively higher amount of longer-chain hydrocarbons (see Figs. 4.4 and 4.5). In contrast, the *n*-alkane fractions in samples from the Serra do Poço Verde of core MAF 42-88 show the opposite trend, with carbonates hosting more longer-chain hydrocarbon than the shales (Olcott, pers. comm.). Whether these n-alkane distributions represent different sources is difficult to determine. Source environment can imprint an odd-over-even or even-over-odd predominance in the *n*-alkane families (Tissot and Welte, 1984), but time and thermal maturity have erased these patterns in the Lapa.

The relative distributions of the three main types of steranes — C_{27}, C_{28} and C_{29} — can indicate variations in source environment of organic matter. Huang and Meinschein (1979) surveyed Phanerozoic oils and showed that the relative

distribution of the three main types of sterols varies according to depositional environment, and that this distribution is retained during the conversion to steranes. In the Lapa, the strongest grouping on the ternary diagram (Fig. 4.9) is of the three bottom shale samples, which are low in carbonate. The three higher samples, including the two highest in carbonate, do not plot in the same region, and are somewhat more variable. The lower three samples could contain organic matter from the same source, either because their depositional environments are similar or because migrated oil is present in all three. One argument against the latter is idea is that the sample at depth 589.90 m does not have as extreme an enrichment in $C_{29}\alpha\alpha$(S) steranes as the two shale samples lower in the core.

A ternary diagram comparing the reported sterane abundances reported by Olcott *et al.* (2005) with those of the Lapa show that the samples from the underlying Poço Verde plot in a significantly different portion of the diagram (Fig. 4.9). This difference is consistent with the suggestion that the Poço Verde organic matter, interpreted as synglacial, experienced a different depositional environment than that in the Lapa, which is interpreted as postglacial.

The ratio of the rearranged sterane (diasterane, C$\alpha\beta$) to all steranes can vary with clay content, because clay can catalyze Diasterane formation (Mackenzie et al., 1980). The diasterane/sterane ratios are fairly consistent among all the samples, with a range of 0.30 to 0.35 and one sample, at depth 572.54m, with a ratio of 0.44. All of these are lower than 1. There is no grouping that coincides with groupings seen in the *n*-alkane fractions and sterane distributions.

Some studies show that the Ts/Tm ratio in the hopane family can also vary according to clay or carbonate content (*cf.* Peters and Moldowan, 1993). These ratios are also fairly consistent among all the samples and less than 1, although the sample at depth 572.64m has a Ts/Tm value much lower than the other samples. Van Graas (1990) suggests that the Ts/Tm ratio can exceed 1 under temperatures extending beyond early oil generation into the oil/condensate threshold.

Chapter 6: Conclusions

The Lapa Formation of the Vazante Group in south-central Brazil is interpreted as a post-glacial, cap carbonate-type deposit. This interpretation is based on similarities in lithology and carbonate carbon and sulfide isotopic compositions between the Lapa Formation and other deposits interpreted as cap carbonates following Neoproterozoic ice ages. This study builds on the Re-Os age constraints of Geboy *et al.* (2006) for the underlying Serra do Poço Verde shale — which suggests low latitude glaciation at about 1.13 Ga — and proposes that the Lapa Formation may also represents a post-glacial Mesoproterozoic event.

The shale portion of the Lapa Formation analyzed in this study hosts high concentrations of organic matter in comparison with other cap carbonate successions. The organic-rich shale was likely deposited during maximum flooding and high primary productivity stimulated by excess nutrients (including sunlight) at the onset of glacial transgression, and is a lithofacies not commonly seen in other capping dolomites worldwide. As relative sea level shallowed, carbonate accumulation proceeded and organic concentrations decreased in the Lapa succession. Carbonate in both the shale and marly facies are characteristically depleted in ^{13}C as noted in cap carbonates worldwide, but $\delta^{13}C$ values do rise in the upper part of the sampled section to near 0‰.

The sulfide values in the basal shale are particularly high (up to +30‰), and could have been driven up by a combination of factors including higher rates of bacterial sulfate reduction and/or a smaller pool of oceanic sulfate. The latter may have been the consequence of long-term anoxia and water column bacterial sulfate

reduction during the ice age, while the former was likely associated with an increased supply of organic carbon from enhanced primary productivity in the glacial aftermath. Upsection there is a marked decrease in $\delta^{34}S$ values, perhaps suggesting an increase in shallow marine sulfate and oxygen concentrations. This view is consistent with measurements of $\Delta^{33}S$ in extracted sulfides, which may be interpreted in terms of an upsection decrease in pyrite burial (Johnston *et al.*, 2006) associated with changing environmental conditions.

The decrease in $\delta^{34}S$ values is not monotonic. This trait, taken together with comparisons between the minor and major isotope values, suggests that deposition occurred in a partially restricted environment. Sulfate reduction may have occurred in the water column of a partially closed basin with periodic communication with sulfate of the open ocean. Alternatively, sulfate reduction may have occurred in sediments, with limited but periodic access to pore-water sulfate.

Soluble organic matter was extracted from Lapa Formation samples in order to understand biological activity during post-glacial deposition and for comparison with the previously studied syn-glacial shale from the underlying Serra do Poço Verde Formation (Olcott *et al.*, 2005). The organic matter preserved in the Lapa progressed at least as far as early oil generation, based on the consistency and equilibrium values of hopane ratios. Whether the organic matter reached temperatures similar to lower greenschist metamorphism cannot be determined.

A distinctive trend of decreasing maturity with depth in the $C_{29}\alpha\alpha$ sterane isomerization ratios suggests that the organic matter in the lower shale samples is less mature than that in the carbonate samples; or that it is enriched in the $C_{29}\alpha\alpha$-20(S)

and $C_{29}\beta\beta$ steranes. Either perspective is consistent with the suggestion that another oil migrated into the Lapa from below. The oil is likely not Phanerozoic, based on sterane distributions

The normal alkane and the sterane fractions in the organic matter demonstrate different characteristics in the shale samples vs. in the carbonate samples, whereas the hopane biomarker ratios tell a consistent story. The differences in the alkane and sterane fractions could reflect variations in the original source of the organic matter, either because of different depositional environments of the host rock or because soluble organic matter from an external source (but Precambrian in age) mixed with indigenous organic matter in the Lapa sediments. As the sediments show signs of fracture and sulfide mineralization in veins, contamination is suspected. The trend of decreasing maturity with depth in the isomerization ratio of the $C_{29}\alpha\alpha$ steranes suggests the introduction of a migrated oil via the unconformity at the base of the Lapa Formation.

Inconsistencies among biomarker abundances — specifically in the *n*-alkane, sterane and naphthalene families — make it difficult to make a strong case that all of the extracted organic matter is indigenous to the host rock. Direct comparisons of source and maturity parameters analyzed in this study with those analyzed in the Olcott *et al.* (2005) study of the underlying Serra do Poço Verde Formation suggest both lateral and horizontal heterogeneities of biomarker distributions in the Vazante Group shales. Differing pathways of migrating fluids through the Vazante Group could be possible causes for this heterogeneity. On the other hand, if these units are of markedly different age, the biomarker variability may be a function of environment

and time. The data from this study and that of Olcott *et al.* (2005) reveal enough inconsistencies to suggest the need for a more comprehensive perspective. Studying samples from additional cores and a variety of depths can help to complete a better picture of both the depositional and postdepositional processes in the Vazante Group.

Appendix

A.1. Additional sulfur minor isotope data

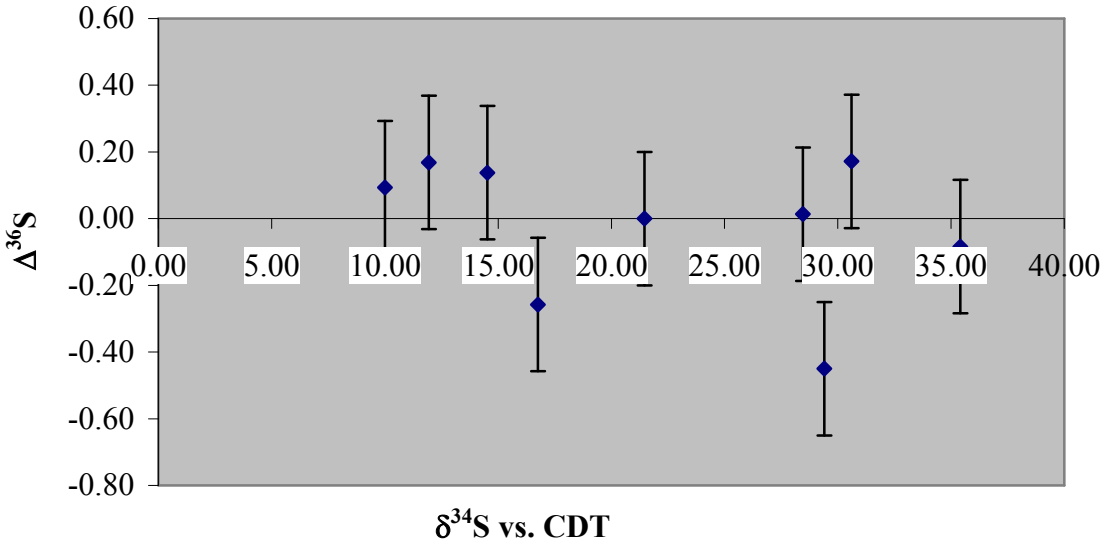

Figure A.1: The d34S vs. D36S values of Lapa sulfides. Data compiled and plotted by David T. Johnston.

A.2 Calculation of sterane distributions

Due to coelution, a quantity for $C_{27}\alpha\beta\beta R$ could not be directly integrated. The $C_{27}\alpha\beta\beta R$ sterane coeluted in the same peak with $C_{29}\beta\alpha S$ sterane. In order to calculate a total amount for C27 sterane to construct a ternary diagram, the quantity of $C_{27}\alpha\beta\beta R$ was estimated using the following equations:

The $C_{29}\beta\alpha S/(C_{29}\beta\alpha S+C_{29}\beta\alpha R)$ ratio was calculated from the *m/z*=259 ion chromatogram. This ratio was used to estimate the quantity of $C_{29}\beta\alpha S$ sterane from the *m/z*=217 chromatogram. This estimated quantity was subtracted from the quantity of the coeluted peak to estimate the $C_{27}\alpha\beta\beta R$ quantity. Using sample 589.90m as an example:

$C_{29}\beta\alpha S_{259}/(C_{29}\beta\alpha S+C_{29}\beta\alpha R)_{259} = 0.4987$

$C_{29}\beta\alpha R_{217} = 3807$

coeluted peak: $(C_{29}\beta\alpha S + C_{27}\alpha\beta\beta R)_{217} = 7226$

Estimate that:
$C_{29}\beta\alpha R_{217} = x$

$0.4987 = x/(3807 + x)$
$(0.4987)(3807) + 0.4987x = x$
$(0.4987)(3807) = x – 0.4987x = x (1 - 0.4987)$
$(0.4987)(3807)/((1 - 0.4987) = x = 3788$

$C_{27}\alpha\beta\beta R = 7226\text{-}3788 = 3438$

Sample	C27/all steranes	C28/all steranes	C29/all steranes
560.72m	0.34	0.27	0.40
572.64m	0.32	0.31	0.37
586.20m	0.28	0.28	0.44
589.90m	0.40	0.26	0.35
591.34m	0.31	0.27	0.42
596.20m	0.35	0.22	0.43

Table A.1: Exact values for the Lapa Formation used to construct the sterane ternary diagram.

A.3 Test for presence of oleanane

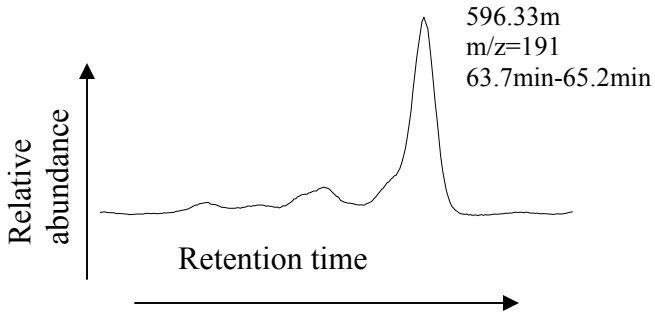

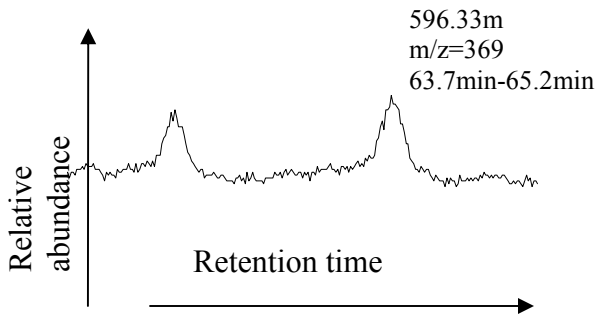

References

Amijaya H., Littke R. (2006). "Properties of thermally metamorphosed coal from Tanjung Enim. Area, South Sumatra Basin, Indonesia with special reference to the coalification path of macerals." *International Journal of Coal Geology* **66** (4): 271-295.

Azmy, K., Kaufman, A.J., Misi, A., de Oliveira, T.F. (2006). "Isotope stratigraphy of the Lapa Formation, Sao Francisco Basin, Brazil: Implications for Late Neoproterozoic glacial events in South America." *Precambrian Research*, **149**, 231-248.

Azmy, K., Veizer, J. Misi, A., de Oliveira, T. F., Sanches, A.L., and Dardenne, M.A. (2001) Dolomitization and isotope stratigraphy of the Vazante Formation, São Francisco Basin, Brazil. *Precambrian Research* **112**, 303-329.

Babinksi, M., Monteiro, L.S., Fetter, A.H., Bettencourt, J.S., and Oliveira, T.F. (2005). "Isotope of the mafic dikes from the Vazante nonsulfide zinc deposit, Brazil." Journal of South American Earth Sciences, **18** (3-4), 293-304.

Bowring, S.A., Grotzinger, J.P., Isachsen, C.E., Knoll, A.H., Pelechaty, S.M. and Kolosov, P. "Calibrating rates of early Cambrian evolution." *Science* **261** (5126): 1293-1298

Brocks, J.J., Logan G.A., Buick, R., and Summons, R.E. (1999). Archean molecular fossils and the early rise of eukaryotes. *Science* **285**: 1033.

Brocks, Jochen J., Buick, Roger, Logan, Graham A., and Summons, Roger E. (2003a). Composition and syngeneity of molecular fossils from the 2.78 to 2.45 billion-year-old Mount Bruce Supergroup, Pilbara Craton, Western Australia. *Geochimica et Cosmochimica Acta*, 67(22), 4289-4319.

Brocks, J.J, Buick, R., Summons, R. and Logan, G. (2003b). A reconstruction of Archean diversity based on molecular fossils from the 2.78 to 2.45 billion-year-old Mount Bruce Supergroup, Hamersley Basin, Western Australia. *Geochimica et Cosmochimica Acta* **67**(22): 4321.

Brody, K.B. Kaufman, A.J., Eigenbrode, J.L. and Cody, G.D. "Biomarker geochemistry of a post-glacial Neoproterozoic succession in Brazil." Geological Society of America *Abstracts with Programs* **36** (5): 477

Burdige, J. (2007). "Preservation of organic matter in marine sediments: Controls, mechanisms, and imbalance in sediment organic carbon budgets?" *Chem. Rev.* 107, 467–485.

Calvo, Eva, Pelejero, Carles, and Logan, Graham A. (2003). Pressurized liquid extraction of selected molecular biomarkers in deep sea sediments used as proxies in paleoceanography. *Journal of Chromatography A*, **989**: 197

Cloud, P. and Dardenne, M.A. (1973). "Proterozoic age of the Bambui Group in Brazil." *Geological Society of America Bulletin* **84**(5), 1673–1676.

Dardenne, M.A. (2000). "The Brasilia Fold Belt" in *Tectonic Evolution of South America*, E.G. Cordoni, Milani E.J., Filho, A.T. and Campos, D.A, eds. 31st International Geological Congress, Rio de Janeiro, Brazil. pp. 231-263.

Derry, L.A., Kaufman, A.J., and Jacobsen, S.B. (1992). Sedimentary cycling and environmental change in the late Proterozoic — evidence from stable and radiogenic isotopes. *Geochimica et Cosmochimica Acta* **56**: 1317.

Dickens, Gerald R. (2004). Methane hydrate and abrupt climate change. *Geotimes*, November 2004.

Eigenbrode, Jennifer L. Goddard Space Flight Center, Greenbelt, MD. and Geophysical Lab, Carnegie Institution of Washington.

Eigenbrode, J.L., and Freeman, K.H. Late Archean shallow- and deepwater sulfur cycles: Molecular and isotopic evidence. *Geochimica et Cosmochimica Acta*, 67(18), p. A85.

Eglinton, G. and Murphy, M.T.J., eds. *Organic Geochemistry: Methods and Results*. Springer-Verlag, 1969.

Erikkson, E. (1968) "Air-ocean-icecap interactions in relation to climate fluctuations and glaciation cycles" *Meteorol. Monogr*. **8**, 68-92.

Evans, DAD (2000). "Stratigraphic, geochronological, and paleomagnetic constraints upon the neoproterozoic climatic paradox." *American Journal of Science* **300** (5): 347-433.

Farquhar, James. Department of Geology, University of Maryland, College Park, MD.

Farrimond, P., Talbot, H.M., Watson, D.F., Schulz, L.K., and Wilhelms, A. (2004). "Methylhopanoids: Molecular indicators of ancient bacteria and a petroleum correlation tool." *Geochimica et Cosmochimica Acta*, v. 68(19), p. 3873-3882.

Frank, T.D., Kah, L.C., and Lyons, T.W. (2003). "Changes in organic matter production and accumulation as a mechanism for isotopic evolution in the Mesoproterozoic ocean." *Geological Magazine* **140**(4): 397-420.

Fuck, R.A., Pimentel, M.M. and Silva, J.H.D. (1994). Compartimentaçäo tectônica na porçäo oriental da Província Tocantins, in *Congresso Brasileiro Geologia 38*, Anais, SBG, pp. 215–216.

Geboy, N., 2006. Rhenium-Osmium Age Determinations of Glaciogeneic Shales from the Mesoproterozoic Vazante Formation, Brazil. Master's thesis.

Gorjan, P., Veevers, J.J., and Walter, M.R. (2000). Neoproterozoic sulfur-isotope variation in Australia and global implications. *Precambrian Research* **100**: 151.

Grotzinger, J.P. and A.H. Knoll (1995). "Anomalous carbonate precipitates: Is the Precambrian the key to the Permian?" *Palaios* **10**, 578-596.

Habicht, K.S., Gade, M. Thamdrup, B., Berg, P. and Canfield, D.E. (2002). "Calibration of sulfate levels in the Archean ocean." *Science* **298** (5602): 2372-2374.

Hambrey, M. J. and Harland, W. B. (1981). "Palaeogene ice-rafted quartz grains in the Sub-Antarctic Pacific". *Earth's pre-Pleistocene glacial record*. 217-219

Hayes, J.M., Kaplan, I.R., and Wedeking, K.W. "Precambrian organic geochemistry, preservation of the record." In *Earth's Earliest Biosphere*, Schopf, W., ed. 1983, Princeton University Press.

Hitzman, M.W., Reynolds, M.A., Sangster, D.F., Allen, C.R., and Carman, C.E. (2003). "Classification, genesis and exploration guides for nosulfides zinc deposits." *Economic Geology* **98**, 685–714.

Hitzman, M.W. and Beaty, D. (1996). "The Irish Zn-Pb-(Ba) Orefield." *Society of Economic Geologists Special Publication 4*, pp. 112–143.

Hoffman, P.F., and Schrag, D.P. (2002) The snowball Earth Hypothesis: testing the limits of global change. *Tera Nova* **14**, 129-155.

Hoffman, P., Kaufman, A J., Halferson, G.P. and Schrag, D. (1998). A Neoproterozoic Snowball Earth. *Science*, v. 281, p. 1342.

Hoffmann, K.H. and Prave, A.R. (1996). "A preliminary note on a revised subdivision and regional correlation of the Otavi Group based on glaciogenic diamictites and associated cap dolostones." *Comms. Geol. Surv. Namibia* **11**: 81–86.

Hsieh Y.P. and Shieh, Y.N. Analysis of reduced inorganic sulfur by diffusion methods: Improved apparatus and evaluation for sulfur isotopic studies. *Chemical Geology* **137**: 255.

Huang, Wen-Yen and Meinschein, W.G. (1979). "Sterols as ecological indicators." *Geochimica et Cosmochimica Acta* **43**: 739-745.

Hughes, William B., Holba, Albert G., and Dzou, Leon I.P. (1995). "The ratios of dibenzothiophene to phenanthrene and pristane to phytane as indicators of depositional environment and lithology of petroleum source rocks." *Geochimica et Coscmochimica Acta*, v. 59(17), p. 3581-3598.

Hunt, J.M., Philp, R.P., and Kvenvolden, K.A. (2002). Early developments in petroleum geochemistry. *Organic Geochemistry* **33**: 1025.

Hurtgen, M.T., Arthur, M.A., Suits, N.S., and Kaufman, A.J. (2002). "The sulfur isotopic composition of Neoproterozoic seawater sulfate: implications for a snowball Earth?" *Earth and Planetary Science Letters* **203** (1): 413–429.

Jacobsen, S.B., (2001) Gas hydrates and deglaciations. *Nature* **412:** 691-693.

Johnston, D.T., Poulton, S.W., Fralick, P.W., Wing, B.A., Canfield, D.E., and Farquhar, J. "Evolution of the oceanic sulfur cycle at the end of the Paleoproterozoic." *Geochimica et Cosmochimica Acta* **70**(23): 5723-5739.

Johnston, D.T., Wing, B.A., Farquhar, J., Kaufman, A.J., Strauss, H., Lyons, T.W., Kah, L.C. and Canfield, D.E. "Active microbial sulfur disproportionation in the Mesoproterozoic." *Science* **310**(5753): 1477-1479.

Kah L.C., Lyons T.W., Frank T.D. "Low marine sulphate and protracted oxygenation of the Proterozoic biosphere." *Nature* **431**(7010): 834-838.

Kah, L.C., Sherman, A.G., Narbonne, G.M., Knoll, A.H. and Kaufman, A.J. (1999). "delta C-13 stratigraphy of the Proterozoic Bylot Supergroup, Baffin Island, Canada: implications for regional lithostratigraphic correlations." *Canadian Journal of Earth Sciences* **36**(3): 313-332.

Kaufman, A.J. Department of Geology, University of Maryland, College Park, MD.

Kaufman, A.J., Knoll, A.H. and Narbonne, G.M. (1997) Isotopes, ice ages, and terminal Proterozoic Earth history. *Proceedings of the National Academy of Sciences* **94**, 6600-6605.

Kaufman, A.J. and Knoll, A.H. (1995) Neoproterozoic variations in the carbon isotopic composition of seawater: Stratigraphic and biogeochemical implications. *Precambrian Research* **73,** 27-49.

Kaufman, A.J., Hayes, J.M., Knoll, A.H., and Germs, G.J.B. Isotopic compositions of carbonates and organic-carbon from upper Proterozoic succession in Namibia — stratigraphic variation and the effects of diagenesis and metamorphism. *Precambrian Research* **49**: 301.

Kaufman, A.J., Hayes, J.M., Knoll, A.J. and Germs, G.J.B. (1991) "Isotopic compositions of carbonates and organic carbon from Upper Proterozoic successions in Namibia — Stratigraphic variation and the effects of diagenesis and metamorphism." *Precambrian Research* **49** (3–4), 301-327.

Kennedy, M.J., Blick-Christie N., and Sohl, L.E. (2001) Are Proterozoic cap carbonates and isotopic excursions a record of gas hydrate destabilization following Earth's coldest intervals. *Geology* **29:** 443-446.

Kennedy, M.J. (1996). "Stratigraphy, sedimentology, and isotopic geochemistry of Australian Neoproterozoic postglacial cap dolostones: Deglaciation, delta C-13 excursions, and carbonate precipitation." *Journal of Sedimentary Research* **66** (6): 1050-1064, Part B.

Kirschvink, J.L. Late Proterozoic low-latitude global glaciation: the Snowball Earth., in *The Proterozoic Biosphere*, Schopf, J.W. and Klein, C., eds. Cambridge University Press, 1992, p. 51.

Klein, C. and Beukes, N.J. (1993). "Sedimentology and geochemistry of the glaciogenic Late Proterozoic Rapitan iron-formation in Canada*." Economic Geology and the Bulletin of the Society of Economic Geologists* 88 (3): 542–565.

Li, R., Chen, J., Zhang, S., Lei, J., Shen, Y., Chen, X. (1999) Spatial and temporal variations in carbon and sulfur isotopic compositions of Sinian sedimentary rocks in the Yangtze platform, South China. *Precambrian Research* **97**: 59.

Logan, G.A., Hayes, J.M., Hieshima, G.B. and Summons, R.E. (1995). "Terminal Proterozoic reorganization of biogeochemical cycles." *Nature* **376** (6535): 53-56.

Mackenzie, A.S., Patience, R.L., Maxwell, J.R., Vandenbroucke, M., and Durand, B. "Molecular-parameters of maturation in the Toarcian shales, Paris Basin, France.1. Changes in the configurations of acyclic isoprenoid alkanes, steranes and triterpanes." *Geochimica et Cosmochimica Acta* **44** (11): 1709–1721.

Mauk, J.L. and Burruss, R.C. (2002). "Water washing of Proterozoic oil in the Midcontinent rift system." *AAPG Bulletin* **86**(6): 1113-1127.

Martins-Neto, M.A., Pedrosa-Soares, A.C., and Lima, S.A.A. (2001). Tectono-sedimentary evolution of sedimentary basins from Late Paleoproterozoic to Late Neoproterozoic in the São Francisco craton and Araçuaí fold belt, eastern Brazil. *Sedimentary Geology*, 141-142, p. 343.

Misi, Aroldo (Universidade Federal da Bahia, Grupo de Metalogenese, Salvador, Brazil); Iyer, Sundaram S. S.; Coelho, Carlos E. S.; Tassinari, Colombo C. G.; Franca-Rocha, Washington J. S.; de Abreu Cunha, Iona; Gomes, Adriana S. Rocha; de Oliveira, Tolentino Flavio; Teixeira, Joao Batista G.; Conceicao Filho, Valter Monaco (2005).

"Sediment hosted lead-zinc deposits of the Neoproterozoic Bambui Group and correlative sequences, Sao Francisco Craton, Brazil; a review and a possible metallogenic evolution model." *Ore Geology Reviews* 26(3–4), 263–304.

Monteiro LVS, Bettencourt JS, Juliani C, de Oliveira TF (2006). "Geology, petrography, and mineral chemistry of the Vazante non-sulfide and Ambrosia and Fagundes sulfide-rich carbonate-hosted Zn-(Pb) deposits, Minas Gerais, Brazil." *Ore Geology Reviews* 28(2): 201–234.

Moraes, Renato. Instituto de Geociências , Universidade de São Paulo. Visiting university research, University of Maryland, College Park, MD.

Olcott, A.M., Sessions, A.L., Corsetti, F.A., Kaufman, A.J. and de Oliveiera, T.F. (2005). "Biomarker evidence for photosynthesis during Neoproterozoic glaciation." *Science* **310** (5747): 471–474.

Ourisson, G., Albrecht, P. and Rohmer, M. (1979). "Hopanoids: Paleochemistry and biochemistry of a group of natural products." *Pure and Applied Chemistry* **51** (4): 709-729.

Pavlov, A.A., Hurtgen, M.T., Kasting, J.F., and Arthur, M.A. (2003) Methane-rich Proterozoic atmosphere? *Geology* **31,** 87-90.

Peters, K.E., Walters, C.C., and Moldowan, J.M. (2005). *The Biomarker Guide*, Cambridge University Press.

Peters, Kenneth E. and Moldowan, Michael J. (1993). *The Biomarker Guide: Interpreting Molecular Fossils in Petroleum and Ancient Sediments*. Prentice Hall, 1993.

Peters, K.E., Moldowan, J.M. and Sundararaman, P. (1990) "Effects of hydrous pyrolysis on biomarker thermal maturity parameters — Monterey phosphatic and siliceous members." *Organic Geochemistry* **15** (3): 249-265.

Petsch, S.T.; Edwards, K.J., Eglinton, T.I. (2005). "Microbial transformations of organic matter in black shales and implications for global biogeochemical cycles." *Palaeogeography, Palaeoclimatology, Palaeoecology* **219**(1-2): 157-170.

Pimentel, M.M., Dardenne, M.A., Fuck, R.A., Viana, M.G., Junges, S.L., Fischel, D.P., Seer, H.J., and Dantas, E.L. (2001). "Nd isotopes and the provenance of detrital sediments of the Neoproterozoic Brasilia Belt, central Brazil." *Journal of South American Earth Sciences* **14**, 571-585.

Plumb, K.A. (1991). "New Precambrian time scale." *Episodes* **14** (2): 139-140.

Radke, M., Vriend, S.P., Schaefer, R.G. (2001). "Geochemical characterization of Lower Toarcian source rocks from NW Germany: Interpretation of aromatic and saturated hydrocarbons in relation to deposition environment and maturation effects." *Journal of Petroleum Geology*, v. 24 (3), p. 287-307.

Rohmer, P. Bisseret and S. Neunlist (1992). "The hopanoids, prokaryotic triterpenoids and precursors of ubiquitous molecular fossils." In: J.M. Moldowan, P. Albrecht and R.P. Philp, Editors, *Biological Markers in Sediments and Petroleum*, Prentice Hall, New York, pp. 1–17.

Rostirolla, S. P., Mancini, F, Reis Neto, M. dos (2001). "Evolução Estrutural da zona da falha de Vazante: Exemplo de deformação Tardi-orogênica na Fasixa Brasília." Simpósio de Estudos Tectônicos. Recife, 2001.

Schrag, D.P., Berner, R.A., Hoffman, P.F., and Halverson, G.P. (2002) On the initiation of a snowball Earth. *Geochemistry, Geophysics, Geosystems* **3**(6).

Seifert, W.K. and Moldowan, J.M. (1979). "Effect of biodegradation on steranes and terpanes in crude oils." *Geochimica et Cosmochimica Acta* **43** (1): 111-126.

Seifert, W.K. and Moldowan, J.M. (1978). "Applications of steranes, terpanes and monoaromatics to the maturation, migration and source of crude oils." *Geochimica et Cosmochimica Acta* **42**:77-95.

Strauss, Harold, Des Marais, David J., Hayes, J.M., and Summons, Roger E. (1992a). Concentrations of Organic Carbon and Maturities and Elemental Compositions of Kerogens, from *The Proterozoic Biosphere*, Schopf, J.W., and Klein, C., eds. Cambridge University Press, 1992, p. 95.

Strauss, Harold, Des Marais, David J., Hayes, J.M., and Summons, Roger E. (1992b). The Carbon-Isotopic Record, from *The Proterozoic Biosphere*, Schopf, J.W., and Klein, C., eds. Cambridge University Press, 1992, p. 117.

Summons, Roger E. Massachusetts Institute of Technology.

Summons, R.E., Jahnke, Linda L., Hope, Janet M. and Logan, Graham A. (1999). 2α-methylhopanoids as biomarkers for cyanobacterial oxygenic photosynthesis. *Nature* **400**: 554 (Letters to Nature).

Teixeira, W., Sabate, P., Barbosa, J., Noce, C.M., and Carneiro, M.A. Archean and Paleoproterozoic Tectonic Evolution of the Sao Francisco Craton in *The Tectonic Evolution of South America*,. 2000. Cordani, U.G., Milani, E.J., Filho, A.T., Campos, D.A., eds, Thirty-First International Geological Congress, August 2000, Rio de Janeiro, p. 101.

Tissot, B.P. and Welte. D.H. (1984). *Petroleum Formation and Occurrence*, Springer-Verlag.

Tohver, E., D'Agrella, M.S., and Trindade, R.I.F. (2006). "Paleomagnetic record of Africa and South America for the 1200-500 Ma interval, and evaluation of Rodinia and Gondwana assemblies." *Precambrian Research* **147** (3-4): 193-222.

van Graas, Ger W. (1989). "Biomarker maturity paremeters for high maturities: Calibration of the working range up to the oil/condensate threshold." *Advances in Organic Geochemistry*, v. 16(4-6), p. 1025-1032.

Volkman, John K. (2005). "Sterols and other triterpenoids: source specificity and evolution of biosynthetic pathways*." Organic Geochemistry*, v. 36, p. 139-159.

Welte, D.H. and Waples, D.W. (1973). "Preference of even-numbered alkanes in sedimentary rock." *Naturwissenschaften* **60** (11): 516-517.

Widdel, F. and Hansen, T.A. "The Dissimilatory Sulfate- and Sulfur-Reducing Bacteria." (1991). In *The Prokaryotes*, Balows, A., Trüper, H.G., Dworkin, M., Harder, W. and Schleifer, Karl-Heinz, eds. Springer-Verlag, pp.583–613.

Wing, Boswell. Department of Earth and Planetary Sciences, McGill University.

Zhusheng, J., Philp, R.P., and Lewes, C.A. "Fractionation of biological markers in crude oils during migration and the effects on correlation and maturation parameters." (1988). *Advances in Organic Geochemistry* 13(1–3): 561–571.